Effects of Ferromagnetic Particles in Viscous Fluids

By

Aaqib Majeed

33-FBAS/PHDMA/F-13

Department of Mathematics and Statistics

Faculty of Basic and Applied Sciences

International Islamic University, Islamabad

Pakistan

2017

Viscous flows.
Mathematical models.
Fluids mechanics.

Effects of Ferromagnetic Particles in Viscous Fluids

By

Aaqib Majeed

Supervised by

Dr. Ahmad Zeeshan

Department of Mathematics and Statistics

Faculty of Basic and Applied Sciences

International Islamic University, Islamabad

Pakistan

2017

Effects of Ferromagnetic Particles in Viscous Fluids

By

Aaqib Majeed

A Thesis

Submitted in the Partial Fulfillment of the

Requirements for the Degree of

DOCTOR OF PHILOSOPHY

IN

MATHEMATICS

Supervised by

Dr. Ahmad Zeeshan

Department of Mathematics and Statistics

Faculty of Basic and Applied Sciences

International Islamic University, Islamabad

Pakistan

2017

Author's Declaration

I, **Aaqib Majeed** Reg. No. **33-FBAS/PHDMA/F13** hereby state that my Ph.D. thesis titled: **Effects of Ferromagnetic Particles in Viscous Fluids** is my own work and has not been submitted previously by my for taking any degree from this university, **International Islamic University, Sector H-10, Islamabad, Pakistan** or anywhere else in the country/world.

At any time if my statement is found to be incorrect even after my Graduate the university has the right to withdraw my Ph.D. degree.

Name of Student: ***(Aaqib Majeed)***
Reg. No. **33-FBAS/PHDMA/F13**
Dated: **19/12/2017**

Plagiarism Undertaking

I solemnly declare that research work presented in the thesis titled: **Effects of Ferromagnetic Particles in Viscous Fluids** is solely my research work with no significant contribution from any other person. Small contribution/help wherever taken has been duly acknowledged and that complete thesis has been written by me.

I understand the zero tolerance policy of the HEC and University, **International Islamic University, Sector H-10, Islamabad, Pakistan** towards plagiarism. Therefore, I as an Author of the above titled thesis declare that no portion of my thesis has been plagiarized and any material used as reference is properly referred/cited.

I undertake that if I am found guilty of any formal plagiarism in the above titled thesis even after award of Ph.D. degree, the university reserves the rights to withdraw/revoke my Ph.D. degree and that HEC and the University has the right to publish my name on the HEC/University Website on which names of students are placed who submitted plagiarized thesis.

Student/Author Signature: _____

Name: **(Aaqib Majeed)**

Certificate of Approval

This is to certify that the research work presented in this thesis, entitled: **Effects of Ferromagnetic Particles in Viscous Fluids** was conducted by **Mr. Aaqib Majeed,** Reg. No. **33-FBAS/PHDMA/F13** under the supervision of **Dr. Ahmed Zeeshan** no part of this thesis has been submitted anywhere else for any other degree. This thesis is submitted to the **Department of Mathematics & Statistics, FBAS, IIU, Islamabad** in partial fulfillment of the requirements for the degree of **Doctor of Philosophy in Mathematics, Department of Mathematics & Statistics, Faculty of Basic & Applied Science, International Islamic University, Sector H-10, Islamabad, Pakistan.**

Student Name: Aaqib Majeed **Signatures:** _____

Examination Committee:

a) **External Examiner 1:**
Name/Designation/Office Address **Signatures:** _____

Prof. Dr. Tasawar Hayat
Department of Mathematics,
QAU, Islamabad.

b) **External Examiner 2:**
Name/Designation/Office Address) **Signatures:** _____

Prof. Dr. Muhammad Ayub
Department of Mathematics,
QAU. Islamabad.

c) **Internal Examiner:**
Name/Designation/Office Address) **Signatures:** _____

Dr. Nasir Ali
Associate Professor

Supervisor Name: **Signatures:** _____
Dr. Ahmed Zeeshan

Name of Dean/HOD **Signatures:** _____
Prof. Dr. Muhammad Sajid, T.I

Dedication

This thesis is dedicated to:

My beloved Father, Mother, Brothers, Sisters, Wife and Children

Acknowledgements

Firstly, I am thankful to Almighty Allah, who created us, taught us everything we did not know, provided us with balance, health, knowledge and intelligence to explore his world. I offer salutation upon the Holy Prophet Hazrat Muhammad (PBUH), who has lightened the life of all mankind with his guidance. He is a source of knowledge and blessings for the entire creations. His teachings make us to ponder and to explore this world with direction of Islam.

Secondly, I express my profound gratitude to my respected supervisor **Dr. Ahmad Zeeshan,** who helped me throughout my PhD study with their cooperation guidance and guided me to complete my thesis within due course of time. This thesis would not have been successfully completed without their valuable intellectual tutelage, words of encouragement, push for tenacity and opportunity to gain from their wealth of knowledge. I am also pay my regards to all my teachers who always directed me to right dimensions and made it possible for me to achieve high goals in my life.

I extend my gratitude to my family for encouragement and support, even in the gloomiest of times. I am also thankful to my friends specially Muhammad Mudassar Maskeen, Nasir shahzad, Nouman Ijaz, Bilal Aryan, Shahid Nadeem, Farooq Hussain and others who always helped me during my studies in all respects.

In the last but not least, it would be sheer injustice and ungratefulness if I make no mention of participation and timely interference of my father **Mr. Abdul Majeed (Sitara-i-Imtiaz)** had been serving as director in esteemed organization Dr. A.Q. Khan research Labs. Kahuta. Being Mathematician, he has helped me to understand mathematical concepts and now I have improved myself a lot due to his inspiring guidance and benevolent attitude in my studies. He has helped me in understanding programming in MATLAB.

Aaqib Majeed

Preface

Human mind strive to achieve more and create smart things, which simplify the work and make the life convenient. One such recent advancement are smart materials, which are designed so that one or more properties of the material are set variable and can be significantly changed external due to stimuli so that it achieve the said purpose. Magnetic smart materials are the material, which are controlled by using external magnetic field. Ferrofluid is an example of such smart materials synthesize by NASA for fuel transport in weightless situation. These fluids are not naturally available, but are to be synthesized. The variety of applications like in instrumentation, electrical and electronics engineering such as, lubricants in bearing and dumpers, heat controller in electric motors and hi-fi speaker systems, sealing of computer hard disk drives, rotating x-ray tubes, rotating shafts rods and sink-float systems for separation of materials. In field of biomedicine, they have been found very useful. These can be used to deliver certain drugs to a certain area of human blood. There is also an idea to use ferrofluids for cancer treating by heating the tumor soaked in ferrofluids by means of an alternating magnetic fields is the prospect of influencing flow by the magnetic field and vice-versa

The purpose of the present thesis is to characterize the flow behavior of non-conducting ferromagnetic fluid under the influence of magnetic field. Mathematical modeling is based upon continuity, momentum and energy equations. The physical problems are first modeled and then the basic governing equations are formulated into a set of dimensionless form by using appropriate transformations. In some cases a numerical procedure is implemented to solve the non-linear boundary value problem by mean of 4^{th} order Runga-kutta based shooting technique. The impact of pertinent parameters: ferromagnetic interaction, Prandtl number, porosity, viscous dissipation, viscoelastic, suction, slip, Deborah, unsteady, relaxation time, mixed convection, heat source/sink, Schmidt number, Soret number, Chemical reaction, radiation and volume fraction of magnetic nanoparticle are demonstrated through graphs and tables. Comparison between the numerical results are made is some cases and found to be an excellent agreement with those published in literature.

This thesis consist of eleven chapters. Chapter one provides literature review, introduction, some basic definitions, governing equations, constitutive relation for Newtonian and non-Newtonian fluids, modelling of ferromagnetic flow and methodology relevant to the material which will use in the subsequent chapters.

In chapter two, the effect of thermal radiation and heat transfer on the flow of ferromagnetic liquid over a stretching surface is investigated under prescribed surface temperature (PST). The appropriate combination of non-magnetic viscous base fluid, magnetic solid and surfactant composes magnetic fluid is considered in the presence of dipole. **This study is published in Journal of Molecular Liquids, 215 (2016) 549-554.**

Chapter three, describes two dimensional steady boundary layer mixed convection flow and heat transfer in ferromagnetic fluid past a stretching surface. Velocity slip is taken into account instead on no-slip. Is this analysis the role of local skin friction, heat transfer rate, ferromagnetic-interaction parameter, slip parameter and buoyancy parameter on velocity and temperature profiles inside the boundary layers are examined through graphs and tables. **This study is published online in the Journal of Thermal Science. DOI: 10.2298/TSCI160610268Z.**

Chapter four, investigates stagnation point flow and heat transfer of a ferrofluid made from a suspension of tiny magnetic particles over a flat stretching or shrinking porous sheet under dipole field. Influence of various pertinent parameters are elaborated with the help of graphs and tables. **This analysis is published in the Caspian Journal of Applied Sciences Research, 5 (2016) 34-44.**

Chapter five illustrates unsteady ferromagnetic boundary layer fluid flow and heat transfer analysis over a stretching sheet. Two different types of thermal boundary conditions namely, (i) prescribed surface temperature (PST) and (ii) prescribed heat flux (PHF) are considered. **This study is published in the Journal of Molecular Liquids, 223 (2016) 528-533.**

Chapter six explores the two-dimensional ferromagnetic viscoelastic boundary layer flow problem and heat transfer over a stretching surface with a linear velocity under the impact of magnetic dipole and suction. Constitutive equation are first derived for viscoelastic fluid and then solved numerically for several controlling parameter. **This study is online available in the Journal of Neural Computing and Applications, Doi: 10.1007/s00521-016-2830-6.**

Chapter seven designates, chemical reaction and heat transfer on boundary layer Maxwell ferro-fluid flow with Soret and suction under the influence of external magnetic field. The sheet is assumed to be permeable in a semi-infinite domain. **This study is published in the Journal of Engineering Science and Technology, 223 (2016) 528-533.**

Chapter eight offers two dimensional boundary layer flow of a Maxwell ferromagnetic fluid toward a flat plate with the occurrence of external magnetic field because of the fact that two equally line dipole which are equidistant from the wall and perpendicular to the flow plane. Cattaneo-Christov heat flux model is utilized in modified form of Fourier's law to disclose the heat transfer characteristic. **This study is published in the Journal Magnetics 22(3), (2017) 472-477.**

Chapter nine describes two-dimensional boundary layer slip flow and heat transfer characteristics of magnetic nanofluid (ferrofluid) via porous medium is investigated. The flow is generated due to stretched surface under the influence of magnetic dipole. Magnetite as a nanoparticle with three different types of base fluids such as water, kerosene and refrigerant-134a is utilized. **The content of this study is submitted in Mathematical Problems in Engineering.**

Chapter ten addresses the boundary layer flow of magnetic nanofluid over a stretching surface with velocity slip condition have been investigated. Water is selected as a base liquid whereas ferromagnetic, paramagnetic, diamagnetic, antiferromagnetic and ferrimagnetic are chosen as nanoparticles. The use of magnetic nanoparticle is to control the flow and heat transfer process via external magnetic field. **The study is online available in the Journal of Neural Computing and Applications, DOI: 10.1007/s00521-017-2989-5.**

Chapter eleven investigates the shapes effect of magnetic nanoparticle on boundary layer flow of ferrofluid over a rotating disk with the presence of low oscillating magnetic field. The disk is rotating about an axis perpendicular to its plane with uniform angular velocity. Water is considered as a base fluid while magnetite (Fe_3O_4) as nanoparticle with three different shapes like platelet, cylinder and brick, which is based on Hamilton-Crosser model. **This study is published in the Journal of Magnetism and Magnetic Materials 443, (2017) 36-44.**

Nomenclature

a^*	Distance from surface to dipole	Pr	Prandtl number
A	Velocity slip factor	Q_o	Heat generation/absorption coefficient
A_1	Ratio of velocity parameter	S	Suction/injection parameter
$c \pm$	Stretching/ shrinking constant	S_c	Schmidt number
C_p	Specific heat	S_r	Soret number
c_s	Concentration susceptibility	q_r	Heat flux
C_f	Skin friction coefficient	Re_x	Reynold number
f	Dimensionless stream function	T	Temperature
G^*	Mixed convection parameter	n	number of particle
H	Magnetic field	T_c	Curie temperature
H_1	Heat source/sink parameter	T_m	Mean fluid temperature
K^*	Pyromagnetic constant	$U(x)$	Free stream velocity
K^{**}	Mean absorption coefficient	u_w	Wall velocity
K	Permeability of porous medium	(u, v)	Velocity components
l	Characteristic length	(x, y)	Cartesian coordinates
K_1	Porosity parameter	M	Magnetization
K_r	Chemical reaction parameter	N	Radiation parameter
I	Some of moment of Inertia	N_{ux}	Nusselt number
		m	Shape factor

Greek symbols

ρ	Density	θ	Dimensionless temperature
σ^*	Stefan-Boltzmann constant	α	Thermal diffusivity

k	Thermal conductivity	α_1	Dimensionless distance
μ	Viscosity	α_2	Thermal relaxation time
ν	Kinematic viscosity	β	Ferrohydrodynamic interaction parameter
v_w	Wall mass flux	γ	Magnetic field strength
Λ	Unsteady parameter	γ_1	Deborah number
μ_0	Permeability	ε	Dimensionless curie temperature
(η, ξ)	Dimensionless coordinate	λ	Viscous dissipation parameter
ϕ	Volume fraction	λ_0	Amplitude
Ψ	Stream function	λ^*	Viscoelastic parameter
Φ	Magnetic potential	λ_1	Relaxation time parameter
τ_{wr}	Radian skin friction	λ_e	Effective magnetic parameter
$\tau_{w\phi}$	Transverse skin friction	τ_s	Small inertia
τ_B	Brownian relaxation	λ_2	Ratio of relaxation to retardation
ω_0	Frequency	δ	Dimensionless slip parameter
ω_p	Angular momentum	Ω	Vorticity
λ	Langevin parameter	$L(\lambda)$	Langevin function

Subscripts

nf	Nanofluid	s	Solid particle
f	Base fluid		

Contents

Chapter 1

Preliminary

1.1 Literature survey

1.1.1 Ferrofluid

Ferrofluids have emerged as a new class of "magnetic nanofluids". Its extraordinary physical properties and usages in many electrical and smart appliances fascinates scientist and engineers over the years. Ferrofluids are stable colloidal dispersions of micron-sized ferromagnetic particles in carrier liquid and its heat transfer properties. Usually ferrofluid comprise 10% surfactant, 5% magnetic solid and 85% liquid. These fluids have potential applications in area of microelectromechanical system (MEMS) and nanoelectromechanical system (NEMS) using ferrofluid particles like nanoduct flows, nanomotors, nanogenerators, purification of molten metals, microfluidic actuators, coolers of nuclear reactors, shock absorbers, leak-proof seals, lithographic patterning, *x*-ray tubes, microfluidic valves and pumps, sealing of hard drives and rotating shafts and rods comprises of ferrofluids. Also, it is utilized as lubrication in bearing and dumpers, to regulator the heat in electric motors systems and speaker systems [1-4]. The contributions of these fluids in biomechanics is also valuable, because it is also useful to supply drugs to unreachable parts of human blood and for the treatment of tumour by heating the lump absorbed ferrofluids by means of substituting external magnetic fields [5, 6]. Maruno et al. [7] utilized ferrofluids as a magnetic ink for high-speed, low-cost and soundless printers. Ferrofluids likewise have exceptionally fascinating shapes, structures and patterns, that can create from ferro-hydrodynamic hazards as sketched in Figs. 1.1 and 1.2. Now the peaking behavior of ferrofluid, consequences of magnetic field which is orthogonal to the layer of ferrofluid. Rrigging-like structure see fig. 1.3, result of radial orthogonal field uncertainty when little magnet is situated beyond a ferromagnetic liquid drop restricted among closely disseminate crystal plates, for labyrinth uncertainty see figs. 1.4 and 1.5 fallouts when external magnetic field is employed tangently to tinny layer of ferromagnetic liquid and restricted among definitely disseminate crystal plates. All images perform a ferrofluid with immersion magnetic polarization of 400 G. In figs. 1.3 to 1.5 ferrofluid is enclosed by 50% deionized water, 50% propanol blend so as to keep impede ferrofluid from wetting the crystal plates.

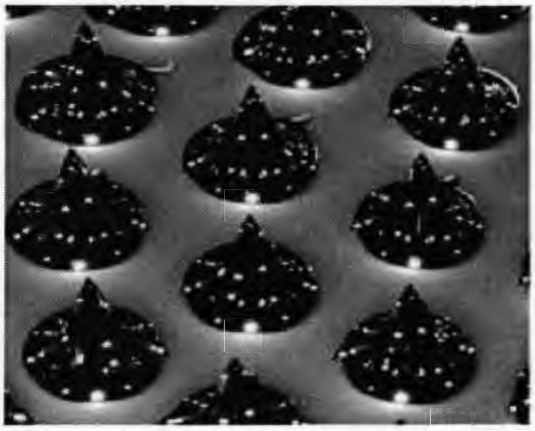

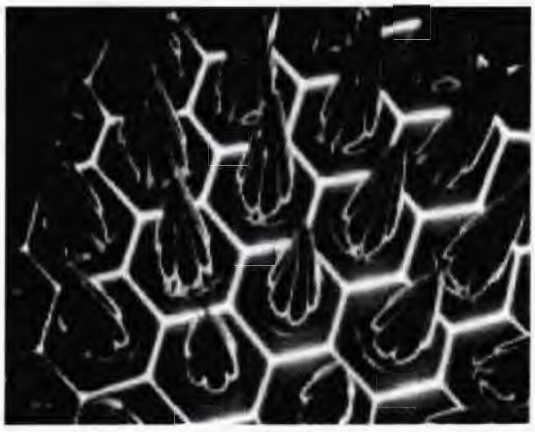

Fig. 1.1 a) Hexagonal peaking patterns. **b)** The chocolate-drop' like shape.

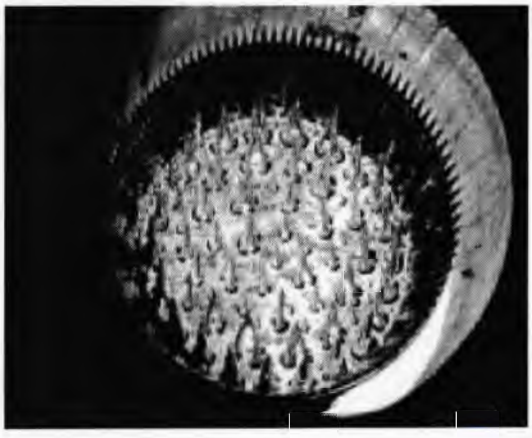

Fig. 1.2. View of the perpendicular field instability including a crown of peaks.

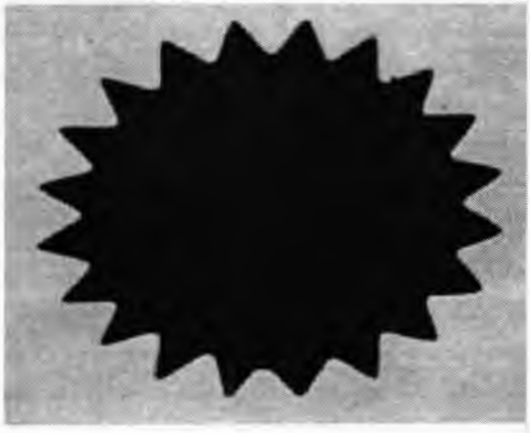

Fig. 1.3. Gear-like structure.

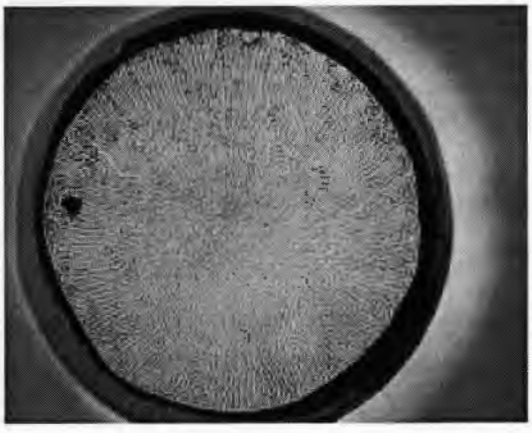

Fig. 1.4. Labyrinth instability.

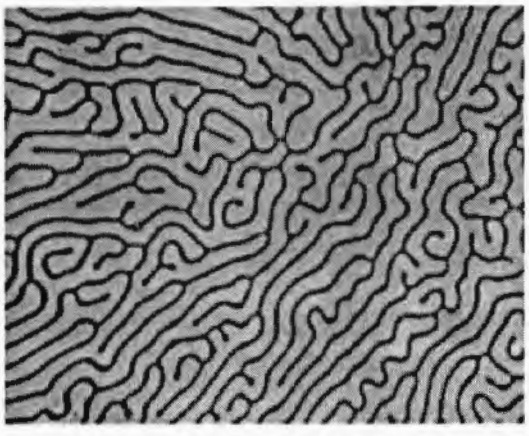

Fig. 1.5. Closer view of the labyrinth instability.

The study of ferrofluid has gained significant importance and have a auspicious potential for heat transport applications because the flow of ferromagnetic liquid can be regulator by applied

field. Ferrofluid was first developed by NASA in the early 1960s to report the distinctive desires of moving fuel in a gravity-free outer-space. Rosensweing [8] has given an influential overview to the investigation on magnetic liquids in his paper and gave the interesting information of the impact of magnetization. Later on Neuringer [9] was the first who considered classical boundary layer flow problem to simulate the effects of applied magnetic field on stagnation point flow to drenched ferromagnetic liquid against a cold wall and parallel flow along flat plate with linearly decreasing surface temperature. Tangthieng et al. [10] elaborated heat transfer enhancement in ferromagnetic fluid flow among the flat surfaces and box by varying magnetic field made with the help of vector potential field and permanent magnet produced by a dipole magnet by utilizing finite element simulation. Yamaguchi et al. [11] have considered ferromagnetic natural convective flow in square cavity with four rigid walls. They found that when the both buoyancy and the magnetic force co-occurs, heat transfer characteristics remain low at lower area of Rayleigh number. Although by rising Rayleigh number, heat transfer improved highly and shows greater value under a strong magnetic field. Snyder et al. [12] examined combined influence of natural and magnetic field on convective energy transport through a ferromagnetic liquid in a cubic enclosure. It was found that magnetoconvection can be predicted numerically and validate the standard theory experiment under constant magnetic field gradient. Ramanathan and Suresh [13] discussed MFD in an anisotropic porous media. It was found that system is destabilizes with the occurrence of anisotropic porous medium, however the stimulus of magnetic field dependent (MFD) viscosity is to stabilize the system. Finlayson [14] analyzed irregularity of ferromagnetic liquid heated from beneath in the appearance of uniform magnetic field. He described the consequence of buoyancy and magnetic field and using linear theory and possibility of oscillatory instability cannot occur. Ganguly et al. [15] considered two-dimensional pressure-driven convective flow and heat transfer in ferrofluid under the inspiration of line-source dipole in a channel. They concluded that the overall heat transfer enhancement relies predominantly on net magnetized current and comparative placement of the line dipoles.

Aminfar et al. [16, 17] analyzed uniform transverse magnetic force effect and non-uniform axial magnetic force on MHD and thermal behaviours of a ferromagnetic mixed convective flow in a pipe. They disclosed that uniform transverse field and negative gradient field act in the same way and enhances skin friction and Nusselt number whereas reverse trend is noted for positive gradient axial field. Aminfar et al. [18] have also employed two phase model and CVT is used to examine the hydrothermal features of a ferrofluid in a rectangular made by an electric current passing through wire situated below the duct embedded with non-uniform

magnetic field. Their outcomes display that Nusselt number and friction factor increases against magnetic field and generates a couple of vertices that improves heat transfer characteristics and precludes alluvium of nanoparticles. Strek and Jopek [19] considered time dependent ferromagnetic fluid flow and transfer of heat among two parallel surfaces beneath the impact of dipole field. Sheikholeslami and Rashidi [20] described finite element technique to stimulate ferrofluid and treatment of heat transport in a lid-driven semi annulus with variable magnetic field. Outcomes illustrate that Nusselt number vary directly to Richardson number and volume concentration of nanoparticle. Ghofrania et al. [21] elaborated an experimental study of ferrofluid and convective heat transport flow in a tube beneath the impact of an alternating magnetic field with a uniform heat flux. It was observed enhancement in convective heat transport against laminar boundary condition. Selimefendigil and Oztop [22] conducted numerical visualization of heat transfer enhancement and fluid flow over a rotating cylinder with dipole field using backward facing step geometry. They showed that the impact of cylindrical rotation at low Reynolds number Nusselt number is more prominent.

Jafari et al. [23] have deliberated kerosene based ferrofluid and transfer of heat in two cylinders with diverse dimensions using CFD. They applied heat flux and uniform magnetic fields over numerous geometries. Sekar and Vaidyanathan [24] have examined instability of convective magnetized ferrofluid in a porous rotating system along a vertical axis using Brinkman model. The result disclose that the porous medium tend to stabilise system for low permeability and higher rotation. Zahn and Rosensweig [25] demonstrated that fingering instability occurs when additional viscous fluid is penetrated across the voids of porous region, which can be controlled if magnetic field is applied along tangential interface to horizontal surface splitting magnetizable and non-magnetizable. Jue [26] have implemented semi-implicit finite element numerical scheme to obtain a ferrofluid flow in a cavity under buoyancy and magnetic force effects. Result shows that flow strength escalations for large magnetic field, whereas there is decline in side-wall heat transfer rate for high magnetic field. Narayana et al. [27] reported micropolar ferromagnetic liquid flow over an elastic stretching sheet for two type of heat process, specifically PST and PHF. It was establish that the impact of ferrohydrodynamic interaction is to slow down fluid movement as compared to pure MHD case. Application of conventional ferromagnetic liquid usages DC magnetic fields from permanent magnets for heat transfer in loudspeakers and usages as a liquid O-ring in rotation and omission seals [28].

The ferromagnetic fluid injecting in a traveling wave magnetic field lack of free surface is discussed by obtaining the time average torque and magnetic force are solved numerically. It is essential that the term of particle spin and fluid convection be important in the

magnetization constitutive law and the spin viscosity must be low in order to forecast the experimentally perceived forward pumping at higher magnetic field and backward pumping at lower magnetic field [29]. Zahn and Pioch [30, 31] investigated anomalous behaviour of ferrofluid in AC magnetic field and examine the infrequent type of pair of electro-mechanical system using the flow model of rectilinear and angular momentum equations involving non-symmetric Maxwell and viscous stress tensors. They examined the magnetic field component transverse and parallel to the duct and fluctuating sinusoidally with time. In uniform magnetic field the magnetization features rely on spin velocity of fluid whereas does not rely on the velocity of fluid. Zakinyan et al. [32] have explored experimentally the performance of magnetic liquid drop lying on a flat surface and bounded by non-magnetic liquid under the inspiration of constant magnetic field which is rotating at low frequency in vertical plane. They also observed the shape deformation and translatory motion of the drop velocity for different field amplitude and frequencies. Buzduga et al. [33] performed experimental studying for the stability of ferrofluids in magnetic fields. Interaction between the ferrofluid and the magnetic field allows us to study the specific properties of both the ferrofluid and the magnetic field in order to develop specific applications. Shliomis and Morozov [34] conducted that under the impact of linearly polarized magnetic field, viscosity of ferrofluid is positive at low frequencies and negative at high frequencies.

Oliveira et al. [35] examined the reaction of ferromagnetic liquid droplet along a radial direction of magnetic field. At the point when the flow of droplet is restrained between two parallel plates they checked how the constancy properties of the boundary interface and shape of evolving arrangements response under the influence of magnetic fluid. Also established the fingering pattern at interface and destabilizing toward radial direction. We have also confirmed that magnetic field praise the development of peaked pattern structures within nonlinear weakly regime, which incline to become sharper and sharper as the magnitude of the magnetic impact is enhanced. Vieru et al. [36] have employed integral transform method to investigated unsteady viscoelastic Maxwell fractional fluid flow on continually hastening plate among two sided walls orthogonal to flat plate. Fetecau et al. [37] considered an incompressible flow of viscous fluid past a porous plate that implements a shear stress to the fluid with thermal radiation effects. Bég et al. [38] demonstrated natural convection and transport of heat of a chemically reactive Newtonian fluid toward a vertically inclined plates under the inspiration of Soret and Dufour effects. Vafai [39] used asymptotic series expansions method to investigate the convective heat transport in a porous region with variable porosity and inertial forces under impermeable boundary condition. Jothimani and Anjali Devi [40] have analyzed the stability

of two superposed ferromagnetic viscous fluids under the action of an oblique magnetic field past an infinite flat plate.

1.1.2 Fluid with nanoparticles

The problems of boundary layer viscous flow and characteristics of heat transport owing to stretching sheet have fascinated many investigator because of several applications and play a vital role in the field of sciences and engineering. like annealing and tinning of copper wires, manufacturing of rubber sheets and plastic, glass blowing, fiber spinning and continuous cooling, manufacturing and extraction of polymer and rubber sheets, glass-fiber and wire drawing etc. In recent years, emergent technology, modern industries like microelectronics, manufacturing, lubricants and oil, cthylene glycol and transportation are facing a problem of limiting cooling efficiency of heat transfer fluids as water etc. On another way, fast cooling is also a fundamental need in food science and innovation. Consequently, heat properties of base liquids may be enhanced by considering minor insertion of nanoparticles into base fluids. This suspension is named "nanofluid" is a comparatively novel type of liquid which comprise of conventional fluid with nanoparticles suspended within them, which first is presented by Choi [41]. Nanoparticles are made from numerous materials, like Cu, Au, Fe, Hg, Ti, Ag, etc. metals and non-metallic TiO_2, SiO_2, Al_2O_3 CuO. Nanofluids have innovative characteristics that make them conceivably valuable in numerous application in transfer of heat transfer, Some applications where nanofluids can be utilized as a regular fluids i.e. engine cooling, cooling of electronics, nuclear reactor, solar water heating, biomedical science, refining the efficiency of diesel generator, domestic refrigerator, cooling of heat exchangeable devices, [42]. Choi et al. [43] exhibited that heat conductivity of the fluid increases twice with the insertion of small amount of nanoparticles to conventional base fluid. A detailed analysis on heat conductivity of nanofluid was discussed by Buongiorno et al. [44]. Variation of heat conductivity and fluid viscosity by dissolving a fine particles TiO2, SiO2 and Al_2O_3 were discussed by Masuda et al. [45]. Abu-Nada et al. [46] studied natural convection flow and heat transport of nanofluid based on Cu-water in an inclined cavity and also considered an angle of inclination as a converging parameter for heat transport. Khan and Pop [47] examined laminar nanofluid flow past a stretchable surface under the presence of thermophoresis and Brownian effect. They establish theat Nusselt number is declining for each non-dimensional number, whereas the Sherwood number is rises for higher value of Pr and reduces for lower value of Pr. The influence of chemically reactive and radiation in the manifestation of a nanoparticle flow over a porous

surface was deliberated by Ismoen et al. [48]. Hady et al. [49] examined viscous nanofluid and heat transfer of nanofluid past a moving nonlinear isothermal flat plate by considering radiation and Rosseland approximation. Nadeem et al. [50] deliberated the influence of velocity slip and heat radiation on MHD stagnation point of nanofluid over a stretchable surface. Das et al. [51] studied two to fourfold rise in thermal conductivity improvement for a nanofluids depend on water comprising CuO or Al_2O_3 nanoparticles for a low temperature. Vajravelu et al. [52] explored the heat transfer characteristic of convective nanofluids based on Ag-water or Cu-water. They pointed out that under the influence of nanoparticles, absolute value of skin friction is increases toward the surface and reduction is noted for the Nusselt number. These effects are establish to be further noticeable for Ag-water as compared to the Cu–water solution. The solution of boundary layer thickness decreases for Ag-water solution more than that of the Cu–water solution. Turkyilmazoglu and Pop [53] inspected two types of heating boundary condition with heat and mass transfer of nanofluid flows over an infinite horizontal plate with radiation effect. They also considered the behavior of dissimilar based on water nanofluids comprising Cu, CuO, Ag, TiO_2 and Al_2O_3. Some of the recent study related to nano and ferrofluids are [54-89].

1.2 Laws of conservation in fluid mechanics

There are three fundamental laws, which are used to solve the fluid dynamics problems [90]. The governing equations of motion can be obtained using a CV technique. This is equal to a "fluidic black box" where we know all about the flow is what is going in and what is coming out of the control volume. We get the expression in differential form by applying the Stoke's theorem to an infinitesimally small volume with in the flow. When investigate a control volume problem following three fundamental laws of fluid dynamics:

1.2.1 Law of conservation of mass

The continuity equation that comes by applying the conservation law of mass to a fluid flow which is mathematically defined as

$$\frac{\partial \rho}{\partial t} + \nabla.(\rho \mathbf{V}) = 0, \tag{1.1}$$

where $\mathbf{V}$ is the velocity of fluid. The 1st term in above equation describes increasing rate of density in control volume and the 2nd term denotes the mass flux rate fleeting out of the control surface. The Eq. (1.1) can be rewrite in following form

$$\frac{D\rho}{Dt} + \nabla.(\rho \mathbf{V}) = 0, \tag{1.2}$$

where

$$\frac{D(\ )}{Dt} \equiv \frac{\partial(\ )}{\partial t} + \mathbf{V}.\nabla(\ ). \tag{1.3}$$

Eq. (1.1) was obtained with the help of Euleriun technique. In this technique, a fixed control volume is used and the deviations to the fluid are documented as the fluid passes with in control volume. On the other hand in Lagrangian approach, the variations in the element of fluid properties are noted by a viewer moving toward the fluid element. The viewpoint of Eulerian is commonly used in fluid mechanics. The Eq. (1.2) in Cartesian coordinate system as follow

$$\frac{\partial \rho}{\partial t} + \frac{\partial}{\partial x}(\rho u) + \frac{\partial}{\partial y}(\rho v) + \frac{\partial}{\partial z}(\rho w) = 0, \tag{1.4}$$

where u, v, w denote the components of velocity toward x, y, z direction. The density of the each fluid element remains constant is termed an incompressible. Mathematically stated as

$$\frac{D\rho}{Dt} = 0, \tag{1.5}$$

which diminish Eq. (1.2) to

$$\nabla.\mathbf{V} = 0, \tag{1.6}$$

or

$$\frac{\partial u}{\partial x} + \frac{\partial v}{\partial y} + \frac{\partial w}{\partial z} = 0. \tag{1.7}$$

1.2.2 Law of conservation of momentum

Conservation equation of linear momentum is recognized as the Navier-Stokes equation. Mathematically

$$\rho \frac{D\mathbf{V}}{Dt} = \nabla.\boldsymbol{\tau} + \rho g. \tag{1.8}$$

Under the directive of an Eulerian explanation, acceleration vector on the left hand side called known material derivative, which is interchanged with the sum of convective and local accelerations to get

$$\rho\left[\frac{\partial}{\partial t} + (\mathbf{V}.\nabla)\right]\mathbf{V} = \nabla.\boldsymbol{\tau} + \rho\mathbf{F}. \tag{1.9}$$

In the above Eq. (1.9), **F** represent the body force per unit volume. If we consider weight of the fluid as bod force then **F** will replace with the gravitational acceleration vector $\boldsymbol{g}$. The 1st term on right hand side (RHS) of Eq. (1.9) shows surface forces. These forces are applied by the external stresses on the fluid element. The stresses comprise of shearing stresses and normal stresses are symbolised by the stress tensor components. Different fluids are defined by different stress tensor. The momentum equation for single dipole described by Andersson and Valnes [91] are

$$\rho(\mathbf{V}.\nabla)\mathbf{V} = -\nabla p + \nabla.\boldsymbol{\tau} + \mu_0(\mathbf{M}.\nabla)\mathbf{H}. \tag{1.10}$$

When two dipoles are taken in account the momentum equation takes the form [92]

$$\rho(\mathbf{V}.\nabla)\mathbf{V} = -\frac{I_0\mu_0 K}{\pi}(T_\theta - T) + \nabla.\boldsymbol{\tau}. \tag{1.11}$$

1.2.3 Law of conservation of energy

Energy equation take the form

$$\rho\left[\frac{\partial h_{enthalpy}}{\partial t}+\nabla.\left(h_{enthalpy}\mathbf{V}\right)\right]=-\frac{Dp}{Dt}+\nabla.\left(k\nabla T\right)+\Psi_1, \tag{1.12}$$

where, $h_{enthalpy}$ represent the enthalpy which is associated to internal energy as $h_{enthalpy}=e+\frac{p}{\rho}$. T is absolute temperature and Ψ_1 is dissipation function indicating the work done against viscous force, which is irrevocably transform into internal energy. Pressure term on RHS of Eq. (1.12) is normally omitted. To get this energy equation it is assumed that the conduction heat transport is regulate by using Fourier's law and thermal conductivity of the fluid. Conservation of energy specified in Eq. (1.12) can be streamline by taking the fact that density is constant for incompressible flows. Also using the definition of enthalpy along with $dh_{enthalpy}=C_p dT$ and $de=C_v dT$ relation, Eq. (1.12) takes the following form

$$\rho C_p\left[\frac{\partial \mathrm{T}}{\partial t}+\left(\mathbf{V}.\nabla\right)\mathrm{T}\right]=k\nabla^2\mathrm{T}+\Psi_1, \tag{1.13}$$

here C_p display specific heat. Also note that $C_p \approx C_v$ for incompressible flows. For single dipole energy equation are of the form [91]

$$\rho c_p\left(\mathbf{V}.\nabla\right)\mathrm{T}=-\nabla p+k\nabla^2\mathrm{T}-\mu_0\mathrm{T}\frac{\partial \mathbf{M}}{\partial \mathrm{T}}.\left(\left(\mathbf{V}.\nabla\right)\mathbf{H}\right)+\mu\,\Psi^*, \tag{1.14}$$

where $\Psi^*=\left[2\left(\frac{\partial u}{\partial x}\right)^2+2\left(\frac{\partial v}{\partial y}\right)^2+\left(\frac{\partial v}{\partial x}+\frac{\partial u}{\partial y}\right)^2\right]$.

1.3 Constitutive relation for Newtonian and non-Newtonian fluid

The stress tensor in Eq (1.8) and (1.9) are defined by nature of fluid. The fluids can be separated into Newtonian and Non-Newtonian fluid base on Newton's law of viscosity defined as a relationship in which shear stress among the adjacent layers of fluid is proportional to the negative value of the velocity gradient between the two layers.

1.3.1 Newtonian fluid

The stress tensor for Newtonian fluids are defined as

$$\boldsymbol{\tau} = -p\mathbf{I}+\boldsymbol{\kappa}, \tag{1.15}$$

where τ represent Cauchy stress tensor, $\boldsymbol{\kappa} = \mu\mathbf{R}_1$ is extra stress tensor, μ is dynamic viscosity. $\mathbf{R}_1$ is first Rivlin-Ericksen tensor

1.3.2 Jeffrey model

The necessary equations for Jeffrey model can be written as [93]. The stress tensor used throughout this thesis defined as follow

$$\boldsymbol{\kappa} = \frac{\mu}{1+\lambda_2}\left[\mathbf{R}_1 + \lambda_1\left(\frac{\partial \mathbf{R}_1}{\partial t} + \mathbf{V}.\nabla\right)\mathbf{R}_1\right], \tag{1.16}$$

where λ_1 is relaxation time and λ_2 is retardation time parameter of Jeffrey fluid.

1.3.3 Maxwell model

The extra stress tensor $\boldsymbol{\kappa}$ for Maxwell fluid satisfies the following relation [94]

$$\left(1+\lambda_1\frac{\partial}{\partial t}\right)\boldsymbol{\kappa}=\mu\mathbf{R}_1. \tag{1.17}$$

1.3.4 Viscoelastic (second grade) model

The extra stress tensor $\boldsymbol{\kappa}$ for viscoelastic fluid can be written as [95]

$$\boldsymbol{\kappa} = \mu\mathbf{R}_1 + \delta_1\mathbf{R}_2 + \delta_2\mathbf{R}_1^2, \tag{1.18}$$

where δ_1 and δ_2 are the material moduli while the kinematic tensors, $\mathbf{R}_1$ and $\mathbf{R}_2$.

1.3.5 Rivlin-Ericksen tensor

$$\begin{aligned}\mathbf{R}_1 &= grad\ \mathbf{V} + (grad\ \mathbf{V})^T \\ \mathbf{R}_2 &= \frac{\partial}{\partial t}\mathbf{R}_1 + \mathbf{R}_1(grad\ \mathbf{V}) + (grad\ \mathbf{V})^T\mathbf{R}_1.\end{aligned} \tag{1.19}$$

1.4 Mechanism of heat transfer

The transfer of energy as heat from a region of high temperature to low region temperature is called heat transfer, which occurs as a temperature difference across the boundary of the system. This temperature difference is thought of a driving force that causes heat to flow. There are three different modes of heat transfer: conduction, radiation and convection. [96]

1.4.1 Conduction

Conduction is a mode of transmit of heat via substance without perceptible motion of the substance itself. Heat can be transfer within a solid, liquids or gas medium or between different mediums which are in physical contact with each other. The conduction may be observed as the energy transfer from more active molecules to neighbouring less active molecules of a substance. When a fast moving molecules of high temperature region strike to slow moving molecules of lower temperature region, energy is transfer between the places. The molecules having low energy absorb energy and then gain a temperature, and high energy molecules obtained lower temperature. The conduction heat transfer in liquids and gases occurs due to collision and diffusion of molecules during their random motion. However, the nature is more complex. Most liquids, except water, become poorer conductors at high temperature. For gasses, the distance between molecules is related to the pressure. However, unless at very high pressure, the molecules is gases are at large distances and, therefore, thermal conduction is almost negligible. The temperature gradient is the potential for heat conduction. If a body in any phase has a temperature gradient, that body will definitely have conduction heat transfer.

[96].

1.4.2 Radiation

Radiation is the energy produced by substance because of its temperature. The radiation energy discharged by a body is communicated in space. Radiation is an electromagnetic phenomenon according to the Maxwell theory [96] and the radiation which is propagated as a result of temperature difference is called radiation. Irrespective of the form of substance (gas, solid, or liquid), the emanation of energy is because of variation in the electron configuration of the constituents' molecules. While the transport of energy by convection or conduction needs the occurrence of material medium, radiation does not. Actually, radiation heat transfer is more effective in a vacuum. A good literature on radiative transfer can be seen in well-presented

texts by Ozisik [98], Sparrow and Cess [97], Siegel and Howell [99], and Howell [100]. Applying Rosseland approximation of radiation we have

$$q_r = -\frac{4\sigma^*}{3k^{**}}\frac{\partial T^4}{\partial y}, \tag{1.20}$$

where k^{**} and σ^* are the mean absorption coefficient and the Stefan–Boltzmann constant, respectively. We consider small temperature difference and the term T^4 exhibit as a linear function of temperature by expanding T^4 in term of Taylor series about T_∞ as below

$$T^4 = T_\infty^4 + 4T_\infty^3(T - T_\infty) + 6T_\infty^2(T - T_\infty)^2 + \ldots \tag{1.21}$$

Ignoring higher power terms in Eq. (1.21), we obtained

$$T^4 \cong 4T_\infty^3 T - T_\infty^4. \tag{1.22}$$

Then, utilizing Eq. (1.22) into Eq. (1.20), we get

$$q_r = -\frac{16T_\infty^3\sigma^*}{3k^{**}}\frac{\partial T}{\partial y}. \tag{1.23}$$

1.4.3 Convection

Convection is the transport of energy by bulk movement of the fluid motion from a region of higher temperature to a region of lower temperature. Such motion in the existence of temperature gradient enhances the heat transfer. In convection problem the examination of fluid mechanics plays a vital role. The convection heat transfer is further classified as natural convection, forced convection and mixed convection [96].

1.4.3.1. Natural convection

Natural convection phenomena is a procedure in which the motion of the fluid fallouts from heat transfer. When a fluid is heated or cooled, its density is changes and buoyance effects produce a natural circulation in the affected region, which caused the increase of warmer fluid and the decrease of colder fluid. Therefore energy transfer from hotter regions to colder regions as long as temperature difference exits in the fluid. It has many applications in industrial and engineering process such as electric absorption heaters in process vessels and steam heated coils, removal of heat from electronic components and electric conductors, heat loss from process piping. Which is suitable suggestion that natural convective boundary layer is designed

owing to divergent viscous force and thus the miracles of natural convection is considered by a non-dimensional recipe of few forces entitled as Grashof number [96].

1.4.3.2. Forced convection

In the mode of forced convection, the fluid is flow due to force past a surface by means of external source like fan or a pump. Many applications of heat transfer utilize forced convection such as heating and cooling of parts of the body through circulation of blood, radiator system in vehicles because the heat transfer rate is more faster than it is with free convection [96].

1.4.3.3. Mixed convection

The mechanisms of natural and forced and convection flows act together to transfer heat in called mixed convection or a situation where both pressure and buoyancy forces interact. This mode of heat transfer is also very significant, occurs in numerous engineering devices and in nature. The ratio of buoyancy force to inertial force and precisely stated as [96]:

$$G^* = \frac{Gr_x}{Re_x^2}, \tag{1.24}$$

where Re indicate Reynolds number and Gr is Grashof number and. When ($G^* << 1$) the inertial force is superseding in flow reign and flow trend is termed as forced convection flow on the other hand for ($G^* >> 1$) the buoyancy force is superseding in flow reign and obviously flow pattern is called natural convection flow. Normally, the mixed convection reign is happened in the central range of mixed convection

1.5. Porous medium

Porous medium means a pores comprising the void space should be interconnected [101]. The interrelated pore space is sometime called efficacious pore space. The unconnected void may be reflected as a part of solid matrix. In simple condition the pore is drenched by a single fluid where as a usual porous medium the circulation of pores based on size and shape is unbalanced such as rye bread, sandstone, limestone, beach sand, the human lung and wood. Most of the time, a porous region is labelled by its porosity and sometimes the other properties like permeability, tensile strength, and electrical conductivity are also measured as a respective aspects of its constituents and the pores [102]. The mathematical expression regarding porosity has been described by Henry Darcy and known as Darcy's law [103]. His experimental investigation on steady state uniform flow in unidirectional exposed a proportionality among

applied pressure gradient and flow rate. In modern way, mathematical communication in refined form as

$$\mathbf{V} = -\frac{K}{\mu}\nabla p. \tag{1.25}$$

After simplifying the above expression we obtained the following relation.

$$\nabla p = -\frac{\mu}{K}\mathbf{V}. \tag{1.26}$$

This is an isotropic case where permeability K is scalar [104]. Hong et al. [105] stated that Darcy model is only effective under small porosity and low velocities with the absence of inertia effect. Therefore it is essential for physical flows to revise the Darcy model to associate non-Darcian impact on the porous medium examination. Further, Forchheimer included an additional term to Eq. (1.25) has converting to new model.

$$\nabla p = -\frac{\mu}{K}\mathbf{V} - \frac{c_F}{\sqrt{K}}\rho|\mathbf{V}|\mathbf{V}, \tag{1.27}$$

where c_F is a non-dimensional form-drag constant. Forchheimer reported that with high permeability Darcy's law was not useable. Darcy's law also not applicable for no-slip case between the porous medium and solid wall [107]. For low Reynolds number the Darcian model is also valid, while for higher Reynolds numbers non-Darcian models has to be considered. Numerous non-Darcy models have been suggested to involve inertia impact. Poulikakos and Bejan [108] and Prasad and Tuntomo [109] employed extended Darcy-Forchheimer equation to scrutinise the flow past a porous medium under inertia impact. Brinkman [110, 111] revised Darcy's law for boundary frictional influence and to integrate a shear stress and no-slip boundary equation at the surface by including a Brinkman term into Equ. (1.25). The transformed equation is of the form

$$\nabla p = -\frac{\mu}{K}\mathbf{V} + \tilde{\mu}\nabla^2\mathbf{V}, \tag{1.28}$$

where $\tilde{\mu}$ is the effective viscosity. Brinkman presumed $\tilde{\mu}$ equal to the fluid viscosity μ.

1.6 Suction and injection

Suction or injection of a fluid through the bounding surface can remarkably variate the flow field. In general, suction tends to magnification the skin friction, although injection behave is reverse manner [112]. The progression of suction/blowing has of great importance in several engineering events like in the design of thermal oil recovery, radial diffusers and thrust bearing [113]. Suction is utilized to chemical processes to eliminate reactants [114]. However, suction or injection of a stretching surface for constant velocity and temperature field was presented by Erickson et al. [115] and Fox et al. [116]. Further Chen and Char [117] examined suction or injection for linearly stretched surface with uniform heat flux and wall temperature, these authors also focused on impermeable case with variable surface heat flux. Mathematically conditions of suction/injection for a flat surface at y=0, can be written as

$$S = -\frac{v_w}{\sqrt{cv}}, \tag{1.29}$$

where S represent the non-dimensional constant which determine the flow rate. $S < 0$ signify injection (blowing) velocity of fluid, $S > 0$ signify suction velocity of fluid and $S = 0$ describes impermeable surface.

1.7 Heat source/sink (generation/absorption)

The investigation of heat source or sink impact on energy transport is most imperative due to its crucial effects in controlling the heat transmit. Abo-Eladahab and El Aziz [118] analyzed the influence of variable heat source under suction or blowing, which is restricted to viscous fluids only

$$Q = \frac{Q_\circ}{\rho c_p}, \tag{1.30}$$

where Q represent heat source $Q > 0$ and sink corresponding to $Q < 0$.

1.8 Soret and Dufour effects

The phenomena in which heat transmit induced through gradient of concentration is named the diffusion-thermo or Dufour effect while mass transfer owing to temperature gradient is termed thermal-diffusion or Soret effects [119]. When both temperature gradient and concentration are high, then influence of these parameter are very prominent. Some studies associated to energy

and mass transport, impact of Soret and Dufour are neglected because of a lower order of magnitude as compared to the influence defined by Fourier's and Fick's laws. Eckert and Drake [120] investigated that there are several cases where Soret and Dufour effects are very prominent for the fluids in the fields such as nuclear waste, geothermal energy, hydrology, isotope separation and in the combination of dissimilar gases Hydrogen or Helium due to their light molecular weight. Mathematically dimensionless form of Soret and Dufour are

$$S_r = \frac{D^* k_T \left(T_c - T_w\right)}{T_m \nu \left(C_\infty - C_w\right)}, D_f = \frac{D^* k_T \left(C_\infty - C_w\right)}{c_p c_s \nu \left(T_c - T_w\right)}, \tag{1.31}$$

here, k_T is thermal diffusion ratio, D^* is mass diffusivity, c_s is concentration susceptibility, T_m is mean fluid temperature and c_p specific heat of fluid,.

1.9 Stagnation point flow in a plane

In fluid mechanics, a point on the flow region where velocity is zero is called stagnation point. The flow in neighbouring of a stagnation point is named stagnation point flow. In fluid dynamics, two dimensional flow problem nearby a stagnation point is one of the most widely studied. Hiemenz [121] was the first one to introduce the stagnation flow in a plane around a stagnation point which is also called the Hiemenz flow. For the potential flow the component of velocity around the stagnation point at $x = y = 0$ are stated as

$$u = a_1 x, \; v = -a_1 y, \tag{1.32}$$

here a_1 is a constant. The flow move toward the y-axis and impinges on solid surface ($y = 0$). The flow accelerates toward the x-axis. Boundary layer grows toward the x-axis due to no-slip condition. For viscous flow, the presumed components of velocity are

$$u = xf'(y), \; v = -f(y), \tag{1.33}$$

which fulfil the equation of continuity. For the pressure distribution, the following Bernoulli's equation can be used for potential flow

$$p_\infty - p = \frac{1}{2}\rho a_1^2 \left(x^2 + y^2\right). \tag{1.34}$$

p_∞ signifies the pressure, for viscous flow, it is supposed that

$$p_\infty - p = \frac{1}{2}\rho a_1^2\left(x^2 + F(y)\right). \tag{1.35}$$

1.10 Governing equations for ferromagnetic flow

The equation described the flow of ferromagnetic particles in fluid are explained hare.

1.10.1 Magnetic force on ferrofluid

In the presence of an applied magnetic field, the suspension of ferromagnetic colloidal particles in carrier fluid, which make fluid magnetized and produce magnetic forces on each particle due to polarization that produce a body force in fluid [122]. The magnetic (Kelvin) force **F** on ferrofluid per unit volume is given by

$$\mathbf{F}=\mu_0(\mathbf{M}.\nabla)\mathbf{H}, \tag{1.36}$$

where μ_0 is magnetic permeability, **H** is strength of external magnetic field, **M** is magnetization.

1.10.2 Magnetic field intensity (H)

Magnetic field intensity at a point is the number of magnetic lines of force crossing per unit area around that point, the area being held perpendicular to the direction of lines of force. In SI system, the unit of magnetic intensity is Ampere/meter.

1.10.3 Magnetic induction (B)

When a magnetic material is located in a uniform magnetizing field **(H)** it acquires magnetism and develops its individual magnetic field because of induction. As a consequence of this induction, the original magnetic field is rehabilitated both outside as well as inside the magnetic material. This modified or resultant field is called magnetic induction and is measured as the number of lines of induction passing normally through unit area of the material and is denoted by **B**. It is expressed in Tesla in SI units. Thus total number of magnetic lines crossing per unit area normally through a magnetic substance is called magnetic induction.

1.10.4 Intensity of magnetization (M)

It is a measure of the extent to which a substance gets magnetized. Intensity of magnetization **M** of a magnetic substance is showed as its magnetic moment per unit volume, the specimen being so small that its magnetization can be supposed to be uniform. In SI system, the unit of intensity of magnetization is Weber/metre^2.

1.10.5 Magnetic susceptibility (χ)

It measures the ease with which a specimen takes magnetism. Magnetic susceptibility of a magnetic substance is defined as the ratio of the intensity of magnetization **M** induced in the substance to the strength of magnetizing field **H** in which the substance is situated. Mathematically, it can be expressed as

$$\mathbf{M}=\chi\mathbf{H}\,. \tag{1.37}$$

Based on this the magnetic response of materials may be categorised into the following five groups

Magnetism	Magnetic susceptibility χ		Illustrations
	Sign	Magnitude	
Diamagnetism	-	Low, Constant	Superconducting materials, Metals like Bi, Organic materials,
Paramagnetism	+	Constant , Low	Alkali and transition metals, Rare earth elements
Ferromagnetism	+	Function of **H** Large,	Transition metals (Ni, Fe, Co), Rare earth elements (Gd)
Antiferromagnetism	+	constant , Low	Salts of transition elements (MnO)
Ferrimagnetism	+	High, Function of **H**	Ferrites ($MnFe_3O_4$, $ZnFeO_4$) and Chromites

1.11 Single dipole field

The characteristic of magnetic field influenced the ferrofluid flow due to dipole field. The scalar potential of magnetic dipole is [91]

$$\Phi = \frac{\gamma}{2\pi}\left(\frac{x}{x^2+\left(y+a^*\right)^2}\right), \tag{1.38}$$

when the magnetic is place at $(0, -a^*)$. The components of magnetic field H are

$$H_x = -\frac{\partial\Phi}{\partial x} = \frac{\gamma}{2\pi}\left\{\left(\frac{x^2-\left(y+a^*\right)^2}{\left(x^2+\left(y+a^*\right)^2\right)^2}\right)\right\}, \tag{1.39}$$

$$H_y = -\frac{\partial\Phi}{\partial y} = \frac{\gamma}{2\pi}\left\{\left(\frac{2x\left(y+a^*\right)}{\left(x^2+\left(y+a^*\right)^2\right)^2}\right)\right\}. \tag{1.40}$$

In Eqs (1.39) and (1.40), H_x and H_x are components toward coordinate axes. The magnetic force and gradient of H are proportionate with each other, so we find the expression

$$H = \left[\left(\frac{\partial\Phi}{\partial x}\right)^2+\left(\frac{\partial\Phi}{\partial y}\right)^2\right]^{\frac{1}{2}}. \tag{1.41}$$

The elements of ∇H in term of scalar potential are

$$\frac{\partial H}{\partial x} = \frac{\frac{\partial\Phi}{\partial x}\frac{\partial^2\Phi}{\partial x^2}+\frac{\partial\Phi}{\partial y}\frac{\partial^2\Phi}{\partial x\partial y}}{\left[\left(\frac{\partial\Phi}{\partial x}\right)^2+\left(\frac{\partial\Phi}{\partial y}\right)^2\right]^{\frac{1}{2}}}. \tag{1.42}$$

$$\frac{\partial H}{\partial y} = \frac{\frac{\partial\Phi}{\partial x}\frac{\partial^2\Phi}{\partial x\partial y}+\frac{\partial\Phi}{\partial y}\frac{\partial^2\Phi}{\partial y^2}}{\left[\left(\frac{\partial\Phi}{\partial x}\right)^2+\left(\frac{\partial\Phi}{\partial y}\right)^2\right]^{\frac{1}{2}}}. \tag{1.43}$$

For single dipole

$$\frac{\partial H}{\partial x} = -\frac{\gamma}{2\pi}\left(\frac{2x}{\left(y+a^*\right)^4}\right) \tag{1.44}$$

and

$$\frac{\partial H}{\partial y} = \frac{\gamma}{2\pi}\left(\frac{-2}{\left(y+a^*\right)^3} + \frac{4x^2}{\left(y+a^*\right)^5}\right). \tag{1.45}$$

1.12 Double dipole field

Magnetic scaler potential Φ at any point (x, y) under the influence of dipole are taken as [92]

$$\Phi = -\frac{\gamma}{2\pi}\left[Tan^{-1}\left(\frac{y+d}{x}\right) + Tan^{-1}\left(\frac{y+d}{x}\right)\right], \tag{1.46}$$

where γ is strength of magnetic field and the corresponding components along the coordinate axes are.

$$H_x = -\frac{\partial \Phi}{\partial x} = -\frac{\gamma}{2\pi}\left[\frac{y+d}{x^2+(y+d)^2} + \frac{y-d}{x^2+(y-d)^2}\right], \tag{1.47}$$

$$H_x = -\frac{\partial \Phi}{\partial x} = -\frac{\gamma}{2\pi}\left[\frac{x}{x^2+(y-d)^2} + \frac{x}{x^2+(y+d)^2}\right]. \tag{1.48}$$

The magnitude H of the force field is specified from Eq. (1.41). Utilizing equation (1.46) in Eqs. (1.42) and (1.43) and expanding order up to x^2, we get

$$\frac{\partial H}{\partial y} = 0, \tag{1.49}$$

since at the surface of wall $\left(\frac{\partial \Phi}{\partial x}\right)_{y=0} = \left(\frac{\partial^2 \Phi}{\partial y^2}\right)_{y=0} = 0$ adjacent to the boundary regions and distance from leading edge is huge as collated with the line dipole from the flat plate that is $x \gg d$ so

$$\frac{\partial H}{\partial x} = -\frac{\gamma}{\pi}\frac{1}{x^2}. \tag{1.50}$$

The dissimilarity of M in term of temperature T [91] is taken as.

$$M = K^*\left(T_0 - T\right), \tag{1.51}$$

here K^* demonstrate pyromagnetic co-efficient, T_g is Curie temperature, although, the following are the important key fact for the existence of ferromagnetic fluid: (a) the external magnetic field is nonhomogeneous and (b) fluid at temperature T differ from T_g. Once the ferromagnetic fluid tend to Curie temperature, where no further magnetization exist. Actually physical characteristics are very important due to very high Curie temperature, which is 1,043 Kelvin for iron.

1.13 Slow oscillating magnetic field

The comprehensive form of equations also contains the Maxwell's equations are

$$\nabla.\left(\boldsymbol{H}+4\pi\boldsymbol{M}\right)=0,\quad \nabla\times\boldsymbol{H}=\boldsymbol{0}. \tag{1.52}$$

and

$$\boldsymbol{M}=\boldsymbol{M}_S\left(\coth\lambda-\frac{1}{\lambda}\right). \tag{1.53}$$

In above, $\boldsymbol{M}$ is fluid magnetization, $\boldsymbol{M}_S=\boldsymbol{M}_0\Gamma$ is the saturation magnetization in fluid, which is represent the produce of instantaneous magnetization $\boldsymbol{M}_0$ and volume concentration Γ of the magnetic component [123, 124]. At $\tau_B=0$, the instantaneous stability magnetization $\boldsymbol{M}_0$ is takes as

$$L(\lambda)=\operatorname{Coth}\lambda-\lambda^{-1},\quad \boldsymbol{M}_0=nmL(\lambda)\frac{\boldsymbol{H}}{H},\quad \lambda=\frac{mH}{\sigma^*T}, \tag{1.54}$$

where σ^* is Boltzmann constant, λ is Langevin parameter, $L(\lambda)$ is Langevin function, n and m denote the number of particle and the magnetic moment.

1.14 Geometries of problems

In this thesis following geometries are used.

1.14.1 Geometry 1

Consider an incompressible, two dimensional electrically non-conducting ferromagnetic fluid induced by stretched horizontal sheet having velocity $u_w(x)=cx$, where c is stretching rate, which is directly dependent to the distance from the origin. A permanent dipole is situated at distance a^* from surface with its center exactly located on y axis as display schematically in

fig. 1.6. The direction of magnetic field is pointed in positive x-direction gives rise to magnetic field of appropriate strength to drench ferromagnetic liquid. It is assume that Curie temperature T_c is higher than the temperature at surface T_w, on the other hand, fluid elements away from the surface is at temperature $T_\infty = T_c$.

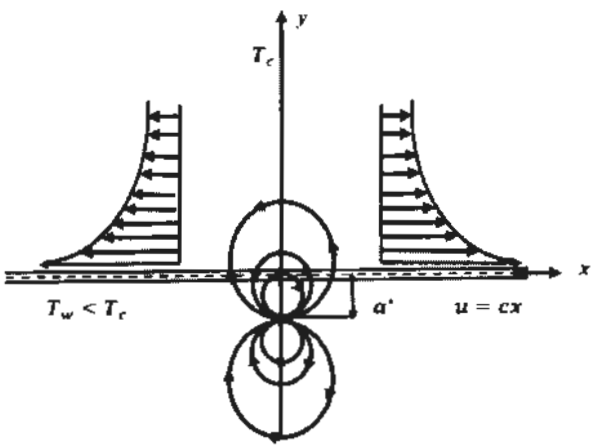

Fig. 1.6. Geometry of the problem, circles indicate magnetic dipole.

1.14.2 Geometry 2

Consider a flat surface with two equally line dipole. Which are equidistant d from the wall and perpendicular to the plane as seen in fig. 1.7.

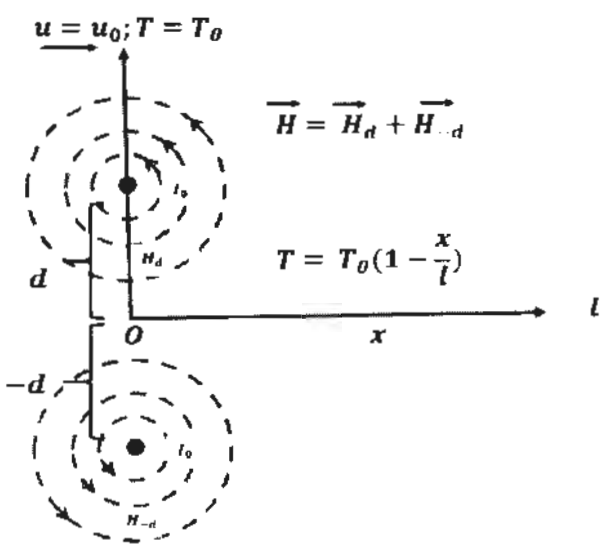

Fig. 1.7. Geometry of the flow model.

1.14.3 Geometry 3

Considering a disk rotating steadily with angular velocity speed $v(r,\theta,z)=\Omega_v r/1-a_3 t$ about z-axis fluctuating with time as shown in fig. 1.8.

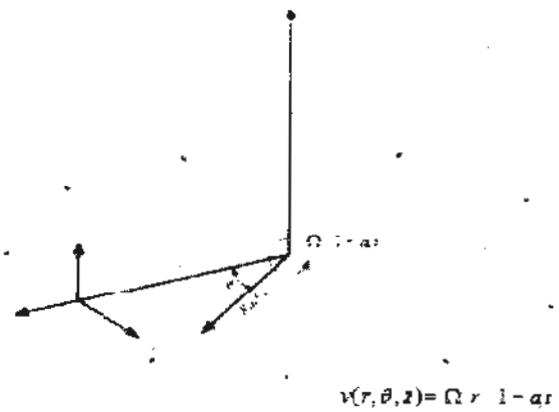

Fig. 1.8. Geometry of the model.

1.15 Boundary conditions

The following type of boundary conditions, we have taken.

1.15.1 Boundary condition on velocity

The boundary conditions on velocity profile rely on the nature of the liquid flow and geometry of the boundary wall. If the boundary sheet is stretched with velocity linearly proportional to x coordinate that is distance from a slit, the boundary equations are

$$u = cx, \quad v = 0, \quad \text{at} \quad y = 0, \tag{1.55}$$

$$u \to 0, \quad y \to \infty. \tag{1.56}$$

Her the boundary sheet is considered to be impermeable. For the permeable stretching surface the boundary equations are assumed in the form

$$\begin{aligned} &u = cx, \quad v = -v_w \quad \text{at} \quad y = 0, \\ &u \to 0, \quad y \to \infty. \end{aligned} \tag{1.57}$$

The condition $v = -v_w$ at $y = 0$, represent the suction/injection in the boundary layer region. The above boundary condition arise as a result of no-slip when we take partial slip into account the velocity condition at $y = 0$ is taken in the following form

$$u = cx + A\frac{\partial u}{\partial y}, \text{ at } y = 0, \tag{1.58}$$

with A representing the velocity slip factor.

1.15.2 Boundary condition on temperature

Boundary conditions on temperature field depend on thermal process. Now we deliberate two types of thermal process

1. Prescribed surface temperature (PST)
2. Prescribes wall heat flux (PHF)

Mathematical forms of such boundary conditions are:

PST Case

$$\begin{aligned} &T = T_w = T_c - D\left(\frac{x}{l}\right)^2 \quad \text{at} \quad y = 0, \\ &T \to T_c, \quad y \to \infty. \end{aligned} \tag{1.59}$$

PHF Case

$$\begin{aligned} &-k\frac{\partial T}{\partial y} = q_w = D\left(\frac{x}{l}\right)^2 \quad \text{at} \quad y = 0, \\ &T \to T_c, \quad y \to \infty. \end{aligned} \tag{1.60}$$

1.16 Similarity transformation

One-parameter (ε) Lie group of infinitesimal transformations in (x, y, t,ψ, P) are [125]

$$\begin{aligned} x^* &= x + \varepsilon\phi_1(x,y,t,\psi_1,P) + O(\varepsilon^2), \\ y^* &= y + \varepsilon\zeta_1(x,y,t,\psi_1,P) + O(\varepsilon^2), \\ t^* &= t + \varepsilon F_1(x,y,t,\psi_1,P) + O(\varepsilon^2), \\ \psi_1^* &= \psi_1 + \varepsilon\eta_1(x,y,t,\psi_1,P) + O(\varepsilon^2), \\ P^* &= P + \varepsilon g_1(x,y,t,\psi_1,P) + O(\varepsilon^2), \end{aligned}$$

where ε is a small parameter ϕ_1, ζ_1, F_1, η_1, g_1 are infinitesimal elements of the group. The Lie symmetry in the set of vector form.

$$X = \phi_1 \frac{\partial}{\partial x} + \zeta_1 \frac{\partial}{\partial y} + F_1 \frac{\partial}{\partial t} + \eta_1 \frac{\partial}{\partial \psi_1} + g_1 \frac{\partial}{\partial P}.$$

Here we considered the non-dimensional variables anticipated by [91]

$$\Psi(\xi,\eta) = \left(\frac{\mu}{\rho}\right)\xi.f(\eta), \tag{1.61}$$

$$P(\xi,\eta) = \frac{P}{c\mu} = -P_1(\eta) - \xi^2 P_2(\eta), \tag{1.62}$$

$$\theta(\xi,\eta) = \frac{T_c - T}{T_c - T_w} = \theta_1(\eta) + \xi^2\theta_2(\eta), \tag{1.63}$$

where dimensionless coordinates ξ and η are defined as

$$\xi = \sqrt{\frac{c\rho}{\mu}}x, \quad \eta = \sqrt{\frac{c\rho}{\mu}}y \tag{1.64}$$

$\theta(\xi,\eta)$ exhibit dimensionless temperature, $\Psi(\xi,\eta)$ is stream function. The comparable velocity constraints u and v are stated as

$$u = \frac{\partial\Psi}{\partial y} = cx.f'(\eta), \quad v = -\frac{\partial\Psi}{\partial x} = -\sqrt{c\nu}f\ (\eta). \tag{1.65}$$

1.17 Numerical tools

It is very difficult to solve highly non-linear coupled differential equation analytically and only few methods are exist to solve it. Additionally, there are several problems which have no analytical solutions. For this here we select numerical method to solve the stretching sheet problem.

1.17.1 Shooting method

Shooting method is one of the popular iterative scheme for solving boundary value problems (BVP's). In this technique, higher order BVP, first converted in to the system of 1st order initial value problem (IVP) by considering the missing initial guess. Our purpose is to obtain the result of IVP directly in place of the given boundary value problem. Now, consider a boundary value problem of second order

$$\frac{d^2y}{dx^2} = f\left(x, y, \frac{dy}{dx}\right) \tag{1.66}$$

along with boundary conditions

$$y(0)=0,\ y(W)=B, \tag{1.67}$$

here f demonstrated arbitrary function and information is given at x=0 and x= W. The above differential equation designates an IVP, if the set of information is described as

$$y(0)=0,\ y'(0)=s. \tag{1.68}$$

For the solution of BVP, reduce the system of equation in two 1st order as

$$\frac{du}{dx}=f(x,y,u),\ \frac{dy}{dx}=u, \tag{1.69}$$

corresponding I.C's

$$y(0)=0,\ u(0)=y'(0)=s, \tag{1.70}$$

here 's' represent missing initial conditions allocated for a starting initial value. Next, we will get the original value of 's', in such a way the solution of Eq. (1.66), with initial conditions (1.68) fulfil the required conditions in Eq. (1.67). Further, if the resulting solution of IVPs are represent by $u(x,s)$ and $y(x,s)$, we are looking for the value of 's' that is

$$y(W,s)-B=0=\phi(s). \tag{1.71}$$

Here Newton's iterative scheme is applied to obtain the value of 's' because we take a solution of the algebraic Eq. (1.69) which is given as

$$s^{(n+1)}=s(n)-\frac{\phi\left(s^{(n)}\right)}{d\phi\left(s^{(n)}\right)/ds}, \tag{1.72}$$

which becomes

$$s^{(n+1)}=s(n)-\frac{y\left(L,\ s^{(n)}\right)-B}{dy\left(L,\ s^{(n)}\right)/ds}. \tag{1.73}$$

Differentiated Eqs. (1.69) and (1.70) w.r.t to 's' we obtained

$$\frac{dY}{dx}=U,\quad \frac{dU}{dx}=\frac{\partial f}{\partial y}Y+\frac{\partial f}{\partial u}U, \tag{1.74}$$

here $U=\partial u/\partial s,\ Y=\partial y/\partial s,$ and corresponding initial conditions are

$$Y(0)=0,\quad U(0)=1. \tag{1.75}$$

1.17.2 Runge-Kutta method

The formula for the forth order Runge-Kutta technique to solve the single IVP.

$$\frac{dy}{dx}=f(x,y);\quad f(x_0)=y_0 \tag{1.76}$$

is defined as

$$y_{j+1}=y_j+h\frac{1}{6}\left(k_1+2k_2+2k_3+k_4\right), \tag{1.77}$$

where

$$k_1=f\left(x_j,y_j\right), \tag{1.78}$$

$$k_2=f\left(x_j+\frac{h}{2},y_j+\frac{k_1}{2}\right), \tag{1.79}$$

$$k_3=f\left(x_j+\frac{h}{2},y_j+\frac{k_2}{2}\right), \tag{1.80}$$

$$k_4=f\left(x_j+h,y_j+k_3\right), \tag{1.81}$$

here h is step size.

Likewise, the classical forth order R-K method for the system of equations

$$\frac{dY}{dX}=f(x,y_1,y_2,\ldots y_n);\quad Y(X_0)=Y_0 \tag{1.82}$$

may be written as

$$Y_{j+1}=Y_j+h\frac{1}{6}\left(K_1+2K_2+2K_3+K_4\right), \tag{1.83}$$

where

$$\mathbf{K}_1 = \begin{pmatrix} k_{11} \\ k_{21} \\ \vdots \\ k_{n1} \end{pmatrix}, \quad \mathbf{K}_2 = \begin{pmatrix} k_{12} \\ k_{22} \\ \vdots \\ k_{n2} \end{pmatrix}, \quad \mathbf{K}_3 = \begin{pmatrix} k_{13} \\ k_{23} \\ \vdots \\ k_{n3} \end{pmatrix}, \quad \mathbf{K}_4 = \begin{pmatrix} k_{14} \\ k_{24} \\ \vdots \\ k_{n4} \end{pmatrix} \tag{1.84}$$

and

$$k_{i1} = f_i\left(x_j,\ y_{1j},\ y_{2j},\ldots,\ y_{nj}\right), \tag{1.85}$$

$$k_{i2} = f_i\left(x_j + \frac{h}{2},\ y_{1j} + \frac{k_{11}}{2},\ y_{2j} + \frac{k_{21}}{2},\ldots,\ y_{nj} + \frac{k_{n1}}{2}\right), \tag{1.86}$$

$$k_{i3} = f_i\left(x_j + \frac{h}{2},\ y_{1j} + \frac{k_{12}}{2},\ y_{2j} + \frac{k_{22}}{2},\ldots,\ y_{nj} + \frac{k_{n2}}{2}\right), \tag{1.87}$$

$$k_{i4} = f_i\left(x_j + h,\ y_{1j} + k_{13},\ y_{2j} + k_{23},\ldots,\ y_{nj} + k_{n3}\right), \tag{1.88}$$

$i = 1(1)\ n.$

Chapter 2

Effect of magnetic dipole on viscous ferro-fluid past a stretching surface with thermal radiation

2.1 Introduction

In this chapter, the impact of magnetic dipole on boundary layer flow of ferromagnetic liquid with thermal radiation has been inspected. Flow is caused by linear stretching of surface. The suitable mixture of non-magnetic viscous base fluid, surfactant and magnetic solid constitutes a magnetic fluid. The boundary layer partial differential equations with the interaction of ferromagnetic fluid are reduced into system of nonlinear ordinary differential equations by implementing similarity procedure. Then resulting set of equations are solved numerically. The influence physical converging flow parameters on dimensionless quantities such as velocity profile, temperature profile, pressure profile, skin friction and Nusselt number are deliberated via graphs.

2.2 Flow assumption and mathematical formulation

Consider a two-dimensional, incompressible viscous flow of ferromagnetic particles electrically non-conducting base fluid over a stretching surface as defined in the geometry of the problem in section 1.15. The flow is assumed to be in the domain $y > 0$. The radiative heat transfer magnetization effect in heat equation is taken in account. By applying boundary layer approximation the governing flow equations in component forms, using Eqs. (1.1), (1.10) and (1.14), we have

$$\frac{\partial u}{\partial x}+\frac{\partial v}{\partial y}=0, \tag{2.1}$$

$$\rho\left(u\frac{\partial u}{\partial x}+v\frac{\partial u}{\partial y}\right)=-\frac{\partial p}{\partial x}+\mu_0 M\frac{\partial H}{\partial x}+\mu\left(\frac{\partial^2 u}{\partial x^2}+\frac{\partial^2 u}{\partial y^2}\right), \tag{2.2}$$

$$\rho\left(u\frac{\partial v}{\partial x}+v\frac{\partial v}{\partial y}\right)=-\frac{\partial p}{\partial y}+\mu_0 M\frac{\partial H}{\partial y}+\mu\left(\frac{\partial^2 v}{\partial x^2}+\frac{\partial^2 v}{\partial y^2}\right), \tag{2.3}$$

$$\rho c_p\left(u\frac{\partial T}{\partial x}+v\frac{\partial T}{\partial y}\right)+\mu_0 T\frac{\partial M}{\partial T}\left(u\frac{\partial H}{\partial x}+v\frac{\partial H}{\partial y}\right)=k\frac{\partial^2 T}{\partial y^2}-\frac{\partial q_r}{\partial y}. \tag{2.4}$$

The radiation flux vector q_r and are explained in Eqs. (1.20) to (1.23), hence.

$$\frac{\partial q_r}{\partial y} = -\frac{16T_\infty^3\sigma^*}{3k^{**}}\frac{\partial^2 T}{\partial y^2}. \tag{2.5}$$

Assuming the stretching boundary conditions

$$\left.\begin{aligned} &u = cx, \quad v = 0, \quad y = 0 \\ &u = 0, \quad p + \frac{1}{2}\rho\left(u^2 + v^2\right) = \text{constant} \quad y \to \infty \end{aligned}\right\}, \tag{2.6}$$

along with PST condition for temperature profile from Eq. (1.59). Using similarity transformation from Eqs. (1.64) and (1.65) to the Eqs. (2.1) to (2.4) and comparing the quantities up to ξ^1, we get equations take the form

$$f''' + ff'' + 2P_2 - \frac{2\beta\theta_1}{(\eta+\alpha_1)^4} = 0, \tag{2.7}$$

$$P_1' - f'' - ff' - \frac{2\beta\theta_1}{(\eta+\alpha_1)^3} = 0, \tag{2.8}$$

$$P_2' - \frac{2\beta\theta_2}{(\eta+\alpha_1)^3} + \frac{4\beta\theta_1}{(\eta+\alpha_1)^5} = 0, \tag{2.9}$$

$$(1+N)\theta_1'' + \Pr(f\theta_1' - 2f'\theta_1) + \frac{2f(\theta_1-\varepsilon)\lambda\beta}{(\eta+\alpha_1)^3} + 2\theta_2 = 0, \tag{2.10}$$

$$(1+N)\theta_2'' - \Pr\left(4f'\theta_2 - f\theta_2'\right) + \frac{2\theta_2 f\lambda\beta}{(\eta+\alpha)^3} - \lambda\beta(\theta_1-\varepsilon)\left[\frac{2f'}{(\eta+\alpha_1)^4} + \frac{4f}{(\eta+\alpha_1)^5}\right] = 0 \tag{2.11}$$

and the boundary equation (2.6) becomes

$$\left.\begin{aligned} &f = 0, \ f' = 1, \ \theta_1 = 1, \ \theta_2 = 0, \quad at \ \eta = 0, \\ &f' \to 0, \ \theta_1 \to 0, \ \theta_2 \to 0, \ P_1 \to -P_\infty, \ P_2 \to 0 \quad as \ \eta \to \infty. \end{aligned}\right\}. \tag{2.12}$$

The dimensionless flow parameters are defined below

$$\left.\begin{aligned} &\Pr = \frac{\mu c_p}{k}, \quad \lambda = \frac{c\mu^2}{\rho k\left(T_c - T_w\right)}, \quad \varepsilon = \frac{T_c}{T_c - T_w} \\ &\beta = \frac{\gamma\rho}{2\pi\mu^2}\mu_0 K\left(T_c - T_w\right), \quad N = \frac{16\sigma^* T_\infty^3}{3kk^{**}}, \quad \alpha_1 = \sqrt{\frac{c\rho}{\mu}}a^* \end{aligned}\right\}, \tag{2.13}$$

where Pr is Prandtl number, λ is viscous dissipation parameter, ε is Curie temperature, α_1 is dimensionless distance and β is the ferromagnetic interaction parameter. The physical quantities in the vicinity of surface, *i.e.*, skin friction coefficient and Nusselt number are stated

as

$$C_{fx} = \frac{-2\tau_w}{\rho(cx)^2}, \qquad Nu_x = \frac{xq_w}{-k(T_c - T_w)}, \tag{2.14}$$

here

$$\tau_w = \mu\left(\frac{\partial u}{\partial y}\right)_{y=0}, q_w = -k\left(\frac{\partial T}{\partial y}\right)_{y=0}. \tag{2.15}$$

In non-dimensional form

$$\mathrm{Re}_x^{1/2} C_f = -2f''(0), \ \mathrm{Re}_x^{-1/2} Nu_x = -\left[\theta_1'(0) + \xi^2\theta_2'(0)\right], \tag{2.16}$$

where $f''(0)$ and $\theta_1'(0)$ are skin friction and heat transfer rate, Re_x represent Reynolds number. Flow region is influenced by ferro-magnetic parameter β. Whereas in case of MHD $(\beta = 0)$, $P_2(0)$ becomes a constant, and flow problem is separated from the thermal energy problem. So, it is more suitable to swap the quantity $-\theta_1' = -\left[\theta_1'(0) + \xi^2\theta_2'(0)\right]$ by ratio $\theta^*(0) = \dfrac{\theta_1'(0)}{\theta_1'(0)|\beta = 0}$ called the dimensionless form of Nusselt number at surface. Also, the quantity $P_2(0)$ is called wall pressure parameter.

2.3. Results and discussion

For the present problem, the numeric values of parameters $\lambda = 0.01$, $\alpha_1 = 1.0$, $\varepsilon = 2.0$ is fixed. To check the legitimacy of the current method, the numeric fallouts of Nusselt number is drawn in table 2.1 for limiting case, which are associated with those existing in open literature Chen [126] and Ishak et al. [127] and found as excellent agreement. Figs. 2.1 to 2.4 are sketched for numerous flow parameters on temperature field. Fig. 2.1 portrays the effect of Prandtl number *Pr* on temperature profile, results shows that temperature decreases by increasing *Pr* in boundary region, for higher values of *Pr* results in diminishes thermal boundary layers. Fig. 2.2 describes the impact of ferromagnetic interaction β on temperature profiles. It is noted that fluid temperature is boost up with an increase in β. This is because to fact that the communication between the ferromagnetic particles and the motion of the fluid. This collaboration increases the frictional heating between the fluid layers or resistance among the fluid particles enhances, so extra energy is produced, consequently increase in temperature and

associated boundary layer thickness. Fig. 2.3 exhibits to perceive the response of radiation parameter N on temperature distribution. It is pointed out that temperature grows up by increasing radiation parameter. Physically, impact of radiation parameter is to improve the thermal diffusivity of the medium.

The consequence of the applied magnetic field due to dipole demonstrates through a ferrohydrodynamic (ferromagnetic) parameter β. The existence of magnetic effects play as retarding force on fluid velocity and thereby as increases, so produce retarding force and hereafter the results in suppressing the velocity profile. Because this occurs owing to the influence of opposing force which confront the fluid flow and produce more resistance to the transport phenomena. Also noted that in fig 2.4 the velocity profile is smaller as compared with hydrodynamic case $(\beta = 0)$. Fig. 2.5 highlights the coefficient of skin friction under the influence of Prandtl number Pr versus β. By scrutinizing the graph it discloses that shear stress $-f''(0)$ accelerate for higher values of Pr as well as β and reduces approximately linearly by increasing thermal radiation parameter N as displayed in fig. 2.6. Fig. 2.7 demonstrates the effect of Pr on local Nusselt number against β. It is observed that that Nusselt number enhances by increasing the value of Pr and opposite trend is noted in the case of for radiation parameter N as shown in Fig. 2.8. Figs. 2.9 to 2.10 are plotted for pressure against β for several values of Pr and N, it can be analyzed that pressure is decline for higher value of Pr and increasing effect is noted for thermal radiation parameter N. Fig. 2.11 is plotted to see the nature of heat transfer rate against thermal radiation parameter N for numerous value of Pr. It is clear that there is improvement in energy transfer rate for higher values of Pr.

Table 2.1 Comparison of Nusselt number $-\theta_1'(0)$ when $\beta = 0,\ N = 0$.

Pr	Chen [126]	Ishak et al. [127]	Present results
0.72	1.0885	--------	1.08862
1	1.3333	1.3333	1.33333
3	2.5097	2.5097	2.50972
10	4.7968	4.7969	4.79682

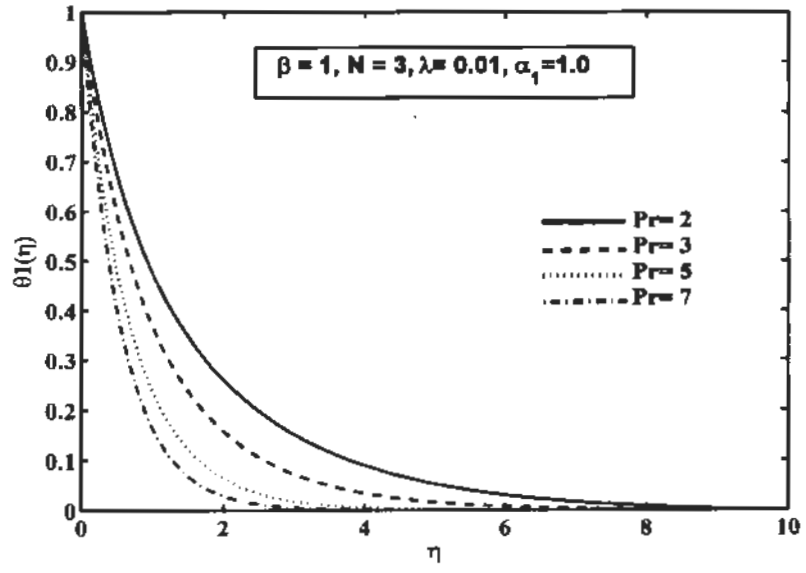

Fig. 2.1. Impact of *Pr* on temperature profile.

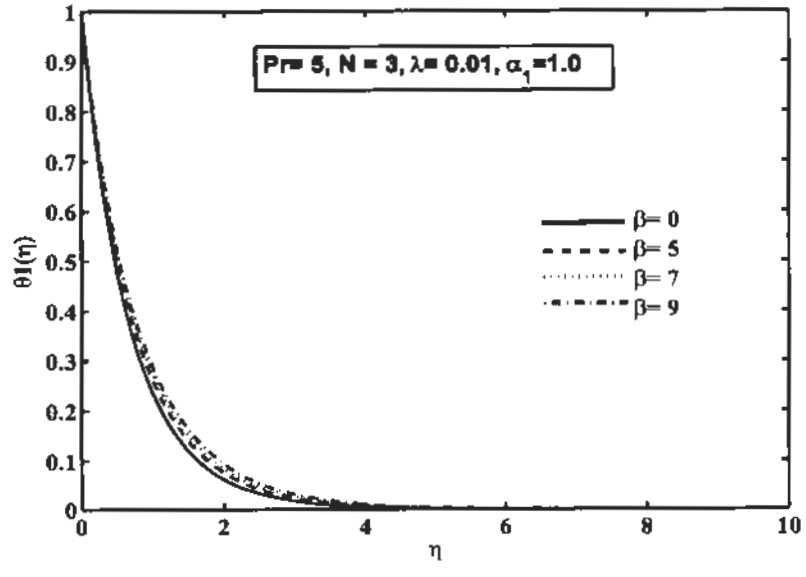

Fig. 2.2. Impact of β on temperature field.

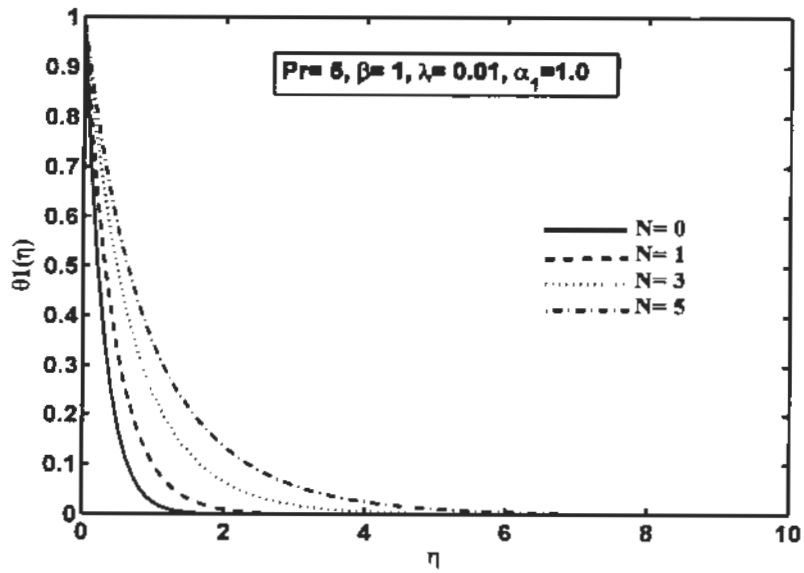

Fig. 2.3. Impact of N on temperature field.

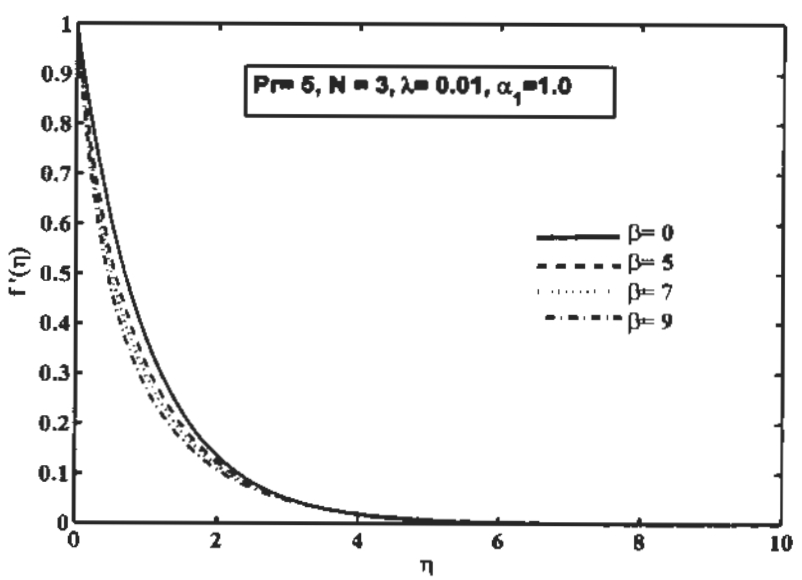

Fig. 2.4. Impact β on velocity field.

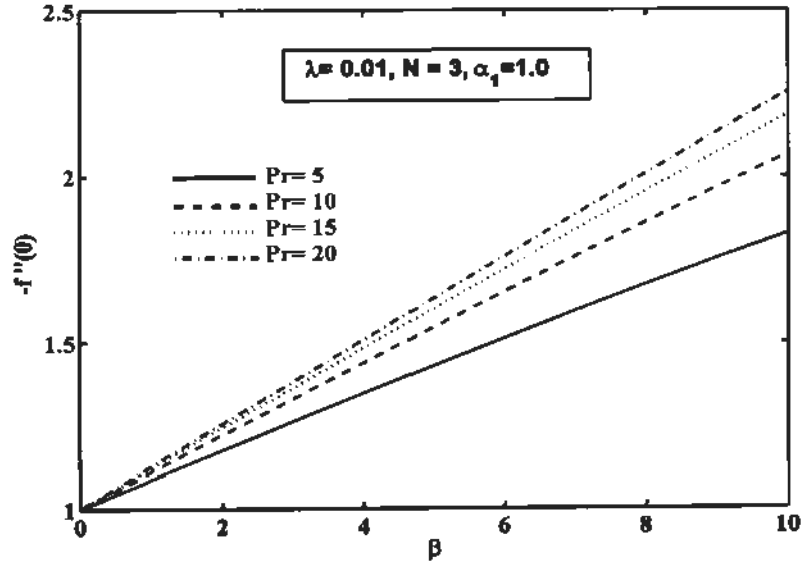

Fig. 2.5. Impact Pr on skin friction against β.

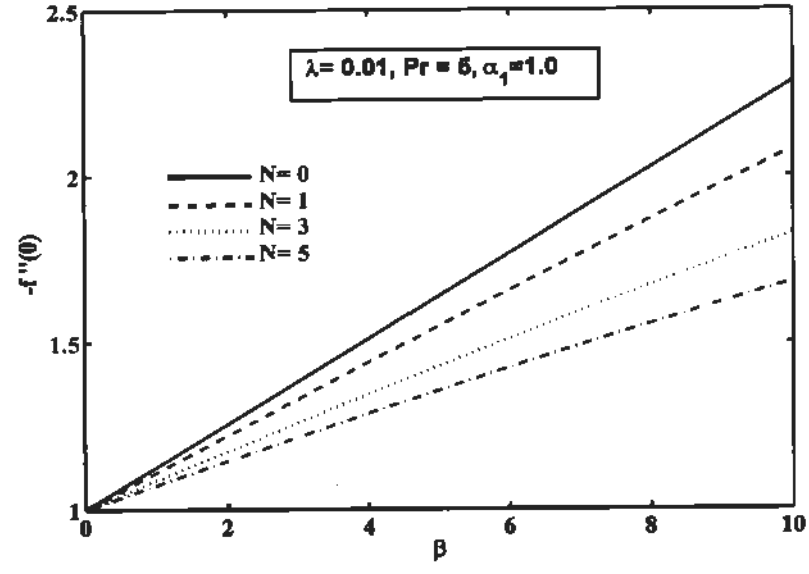

Fig. 2.6. Impact Effect of N on skin friction against β.

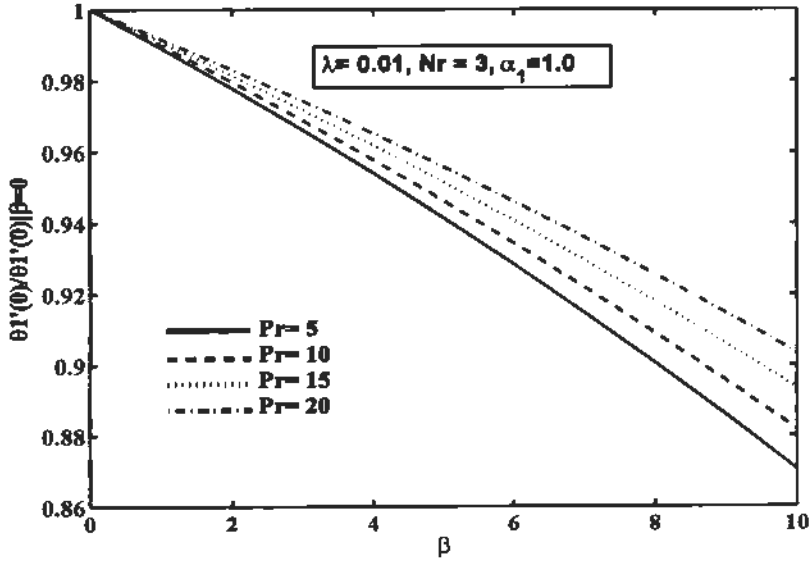

Fig. 2.7. Impact Pr on Nusselt number against β.

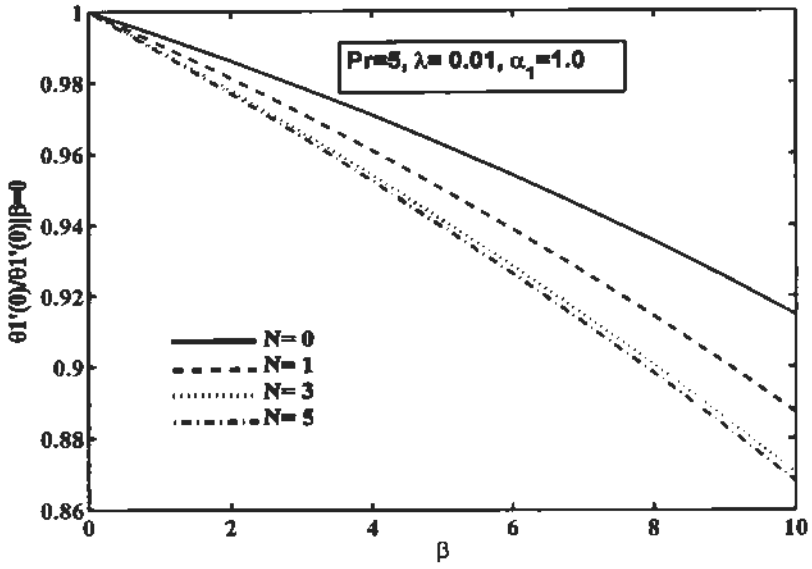

Fig. 2.8. Impact of N on Nusselt number against β.

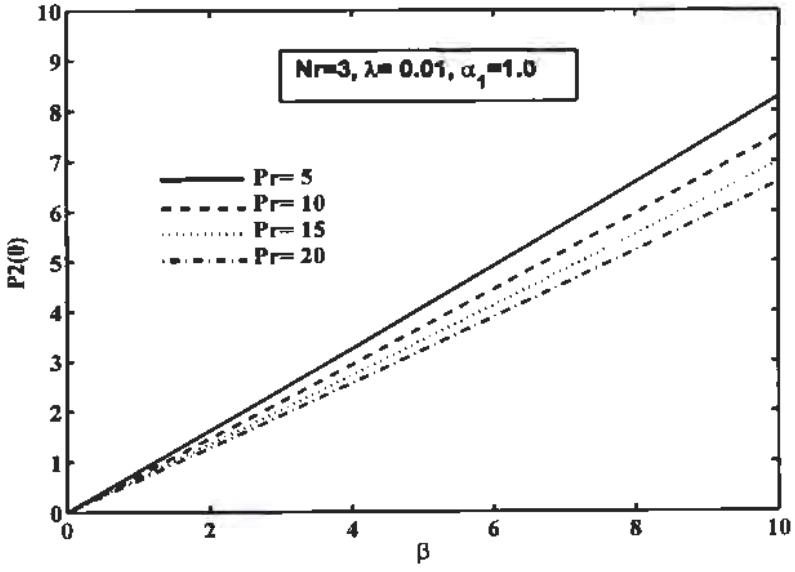

Fig. 2.9. Impact of Pr on pressure against β.

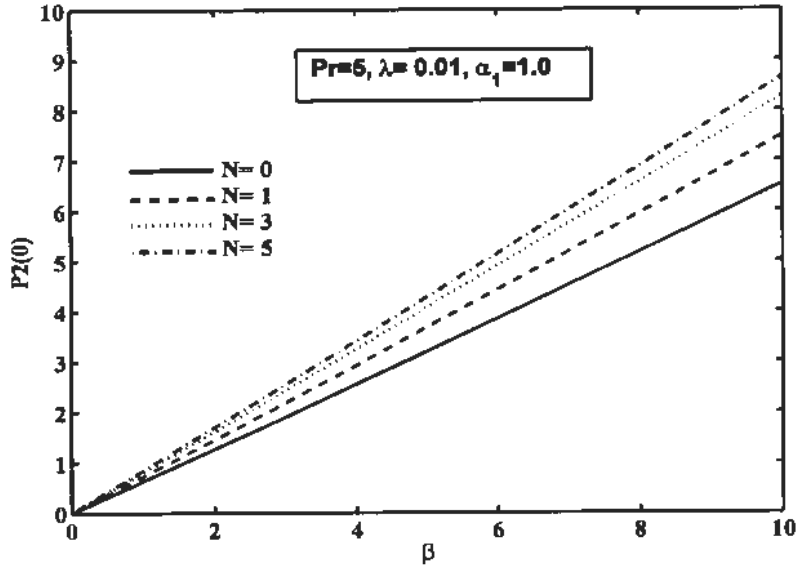

Fig. 2.10. Impact of N on pressure against β.

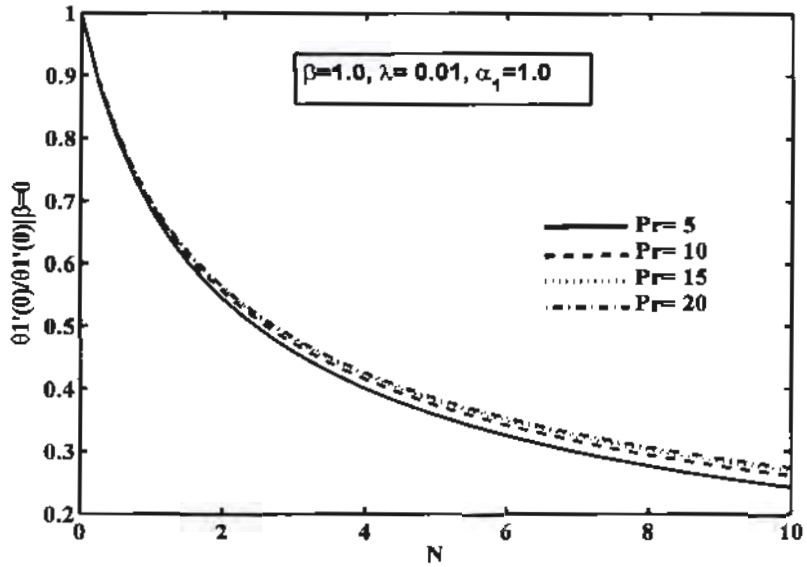

Fig. 2.11. Impact of Pr on Nusselt number against N.

2.4 Conclusion

Mathematical analysis has been performed to inquiry the combine effect of dipole magnetic field and thermal radiation on viscous fluid flow over a stretchable surface. PDE's are converted in to system of ODE's by applying similarity approach. The behavior of feasible controlling parameters on flow field (velocity, temperature) is presented via graphs. The important conclusion are

- Velocity profile decreases for larger value of the ferromagnetic parameter and Prandtl number.
- Temperature field shows an increasing function of β and N whereas it reduces for larger values of Prandtl number.
- Skin friction coefficient boost up by increasing Prandtl number but declines for radiation parameter.
- Nusselt number increases for greater values of Pr and opposite response in seen for thermal radiation parameter.

Chapter 3

Mixed convection flow and heat transfer in ferromagnetic fluid over a stretching sheet with partial slip effects

3.1 Introduction

The purpose of the current exploration is to study heat transport and mixed convection analysis in ferromagnetic liquid flow over a stretchable surface. The influence of momentum slip is also considered. Similarity approach is adopted to convert the boundary layer model into a system of differential equations which are then elucidated numerically by R-K based shooting technique. The characteristic of friction factor, Nusselt number, slip parameter ferrohydrodynamic thermo-mechanical parameter and mixed convection parameter on flow fields on boundary layer region are deliberated through graphs and tables. Lastly an assessment is also made with the available data and establish a tremendous agreement.

3.2 Flow assumption and mathematical formulation

A mixed convection heat transfer for two-dimensional, incompressible ferromagnetic liquid, electrically non-conducting base fluid with linear stretching velocity $u_w = cx$. Using the boundary layer assumption, the flow equations established due to conservation of mass, momentum and energy transport with viscous dissipation in component form are

$$\frac{\partial u}{\partial x}+\frac{\partial v}{\partial y}=0, \tag{3.1}$$

$$\rho\left(u\frac{\partial u}{\partial x}+v\frac{\partial u}{\partial y}\right)=-\frac{\partial p}{\partial x}+\mu_0 M\frac{\partial H}{\partial x}+\mu\left(\frac{\partial^2 u}{\partial x^2}+\frac{\partial^2 u}{\partial y^2}\right)+g\beta^*(T_c-T)\,, \tag{3.2}$$

$$\rho\left(u\frac{\partial v}{\partial x}+v\frac{\partial v}{\partial y}\right)=-\frac{\partial p}{\partial y}+\mu_0 M\frac{\partial H}{\partial y}+\mu\left(\frac{\partial^2 v}{\partial x^2}+\frac{\partial^2 v}{\partial y^2}\right)+g\beta^*(T_c-T), \tag{3.3}$$

$$\begin{aligned}\rho c_p\left(u\frac{\partial T}{\partial x}+v\frac{\partial T}{\partial y}\right)+\mu_0 T\frac{\partial M}{\partial T}\left(u\frac{\partial H}{\partial x}+v\frac{\partial H}{\partial y}\right)&=k\frac{\partial^2 T}{\partial y^2}\\ +\mu\left[2\left(\frac{\partial u}{\partial x}\right)^2+2\left(\frac{\partial v}{\partial y}\right)^2+\left(\frac{\partial v}{\partial x}+\frac{\partial u}{\partial y}\right)^2\right].&\end{aligned} \tag{3.4}$$

Corresponding boundary equations are

$$\left.\begin{aligned} &u = u_w + A\frac{\partial u}{\partial y}, \quad v = 0, \quad \text{at} \quad y = 0 \\ &u = 0, \quad p + \frac{1}{2}\rho(u^2 + v^2) = \text{constant} \quad \text{as} \quad y \to \infty \end{aligned}\right\}, \tag{3.5}$$

along with PST condition for temperature described in Eq. (1.59). Using similarity transformation Eqs. (1.64) and (1.65) in to the Eqs. (3.1) to (3.5) and equationg the coefficients up to order ξ^1. The system of equations along with Eqs. (3.5) and (1.59) takes the form

$$f''' + ff'' - f'^2 - \frac{2\beta\theta_1}{(\eta+\alpha_1)^4} + 2P_2 + G^*\theta_1 = 0, \tag{3.6}$$

$$P_1' - f'' - ff' - \frac{2\beta\theta_1}{(\eta+\alpha_1)^3} + G^*\theta_1 = 0, \tag{3.7}$$

$$P_2' - \frac{2\beta\theta_2}{(\eta+\alpha)^3} + \frac{4\beta\theta_1}{(\eta+\alpha_1)^5} + G^*\theta_2 = 0, \tag{3.8}$$

$$\theta_1'' - \Pr(2f'\theta_1 - f\theta_1') + \frac{2f(\theta_1-\varepsilon)\lambda\beta}{(\eta+\alpha_1)^3} - 4\lambda(f')^2 = 0, \tag{3.9}$$

$$\begin{aligned} &\theta_2'' - \Pr\left(4f'\theta_2 - f\theta_2'\right) - \left(\theta_1 - \varepsilon\right)\lambda\beta\left[\frac{2f'}{(\eta+\alpha_1)^4} + \frac{4f}{(\eta+\alpha_1)^5}\right] \\ &+ \frac{2f\theta_2\lambda\beta}{(\eta+\alpha_1)^3} - \lambda(f'')^2 = 0, \end{aligned} \tag{3.10}$$

$$\left.\begin{aligned} &f' = 1 + \delta f''(0), f = 0, \quad \theta_1 = 1, \quad \theta_2 = 0, \quad \text{at} \quad \eta = 0 \\ &f' \to 0, \quad \theta_1 \to 0, \quad \theta_2 \to 0, \quad P_1 \to -P_\infty, \; P_2 \to 0 \quad \text{as} \quad \eta \to \infty \end{aligned}\right\}. \tag{3.11}$$

The non-dimension parameters occurring in Eqs. (3.6) to (3.11) are

$$\left.\begin{aligned} &G^* = \frac{Gr_x}{\mathrm{Re}_x^2}, \; Gr_x = \frac{g\beta^*(T_C - T_W)}{\nu^2}, \quad \delta = A\sqrt{\frac{c}{\nu}} \end{aligned}\right\}, \tag{3.12}$$

where $G^* \geq 0$ is mixed convection, Gr_x is Grashof number, δ is slip parameter. Skin friction and Nusselt number are mentioned in Eq. (2.15).

3.3. Results and discussion

Influence of numerous pertinent parameter like ferrohydrodynamic interaction parameter β, partial slip parameter δ, Prandtl number Pr, mixed convection parameter G^*, and heat transfer characteristic on boundary layer ferromagnetic fluid are investigated with the help of figures and table. Throughout the problem the values to physical parameter for computational work as $Pr = 0.72$, $\lambda = 0.01$, $\varepsilon = 2.0$, $\alpha_1 = 1.0$. To authorize the convergence of the current numerical technique, numeric values of Nusselt number $-\theta_1'(0)$ are matched with available published data described by Chen [126], Abel et al. [128] and Ali [129] for innumerable values of Pr when $\beta = 0$ are given in table 3.1. It can be realized that superb agreement is obtained with those availabe results. Further table 3.2. display the values of Nusselt number and skin friction are given in the presence of β.

The behavior of various sundry parameter on dimensionless velocity and temperature fields are elaborated through figs. 3.1 to 3.7. Figs. 3.1 and 3.2 outlined the inspiration of slip parameter δ on flow velocity and temperature field. From fig. 3.1 it is witnessed that the velocity reduces under the attendance of δ. Also fluid velocity decreases monotonically and approaches to zero away from the solid surface, whereas under no slip circumstance, Near the solid surface the velocity of the fluid and stretching surface is equal, then $f'(0) = 1$, which is obviously justified in the figure. Fig. 3.2 indicate that temperature of the fluid increases by enlarging velocity slip parameter δ, therefore reduction in temperature gradient, which illustrate the heat transfer rate. This statement is validated through the results presented in fig.3.9. Fig. 3.3 and 3.4 describes the impact of ferromagnetic interaction parameter β on velocity and temperature field which is due to magnetic force prompted via dipole field on the fluid dynamics. The existence of magnetic field, reduction is observed in fluid velocity for higher values of β. Because this happen due to Lorentz force which has tendency to opposes the flow and hereafter declines in the axial velocity as shown in fig. 3.3, whereas inverse behavior is noted for temperature field as shown in fig. 3.4.

Fig. 3.5 interprets the impact of G^* on $f'(\eta)$. Results indicate increasing behavior for velocity profile for G^* and associated boundary layer thickness. Fig. 3.6 represent the behavior of G^* on temperature field $\theta_1(\eta)$. It is manifest that reduction is noted for temperate and thermal boundary layer thickness against buoyancy parameter. Behavior of Pr on θ_1 is outlined in fig.

3.7. Decreasing effect is noted for temperature profile and associated boundary layer thickness by enhancing *Pr*. Physically higher *Pr* fluids have weaker thermal diffusivity and smaller *Pr* means stronger thermal diffusivity. Figs. 3.8 and 3.9 are drawn for local skin friction coefficient and rate of heat transfer against β for numerous values δ. It is evaluated form fig. 3.8, that skin friction coefficient increases for β, whereas it declines corresponding to δ. It implies that, for no-slip case $(\delta = 0.0)$, the maximum shear stress arises at surface for ferromagnetic fluid $(\beta = 0)$.

Fig. 3.9 is scrutinized to display the rate of heat transfer for several values of velocity slip parameter δ against β. Apparently graph discloses that Nusselt number reduces for larger values of β and δ. Fig. 3.10 is plotted to see the behavior of pressure profile against β for some values of δ. The fallouts indicate that pressure is enhances for β as well as δ. Figs. 3.11 to 3.13 are sketched to see the impact of mixed convection parameter G^* on skin friction, heat transfer rate, and pressure versus β. It is examined from fig. 3.11 that Nusselt number is declines for larger values of β, whereas it is increasing function of mixed convection parameter and skin friction coefficient enhances with β as seen in Fig 3.12, whereas inverse response is noted for G^*. Fig. 3.13 exhibit the pressure profile for a set of values of mixed convection parameters. It is perceive that pressure is reduces by rising the valued of G^*, whereas increasing linearly with the variation of β.

Table 3.1. Comparison of Nusselt number $-\theta_1'(0)$ in case of Pr once $G^* = \beta = \lambda = \delta = 0$.

Pr	Chen [126]	Abel et al. [128]	Ali [129]	Present results
0.72	1.0885	1.0885	----	1.08863
1	1.3333	1.3333	1.3333	1.33334
3	2.5097	----	2.5097	2.50967
10	4.7968	4.7968	4.7968	4.79671

Table 3.2. Skin friction $-f''(0)$ and heat transfer rate $-\theta_1'(0)$ for some values of β when Pr=1.0.

β	$-f''(0)$	$-\theta_1'(0)$
0.0	1.0000	1.3333
0.5	1.0507	1.3286
1.0	1.1015	1.3237
1.3	1.1524	1.3187

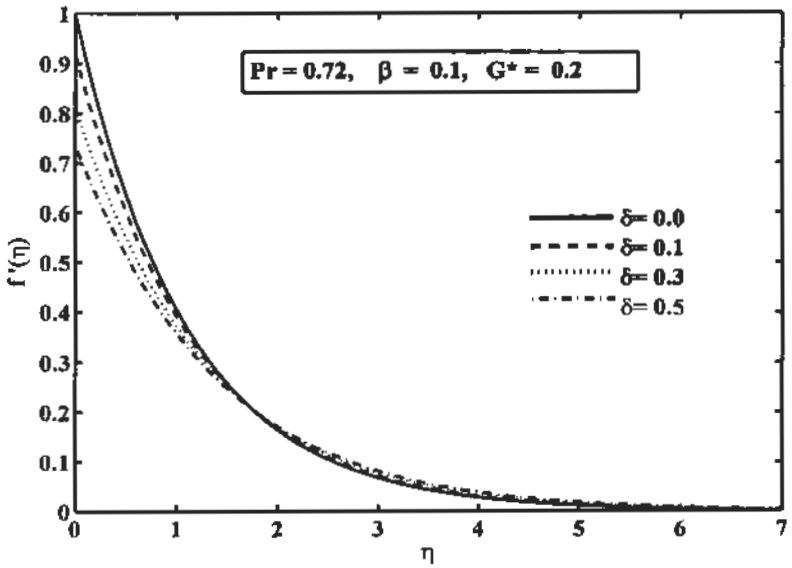

Fig. 3.1. Impact of δ on velocity field against η .

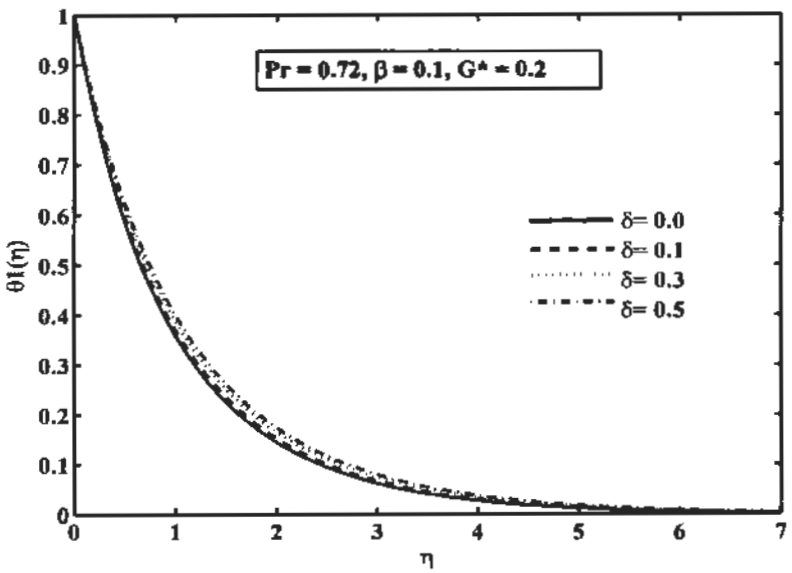

Fig. 3.2. Impact of δ on temperature field against η .

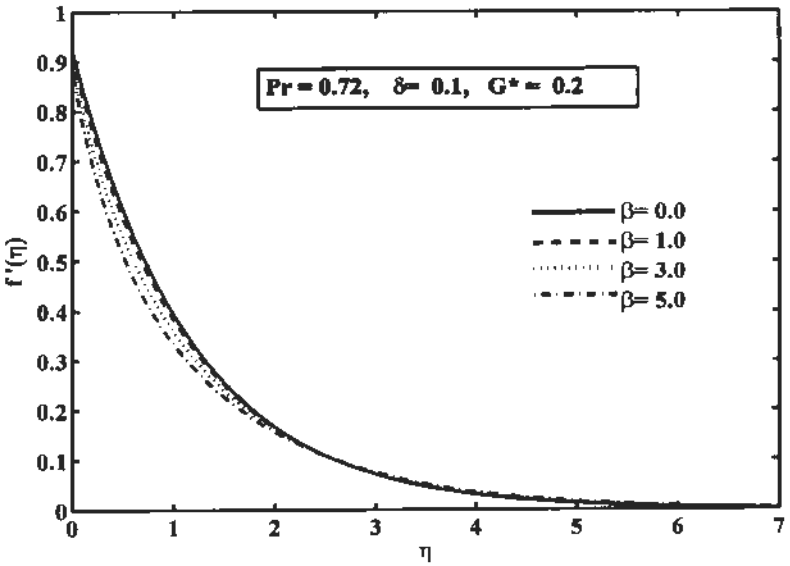

Fig. 3.3. Impact of β on velocity field against η .

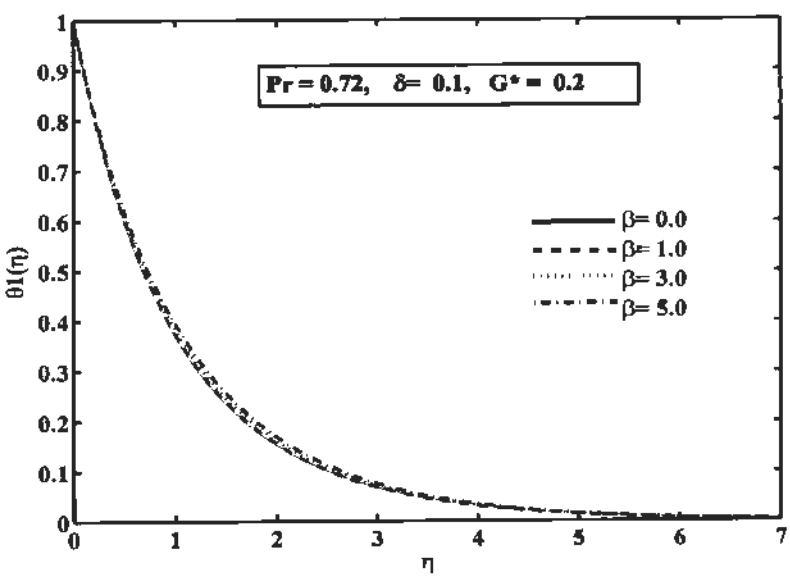

Fig. 3.4. Impact of β on temperature field against η .

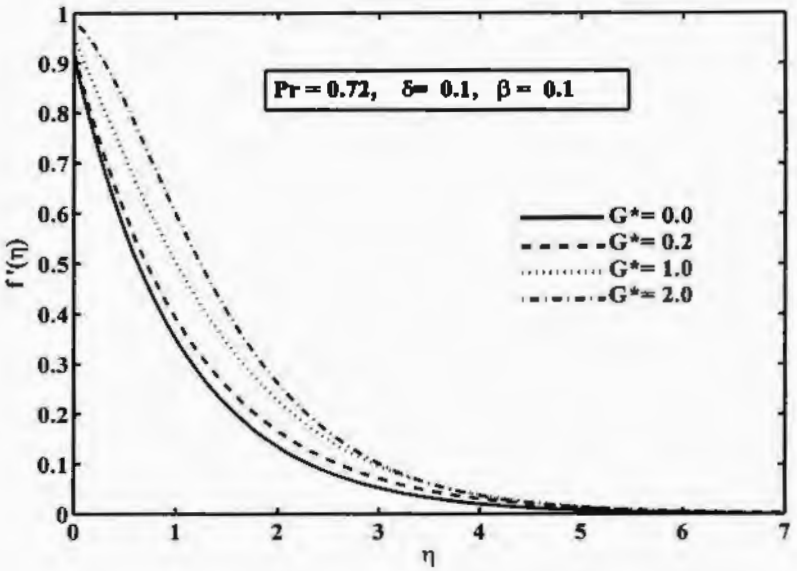

Fig. 3.5. Impact of G^* on velocity field against η .

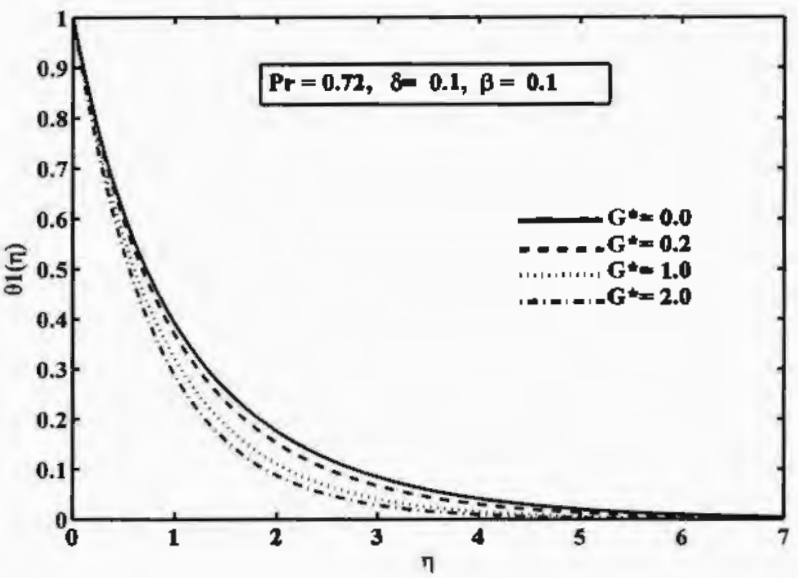

Fig. 3.6. Impact of G^* on temperature field against η .

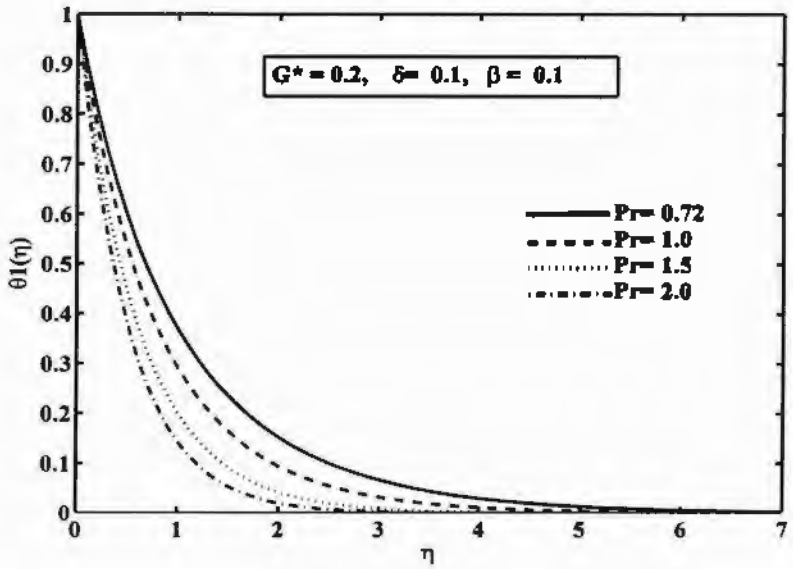

Fig. 3.7. Impact of *Pr* on temperature field against η .

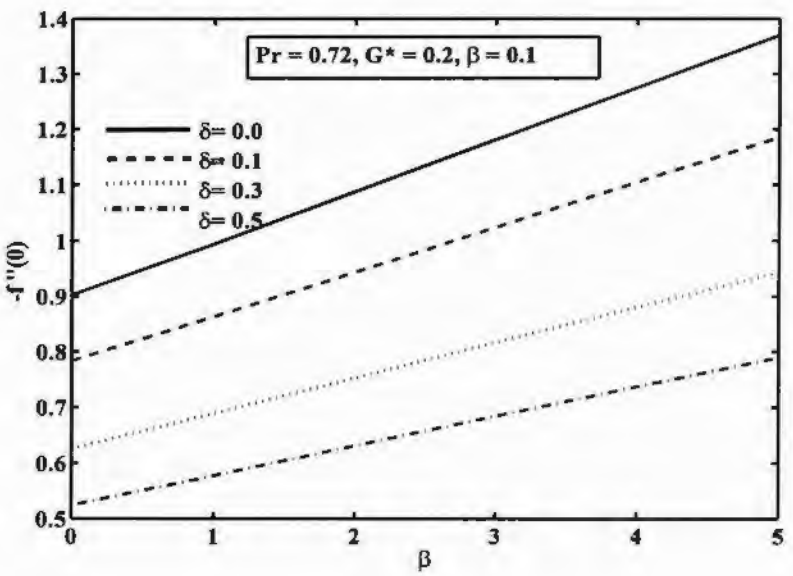

Fig. 3.8 Impact of δ on skin friction coefficient versus β .

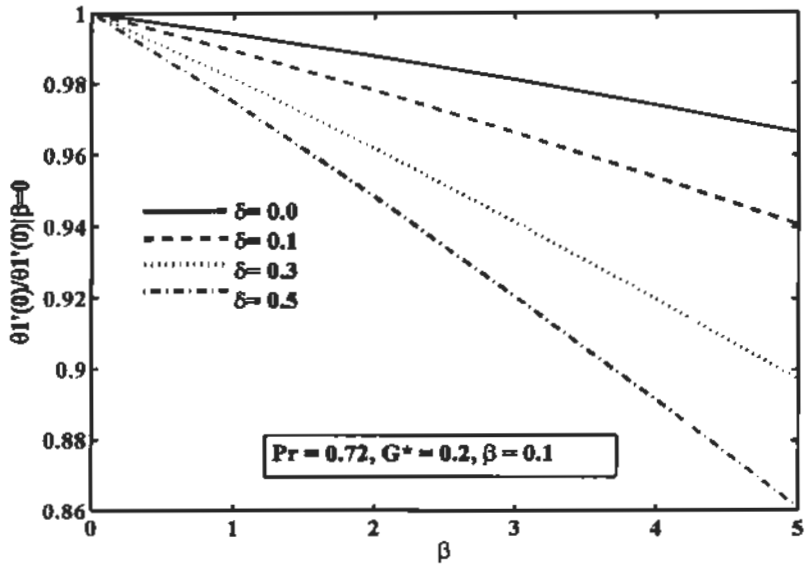

Fig. 3.9. Impact of δ on Nusselt number versus β.

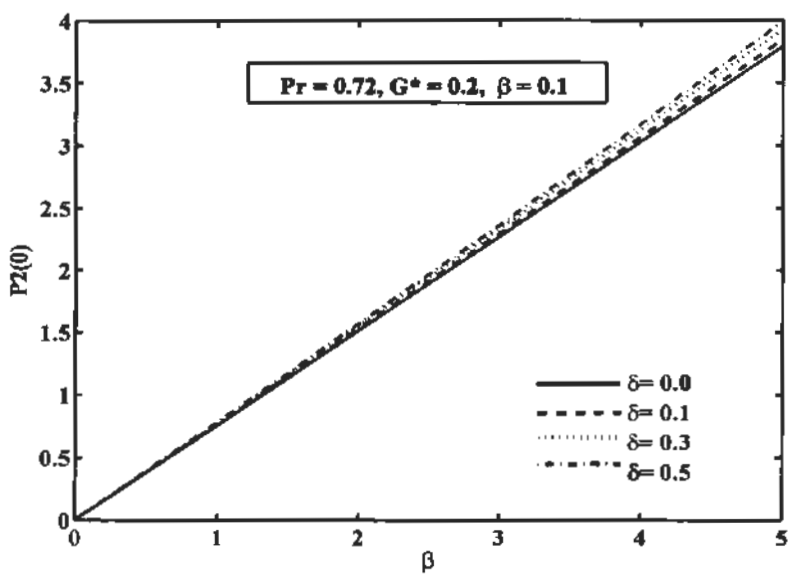

Fig. 3.10. Impact of δ on pressure profile versus β.

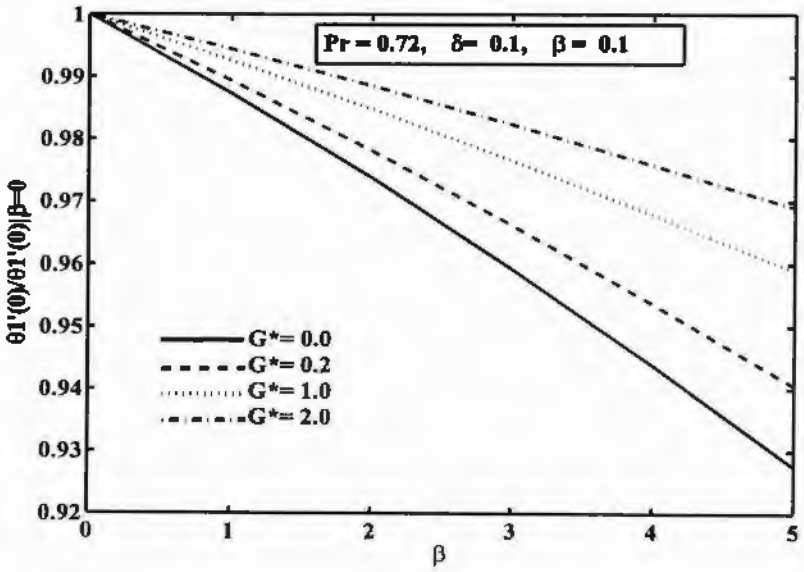

Fig. 3.11. Impact of G^* on Nusselt number versus β.

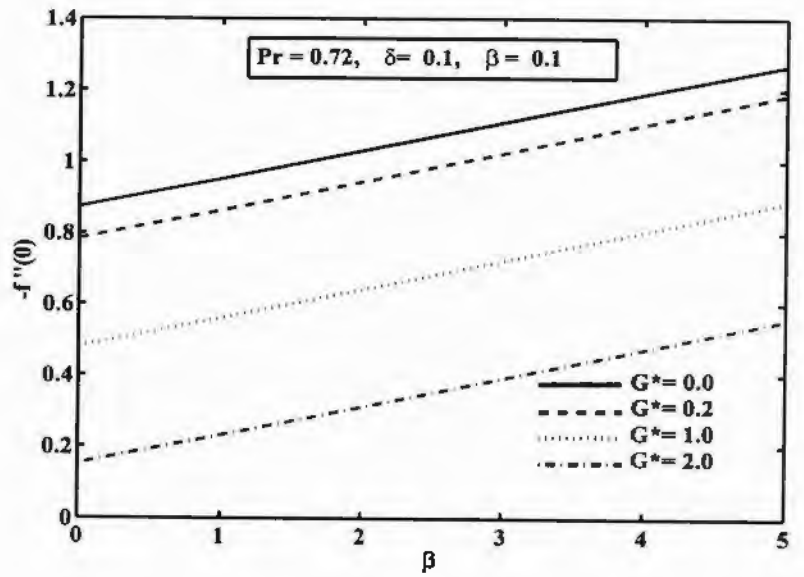

Fig. 3.12. Impact of G^* on local skin friction versus β.

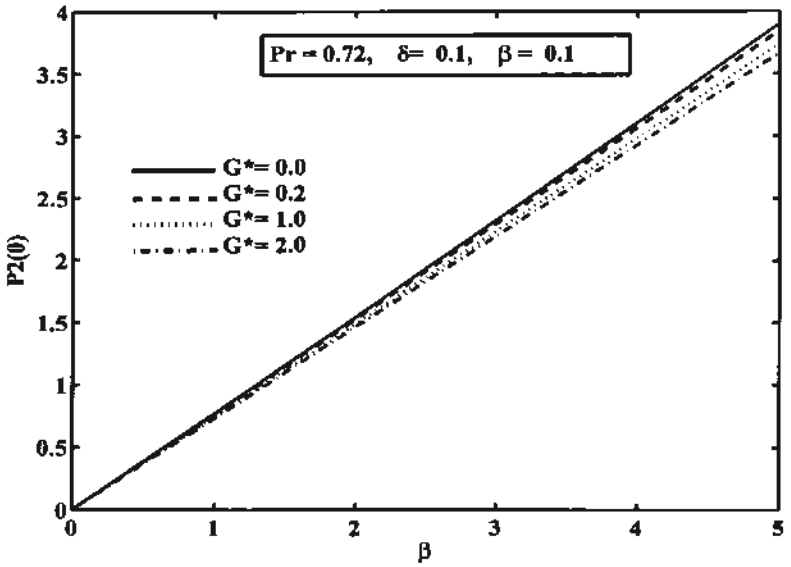

Fig. 3.13. Impact of G^* on pressure profile versus β.

3.4 Conclusion

In this chapter two-dimensional viscous flow of ferrofluid over a horizontal stretched surface is examined. The impact of mixed convection parameter and partial slip also taken in to account. Governing equestions are obtained through similarity approach and handle via numerically. The effects of involving flow field quantities are elaborated graphically. The present problem has the following key points.

- Velocity profile is an increasing function of G^* and decreases for larger δ and β.
- Temperature of the fluid enhances for β and δ, on the other end it declines for Pr and G^*.
- Heat transfer rate is increases for G^* and decreases for δ.
- Skin friction is reduces for δ and G^* whereas it increases for higher values of ferrohydrodynamic parameter.

Chapter 4

Stagnation point flow of ferromagnetic particle-fluid suspension over a stretching/shrinking surface in a porous medium with heat source/sink

4.1 Introduction

This chapter scrutinizes stagnation point flow with heat transfer of a ferromagnetic liquid made from a suspension of tiny magnetic particles in a fluid move along a flat stretching or shrinking surface through a porous media with the existence of magnetic dipole. The influence of suction or injection parameters are also deliberated. By employing similarity approach mentioned in section 1.17, the resulting system of coupled equations are solved numerically by 4th order Runge-Kutta method. The impact of controlling flow quantities, like ferrohydrodynamic interaction parameter, porosity parameter, velocity parameter, wall mass flux parameter and heat source/sink parameter on dimensionless form of (velocity, temperature field) and skin friction and Nusselt numbers are explained pictorially and tabular form. A comparison with already published studies in limited case revealed an excellent agreement.

4.2 Flow assumption and mathematical formulation

Consider an incompressible, stagnation point flow of ferromagnetic fluid over a stretching or shrinking surface with wall velocity $u_w = \pm cx$, where '+' indicates stretching and '-' indicates shrinking surface and free stream velocity $U(x) = ax$. The flow transpires in the domain at $y > 0$. The flow equations modelled due to conservation of mass, momentum and energy along with boundary layer assumption with standard representation are of the form

$$\frac{\partial u}{\partial x} + \frac{\partial v}{\partial y} = 0, \tag{4.1}$$

$$\left(u\frac{\partial u}{\partial x} + v\frac{\partial u}{\partial y}\right) = U(x)\frac{dU(x)}{dx} + \frac{\mu_0}{\rho}M\frac{\partial H}{\partial x} + \frac{\mu}{\rho}\left(\frac{\partial^2 u}{\partial x^2} + \frac{\partial^2 u}{\partial y^2}\right) + \frac{\mu}{\rho K}(U(x) - u), \tag{4.2}$$

$$\left(u\frac{\partial v}{\partial x} + v\frac{\partial v}{\partial y}\right) = \frac{\mu_0}{\rho}M\frac{\partial H}{\partial y} + \frac{\mu}{\rho}\left(\frac{\partial^2 v}{\partial x^2} + \frac{\partial^2 v}{\partial y^2}\right) - \frac{\mu}{\rho K}v, \tag{4.3}$$

$$\rho c_p\left(u\frac{\partial T}{\partial x}+v\frac{\partial T}{\partial y}\right)+\mu_0 T\frac{\partial M}{\partial T}\left(u\frac{\partial H}{\partial x}+v\frac{\partial H}{\partial y}\right)=k\frac{\partial^2 T}{\partial y^2}+$$
$$\mu\left[2\left(\frac{\partial u}{\partial x}\right)^2+2\left(\frac{\partial v}{\partial y}\right)^2+\left(\frac{\partial v}{\partial x}+\frac{\partial u}{\partial y}\right)^2\right]+Q_0(T_c-T) \tag{4.4}$$

with relevant boundary equations

$$\left.\begin{aligned} &u=u_w(x)=\pm cx,\ v=v_w,\ T=T_w,\quad y=0\\ &u\to U(x)=ax,\ T\to T_\infty,\qquad y\to\infty \end{aligned}\right\}. \tag{4.5}$$

Substituting Eqs. (1.64) and (1.65) into the Eqs. (4.1) to (4.5) and matching, we find following self-similar equations.

$$f'''+ff''-f'(f'+K_1)+A_1(A_1+K_1)-\frac{2\beta\theta_1}{(\eta+\alpha_1)^4}=0, \tag{4.6}$$

$$f''+f(f'-K_1)+\frac{2\beta\theta_1}{(\eta+\alpha_1)^3}=0, \tag{4.7}$$

$$\theta_1''-\Pr(-f\theta_1'-H_1\theta_1)+\frac{2\lambda\beta(\theta_1-\varepsilon)f}{(\eta+\alpha_1)^3}-4\lambda(f')^2=0, \tag{4.8}$$

$$\theta_2''-\Pr\left(2f'\theta_2-f\theta_2'-H_1\theta_2\right)-\lambda\beta\left(\theta_1-\varepsilon\right)$$
$$\times\left[\frac{2f'}{(\eta+\alpha_1)^4}+\frac{4f}{(\eta+\alpha_1)^5}\right]+\frac{2\lambda\beta f\theta_2}{(\eta+\alpha_1)^3}-\lambda(f'')^2=0. \tag{4.9}$$

Also the Eq. (4.5) takes the form

$$\left.\begin{aligned} &f=S,\ f'=1,\ \ \theta_1=1,\ \ \theta_2=0,\ \text{at}\ \ \eta=0\ \ \text{For stretching sheet}\\ &f=S,\ f'=-1,\ \ \theta_1=1,\ \ \theta_2=0,\ \text{at}\ \ \eta=0\ \ \text{For shrinking sheet} \end{aligned}\right\}, \tag{4.10}$$

$$f'\to A_1,\ \theta_1\to 0,\ \theta_2\to 0,\ \ as\ \ \eta\to\infty. \tag{4.11}$$

The new emerging constraints occurring in the dimensionless equations are

$$\left.A_1=\frac{a}{c},\ K_1=\frac{\nu}{cK},\ H_1=\frac{Q_0}{c\rho c_p},\ S=\frac{-v_w}{\sqrt{c\nu}}\right\}. \tag{4.12}$$

Here A_1 is the ratio of velocity parameter, K_1 is porous parameter, $H_1>0$ and $H_1<0$ correspond to heat source and sink, and S is mass flux $S>0$ correspond to suction and $S<0$ correspond to injection. The dimensionless form of skin friction and heat transfer rate are defined in Eq. (2.15).

4.3. Results and discussion

This chapter mainly focuses on heat transfer characteristic and stagnation-point flow of ferromagnetic fluids over a stretching and shrinking surface with the existence of porous medium. Calculated numerical conclusions are displayed pictorially and tabular forms for some values of physical parameters. Throughout the problem the values of parameters $\lambda = 0.01$, $\varepsilon = 2.0$ and $\alpha_1 = 1.0$ are considered, fixed. Present results is compared in the case of $\beta = 0$ for $f''(0)$ and $-\theta_1'(0)$ with those of Wang [130], Hammad and Ferdows [131], Pal et al. [132] and Hammad and Pop [133] for numerous values of Pr, κ_1 and a/c are displayed in Table 4.1 to 4.3, which shows an excellent agreement with published data and confirm the validity of our numerical technique. Also the calculated values of $f''(0)$ and $-\theta_1'(0)$ for stretching and shrinking sheet are exhibited in table. 4.4 for several values of pertinent parameter such as a/c, β, κ_1, H_1, S and Pr. Effect of ferromagnetic parameter β on velocity and temperature fields can be examined from figs. 4.1 and 4.2. The change in velocity profile against η is simplified in fig. 4.1 for several values of ferromagnetic parameter $\beta(=2,4,6)$ when $a/c = 2$. From fig. 4.1, it is noted that there is reduction in the thickness of boundary layer by rising β for both type of sheet. Infect ferromagnetic fluid basically has a Newtonian carrier fluid with micron sized suspended particles of ferrite which enhance the viscosity of the liquid and hence velocity of the field is decreased as the values of β increased. It is also noticed that velocity profile for stretching is higher than shrinking sheet. Fig. 4.2 determined temperature distribution for some values of ferromagnetic parameter β. It is also pointed out that temperature is an increasing function of β for both type of sheets, this is due to the collaboration among fluid motion and act of external dipole. This collaboration diminishes the velocity field and enlarging frictional heating among the fluid layers. In both cases temperature profile gradually decreases with the variation of η, the value of temperature profile approaches to zero when $\eta \to 0.8$ (stretching) and $\eta \to 1.4$ (shrinking) sheet (meeting the end point condition $\theta_1 \to 0$ as $\eta \to \infty$). It is also viewed that for shrinking sheet temperature field is greater than stretching sheet.

Fig. 4.3 shows effect of several values of suction/injection parameter S on θ_1. From the figure, it is perceived that temperature profile decline by snowballing the value of S for stretching/shrinking surface. Figs. 4.4 and 4.5 are sketched to perceive the influence of S on

skin friction and rate of heat transfer with the deviation of ferro-magnetic parameter β. From the figures it is noticed that friction factor depresses for large value of S for stretching/shrinking sheets when $a/c=2$, whereas the reverse effect occurs on heat transfer rate for stretching and shrinking surface as noted in fig. 4.5.

Fig. 4.6 illustrate the behavior of local Nusselt number against ferromagnetic parameter β for few values of H_1. It is detected that Nusselt number is rising for stretching sheet and converse behavior is pointed out for shrinking sheet against the variation of H_1.

Fig. 4.7 display the effects of K_1 on Nusselt number with the variation of β. From the figure it is establish that Nusselt number is an increasing function of K_1 for both type of surface. Also noted that the Nusselt number for shrinking sheet rises very slowly as compared to stretching sheet when $a/c=2$. Fig. 4.8 exemplify the influence of porosity parameter K_1 on shear stress for some values of β. It is found that there is reduction in skin friction coefficient as value of K_1 increases, whereas it increases with the values of β for both type of sheets. figs. 4.9 and 4.10 depict the effect of velocity parameter a/c with $Pr=1.0$ on the functions like $f'(\eta)$ and $f''(\eta)$ with the variation of η. From the figures it is observed that all the functions are monotonically increasing/decreasing with η. Also notice that the velocity profile for stretching sheet is decreases and inverse response occurs for shrinking surface and meeting the end point condition for definite values of a/c. Fig. 4.11 demonstrate the influence of source/sink parameter H_1 on temperature profile when $\beta=0.1$ for both types of sheets. From the figure it perceived that temperature field gradually decreases with η, and approaches to zero as $\eta\to 0.9$ for stretching sheet, whereas there is a formation of peak near $\eta=0.5$ for shrinking sheet, then decreases linearly until the temperature approaches zero as $\eta\to 1.5$ and (meeting the boundary condition $\theta_1\to 0$ as $\eta\to\infty$). Also publicized temperature profile increases against H_1 for both type of sheet. In spite of the fact that the outcome of shrinking sheet is more generous than stretching sheet. Fig. 4.12 shows change of $\theta_1(\eta)$ for some values of injection parameter. When $S<0$ there is a formation of a peak as $\eta\to 12.5$, thereafter temperature decreases gradually until approaches to 0 as.

Table 4.1. Comparison of $-\theta_1'(0)$ for stretching sheet in the case when $\beta = 0$, $a/c = 0$, $K_1 = 0$, $H_1 = 0$, $S = 0$.

Pr	Wang [130]	Hamad and Ferdows [131]	Pal et al. [132]	Present results
0.2	0.1691	0.16909	0.16952	0.169522
0.7	0.4539	0.45391	0.45391	0.453907
2	0.9114	0.91136	0.91135	0.911359
7	1.8954	1.89540	1.89540	1.895412
20	3.3539	3.35390	3.35390	3.353902

Table 4.2. Comparison of $f''(0)$ when $\beta = H_1 = S = 0$, $Pr = 0.05$.

a/c	K_1	Hamad and Ferdows [131]	Pal et al. [132]	Present results
2	0.0	1.99907	2.017	2.017416
	0.1	2.01021	2.041	2.041706
	0.5	2.11021	2.136	2.136219

Table 4.3. Comparison of $-\theta_1'(0)$ in the case when $\beta = K_1 = H_1 = S = 0$

Pr	a/c	Hammad and Pop [133]	Pal et al. [132]	Present results
1	0.1	0.6216	0.6244	0.602138
	0.5	0.6937	0.6924	0.692449
	1.0	0.8001	0.7978	0.797896
	2.0	0.9788	0.9782	0.978724
	3.0	1.1221	1.1327	1.132100
1.5	0.1	0.7952	0.7971	0.776822
	0.5	0.8673	0.8647	0.864818
	1.0	0.9774	0.9772	0.977201
	2.0	1.1721	1.1780	1.178113
	3.0	1.3419	1.3519	1.351950

Table 4.4. Computed values of skin friction $f''(0)$, and Nusselt number $-\theta_1'(0)$.

						Stretching sheet		Shrinking sheet	
a/c	β	K_1	H_1	S	Pr	$f''(0)$	$-\theta_1'(0)$	$f''(0)$	$-\theta_1'(0)$
2						2.0671	1.0017	4.4805	0.6115
1.8						1.5861	0.9662	3.8717	0.5519
1.5						0.9186	0.9100	2.9908	0.4488
1.5	0.1					0.9186	0.9100	2.9908	0.4488
	0.2					0.8864	0.9102	2.9462	0.4467
	0.3					0.8541	0.9104	2.9016	0.4445
		0.1				0.9186	0.9100	2.9908	0.4488
		0.2				0.9319	0.9106	3.0979	0.4569
		0.3				0.9451	0.9111	3.2012	0.4644
			0.1			0.9186	0.9100	2.9908	0.4488
			0.2			0.9448	0.8615	2.9901	0.3746
			0.3			0.9446	0.8099	2.9894	0.2948
				0.1		0.9186	0.9100	2.9908	0.4488
				0.2		0.9473	0.9777	3.1536	0.5191
				0.3		0.9766	1.0471	3.3205	0.5925
					0.1	0.9186	0.9100	2.9908	0.4488
					0.2	0.9212	1.3009	2.9918	0.5017
					0.3	0.9231	1.6131	2.9922	0.5148

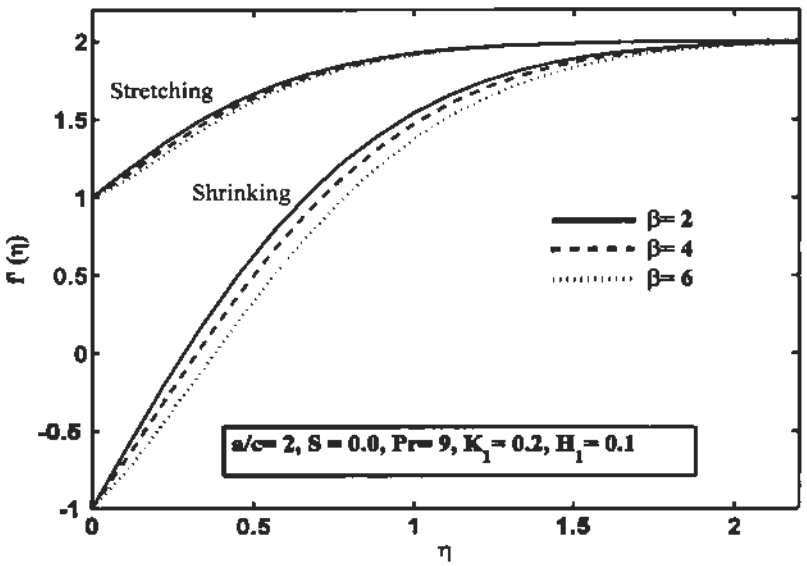

Fig. 4.1. Influence of β on $f'(\eta)$.

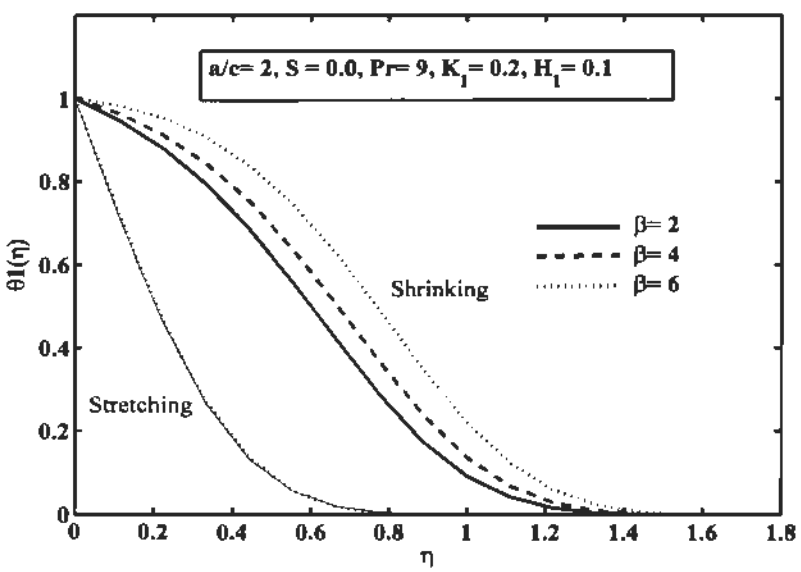

Fig. 4.2. Effect of β on $\theta_1(\eta)$.

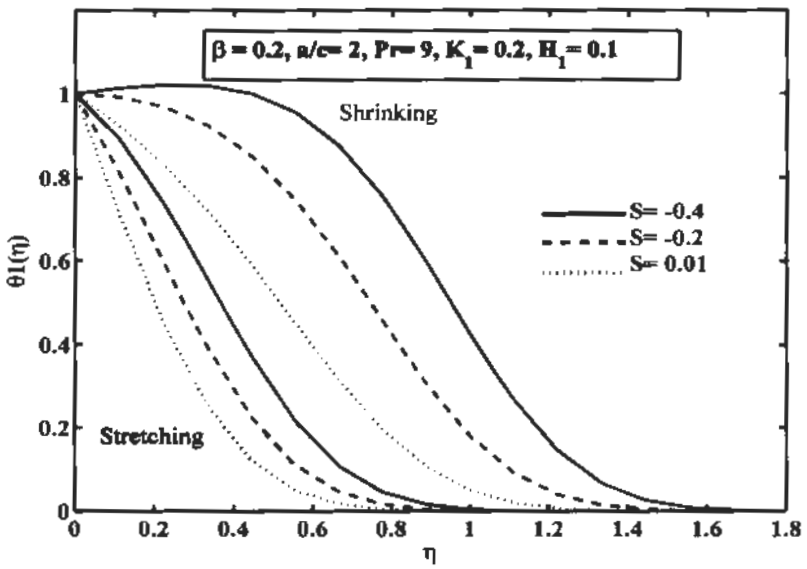

Fig. 4.3. Effect of S on $\theta_1(\eta)$.

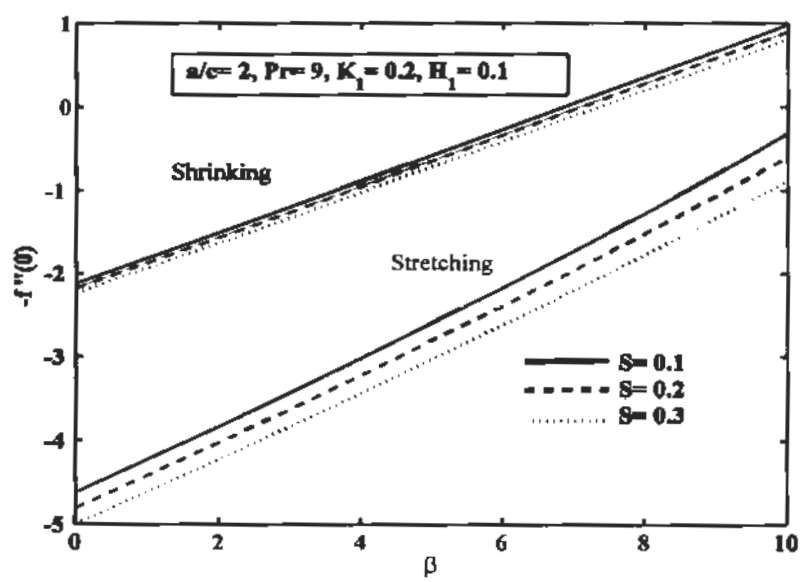

Fig. 4.4. Influence of S on Skin friction coefficient versus β.

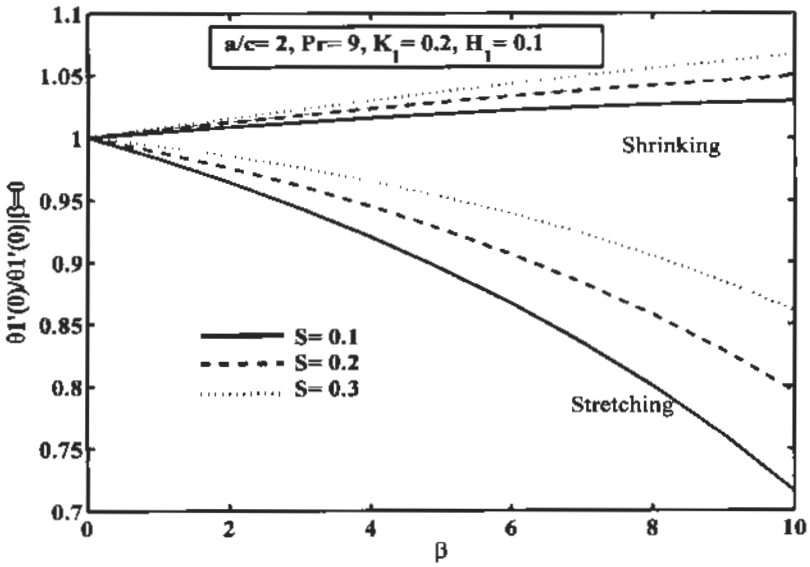

Fig. 4.5. Influence of S on Nusselt number versus β .

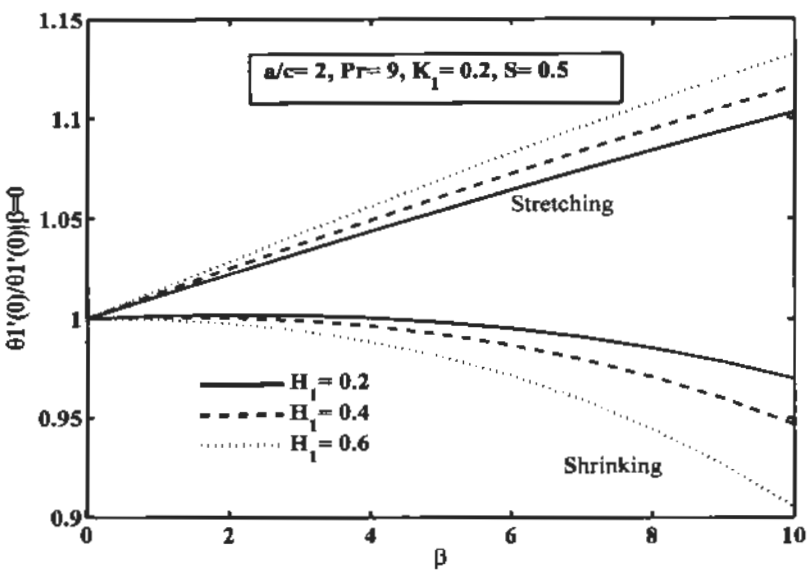

Fig. 4.6. Influence of H_1 on Nusselt number versus β .

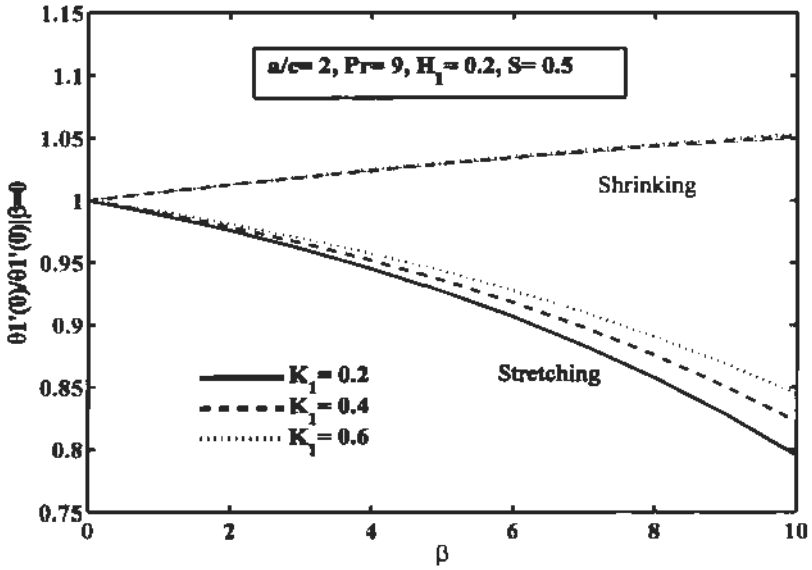

Fig. 4.7. Influence of K_1 on Nusselt number versus β .

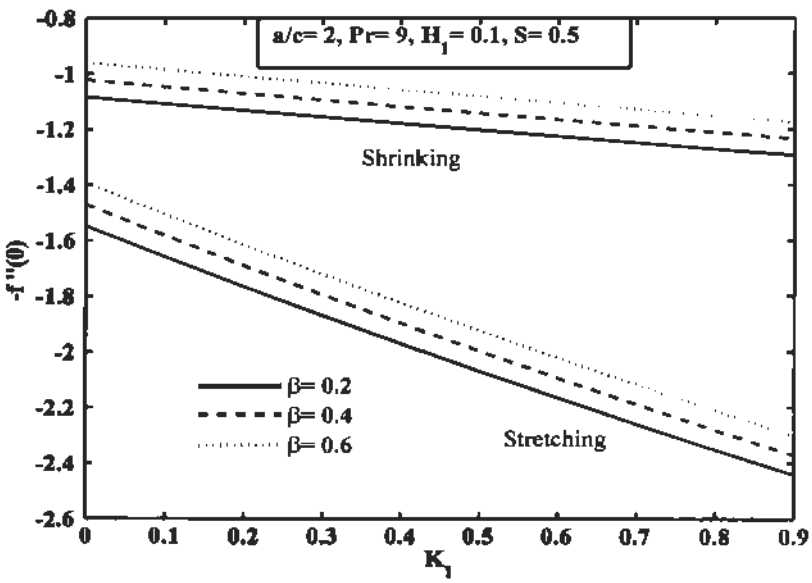

Fig. 4.8. Influence of β on Skin friction coefficient versus K_1.

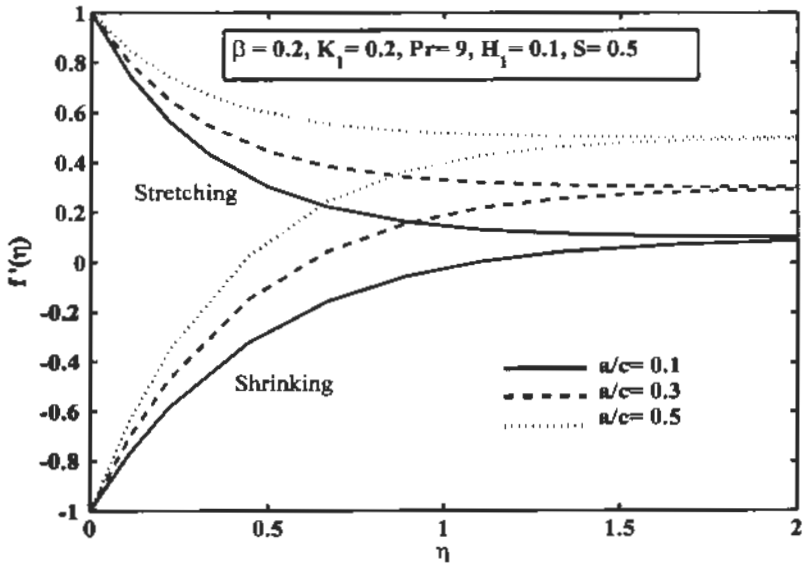

Fig. 4.9. Influence of a/c on $f'(\eta)$.

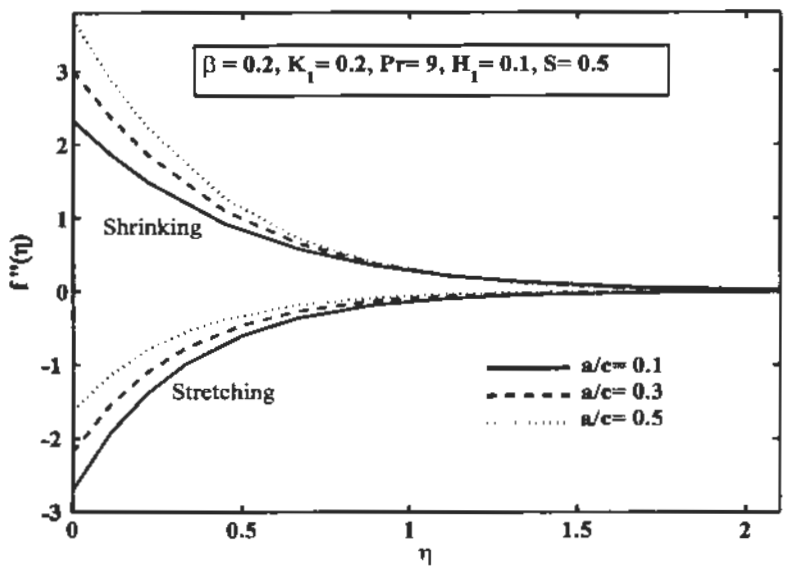

Fig. 4.10. Influence of a/c on $f''(\eta)$.

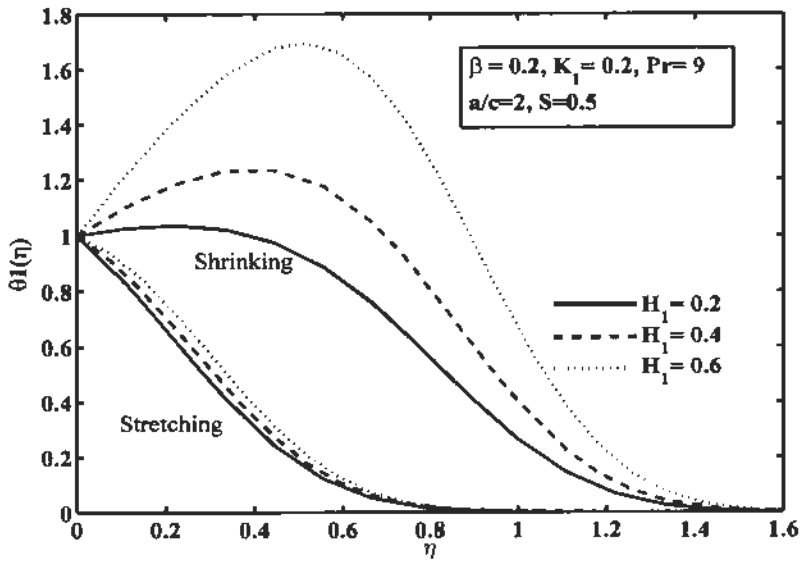

Fig. 4.11. Influence of H_1 on $\theta_1(\eta)$.

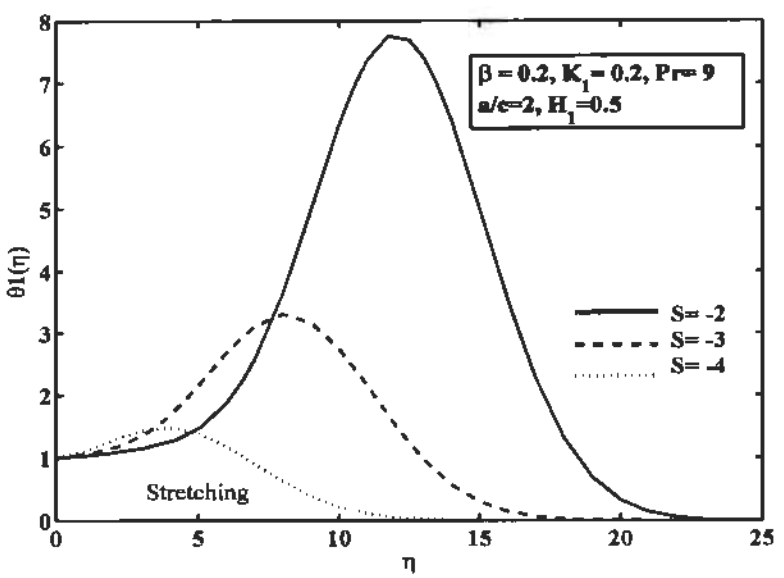

Fig. 4.12. Influence of $S<0$ on $\theta_1(\eta)$.

4.4 Conclusion

We explore boundary layer flow and heat transport behavior under porous medium over a stretching and shrinking surface with the impact of mass flux. The governing flow model of momentum and energy transport are renovated into ODE's by employing similarity approach. The obtained coupled nonlinear ODE's are then solved with the help of shooting technique. Impact of various converging parameters like suction/injection parameter S, ferromagnetic interaction parameter β, porous parameter K_1, heat source/sink parameter H_1 and Prandtl number Pr on flow field are studied in detail. The major findings are in compact form as follows:

- Velocity profile shows decreasing behavior for larger values of ferromagnetic parameter β, whereas temperature field increases with β.
- Temperature profile increases by increasing the value of H_1, but revers effect is occur for few values of injection parameter $S < 0$.
- Skin friction coefficient decreases by enlarging S for both type of sheet, whereas opposite behavior is noted against β.
- Nusselt number rises for both type of sheets by increasing values of K_1 with the variation of β.

Chapter 5

Unsteady ferromagnetic liquid flow and heat transfer analysis over a stretching sheet with the effect of dipole and prescribed heat flux

5.1 Introduction

In this chapter, focus in on time dependent ferromagnetic liquid flow on boundary region and heat transfer characteristics over a stretchable surface under the action of dipole field. The problem of momentum and energy transport equation are first modeled into system of ODE's by utilizing similarity approach, then numerically solved by using RKF-45 based shooting technique. Two kinds of heating process are considered, specifically (i) prescribed surface temperature (PST) and (ii) prescribed heat flux (PHF). The influence of the innumerable emerging parameters involving in the problem namely ferrohydrodynamic parameter, viscous dissipation parameter, unsteady parameter, Prandtl number on flow velocity, temperature fields, Nusselt number and skin friction are illustrated through pictorially and tabular form.

5.2 Flow assumption and mathematical formulation

Consider an incompressible, two dimensional unsteady boundary layer viscous flow of ferromagnetic liquid past a stretching surface (see section 1.17) located at y=0 stretching with velocity $U_w(x,t)=cx/(1-\alpha_1 t)$. Here, c is stretching rate, while effective stretching rate $c/(1-\alpha_1 t)$ is growing with time. Boundary layer equations for the current system takes the form

$$\frac{\partial u}{\partial x}+\frac{\partial v}{\partial y}=0, \tag{5.1}$$

$$\frac{\partial u}{\partial t}+u\frac{\partial u}{\partial x}+v\frac{\partial u}{\partial y}=\frac{\mu_0}{\rho}M\frac{\partial H}{\partial x}+\frac{\mu}{\rho}\frac{\partial^2 u}{\partial y^2}, \tag{5.2}$$

$$\rho c_p\left(\frac{\partial T}{\partial t}+u\frac{\partial T}{\partial x}+v\frac{\partial T}{\partial y}\right)+\mu_0 T\frac{\partial M}{\partial T}\left(u\frac{\partial H}{\partial x}+v\frac{\partial H}{\partial y}\right)=k\frac{\partial^2 T}{\partial y^2}\mu\left(\frac{\partial u}{\partial y}\right)^2+2\mu\left(\frac{\partial v}{\partial y}\right)^2, \tag{5.3}$$

associated boundary equations are

$$\left.\begin{aligned} &u = U_w(x,t) = \frac{cx}{1-\alpha_3 t},\ v = 0, \\ &T = T_w(x,t) = T_\infty - \frac{b_1 x}{1-\alpha_3 t} \qquad \text{for PST} \\ &-k\frac{\partial T}{\partial y} = q_w(x,t) = T_\infty - \frac{d_1 x}{1-\alpha_3 t} \qquad \text{for PHF} \end{aligned}\right\} \quad \text{at } y = 0, \tag{5.4}$$

$$u \to 0, \quad T \to T_\infty, \qquad \text{as } y \to \infty, \tag{5.5}$$

where $q_w = d_1 x/(1-\alpha_3 t)$ is heat flux, c, b_1, d_1 and α_3 are positive constant with $b_1 > 0$, $c \geq 0$ and $\alpha_3 \geq 0$ (such that $\alpha_3 t < 1$), and both b_1 and c have dimension of inverse time. It is important to know that at t = 0, Eqs. (5.1) to (5.3) obtained steady flow past a stretching surface. $U_w(x,t)$ and $T_w(x,t)$ are selected in such a way to refurbish the PDE's (5.1) to (5.3) into ODE's. Substituting Eqs. (1.64) and (1.65) into the Eqs. (5.2) and (5.3) and equating the coefficients up to power of ξ^2, we acquire

$$f''' + ff'' - (f')^2 - \Lambda\left(f' + \frac{1}{2}\eta f''\right) - \frac{2\beta\theta_1}{(\eta+\alpha_1)^4} = 0, \tag{5.6}$$

$$\theta_1'' - \Pr(f'\theta_1 - f\theta_1') + \frac{2\lambda\beta(\theta_1 - \varepsilon)f}{(\eta+\alpha_1)^5} - \Pr\Lambda\left(\theta_1 + \frac{1}{2}\eta\theta_1'\right) - 2\lambda(f')^2 = 0, \tag{5.7}$$

$$\begin{aligned} &\theta_2'' - \Pr\left(4f'\theta_2 - f\theta_2'\right) - \lambda\beta\left(\theta_1 - \varepsilon\right)\left[\frac{2f'}{(\eta+\alpha_1)^4} + \frac{4f}{(\eta+\alpha_1)^5}\right] \\ &- \Pr\Lambda\left(\theta_2 + \frac{1}{2}\eta\theta'\right) + \frac{2\lambda\beta\theta_2 f}{(\eta+\alpha_1)^5} - \lambda(f'')^2 = 0. \end{aligned} \tag{5.8}$$

In Eqs. (5.4) and (5.5) representation of boundary conditions take the form

$$\left.\begin{aligned} &f = 0,\ f' = 1,\ \theta_1 = 1,\ \theta_2 = 0, \text{ for PST} \\ &f = 0,\ f' = 1,\ \theta_1' = -1,\ \theta_2' = 0, \text{for PHF} \end{aligned}\right\} \quad \text{at } \eta = 0, \tag{5.9}$$

$$f' \to 0, \quad \theta_1 \to 0, \quad \theta_2 \to 0, \qquad \text{as } \eta \to \infty. \tag{5.10}$$

Here $\Lambda = \alpha_3/c$ is the unsteady parameter, by applying Eqs. (1.64) and (1.65), the non-dimensional form of skin friction and Nusselt number for PST and PHF defined in Eq. (2.14) are

$$\left.\begin{aligned} &C_f \,\mathrm{Re}_x^{1/2} = -2f''(0), \\ &Nu_x / \mathrm{Re}_x^{1/2} = -\left(\theta_1'(0) + \xi^2\theta_2'(0)\right) \quad \text{PST} \\ &Nu_x / \mathrm{Re}_x^{1/2} = 1/\left(\theta_1(0) + \xi^2\theta_2(0)\right) \quad \text{PHF} \end{aligned}\right\}. \tag{5.11}$$

5.3. Results and discussion

For evaluating numerical results, we have taken two kind heating process PST and PHF, impact of numerous convergence flow quantities, like viscous dissipation parameter λ, ferromagnetic (ferrohydrodynamic) parameter β, Prandtl number Pr, and unsteady parameter Λ on flow fields are discussed via graphs and in tabular form. We have used the values $Pr = 0.72$, $\beta = 0.1$, $\Lambda = 0.1$, $\lambda = 0.01$, $\varepsilon = 2.0$, $\alpha_1 = 1.0$ in our problem. To confirm the accuracy and exactness of current results, the numeric values of Nusselt number $-\theta_1'(0)$ are matched with Ali [129], Grubka and Bobba [134], and Bachok et al. [135] when $(\beta = 0)$ and steady parameter ($\Lambda = 0$) against some values of Pr are define in table 5.1. From the table it can be analyzed that splendid agreement achieved between the current and earlier publicized results. Additionally, influence of various parameter of interest on wall temperature (PHF), skin friction, and wall temperature gradient (PST) are exhibited in table 5.2. Ferromagnetic parameter β demonstrate the significance of applied magnetic field persuaded by dipole field on the dynamics of fluid. The presence of magnetization perform as a repelling force on the velocity field, as β enhances, so does resisting force, therefore reduces axial velocity. From graphs it is observed that under the impact of magnetic field fluid velocity $f'(\eta)$ is lower as compared to hydrodynamic case $(\beta = 0)$ for PHF and PST as shown in figs. 5.1 and 5.2. The reason behind is that there occur intervention among fluid motion and stroke of external dipole field. This involvement decreases velocity and enhances frictional heating among the layers of fluid which is responsible for the increment in the thickness of thermal boundary layer as portrayed in figs. 5.3 and 5.4. Also observed that temperature $\theta_1(\eta)$ for prescribes heat flux is higher than that of prescribes surface temperature. Figs 5.5 to 5.8 highlights the influence of unsteady parameter Λ on temperature and velocity profile. Form the fallouts it is identified that $f'(\eta)$ reduces with the deviation of unsteady parameter Λ for PST and PHF, which consequently reduction in the thickness of momentum boundary layer. The non-dimensional temperature reduces monotonically against η for numerous values of Λ as exposed in fig. 5.8. Also witnessed that

the influence of unsteady parameter Λ on temperature is more noticeable than velocity field. Figs. 5.9 and 5.10 portrays the temperature field $\theta_1(\eta)$ versus η for PST and PHF against numerous values of Prandtl number Pr. By studying the graph, we conclude that temperature declines for higher values of Pr, which indicates that viscous boundary region is thicker than thermal boundary region. By increasing Pr means that thermal diffusion rate is slow. Though, for larger value of Pr, temperature enhances near the boundary layer and declines when far away from boundary in PST. While it might be dissimilar other than unity in PHF due to adiabatic surface temperature. The significance of frictional heating owing to magnetic field and viscosity on temperature profile is signifies by dissipation parameter λ. Figs. 5.11 and 5.12 demonstrate the impact of λ on $\theta_1(\eta)$ for PST and PHF. Resets shows decreasing impact in the thickness of thermal boundary region for higher value of λ for both PST and PHF. For lesser values of λ, it disclose that temperature in PST is less than PHF. Due to extra ordinary behavior of ferrofluid, this is contradictory to hydro-dynamic case $(\beta = 0)$ whereas snowballing the value of λ, result is enhanced temperature field near the boundary region. The influence of unsteady parameter and ferromagnetic interaction parameter on skin friction and heat transfer rate are presented in figs. 5.13 and 5.14. It is perceived that by enlarging the unsteady parameter, the amount of skin friction and Nusselt number increases significantly. Also heat transfer rate is reduces with the variation of β but opposite trend is noted for skin friction, this is because of the fact that there is a resistive Lorentz force is produced. This force has propensity to slow down the fluid motion on boundary region and hence an increasing in skin-friction coefficient.

Table 5.1. Comparing Nusselt number $-\theta_1'(0)$ for few values of Λ, β, Pr when $\lambda = 0$.

Λ	β	Pr	Grubka and Bobba [134]	Ali [129]	Bachok et. al. [135]	Present results
0	0	0.01	0.0197	--	0.0197	0.079813
		0.72	0.8086	0.8058	0.8086	0.808640
		1	1.0000	0.9961	1.0000	1.000000
		3	1.9237	1.9144	1.9237	1.923609
		10	3.7207	3.7006	3.7207	3.720580
1.0	0	0.72	--	--	1.1005	1.100529
		1	--	--	1.3205	1.320529
		3	--	--	2.4024	2.402342
		7	--	--	3.7682	3.768204
		10	--	--	4.5428	4.542738
0	1.0	0.72	--	--	--	0.771890
		1	--	--	--	0.962935
		3	--	--	--	1.888929
		7	--	--	--	3.041760
		10	--	--	--	3.692413

Table 5.2. Variation of skin friction, heat transfer rate (PST) and wall temperature (PHF) for numerous values of Pr, Λ, β, λ.

β	Λ	λ	Pr	$-f''(0)$	$-\theta_1'(0)$ PST	$1/\theta_1(0)$PHF
0.0	0.1	0.01	0.72	1.0341	0.8498	0.8499
1.0				1.4011	0.8169	0.8051
1.5				1.5890	0.7984	0.7761
0.1	0.0	0.01	0.72	1.0366	0.8143	0.8131
	0.5			1.2020	0.9697	0.9700
	1.0			1.3537	1.1054	1.1068
0.1	0.1	0.01	0.72	1.0704	0.8467	0.8459
		0.2		1.0693	1.0135	1.0517
		0.3		1.0687	1.1014	1.2059
0.1	0.1	0.01	0.72	1.0704	0.8467	0.8459
			1.0	1.0689	1.0389	1.0403
			2.0	1.0653	1.5684	1.5742

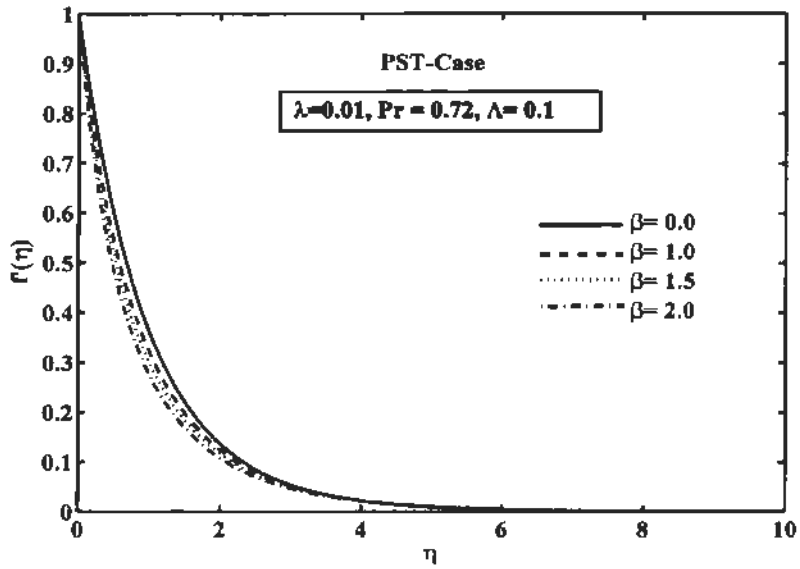

Fig. 5.1. Impact of β on velocity profile for PST.

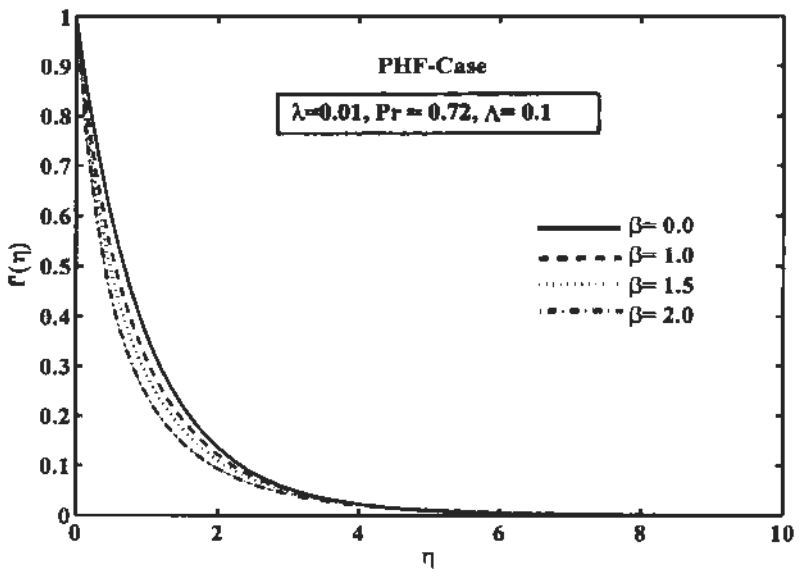

Fig. 5.2. Impact of β on velocity field for PHF.

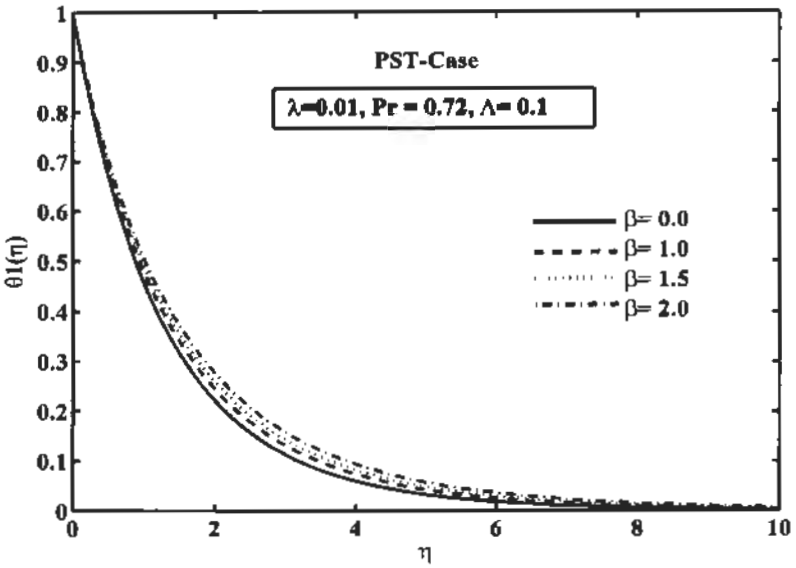

Fig. 5.3. Impact of β on temperature field for PST.

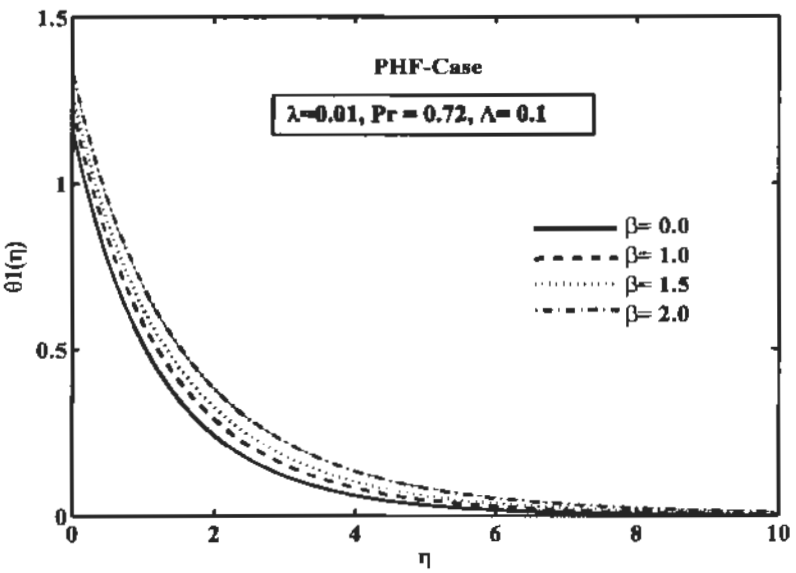

Fig. 5.4. Impact β on temperature profile for PHF.

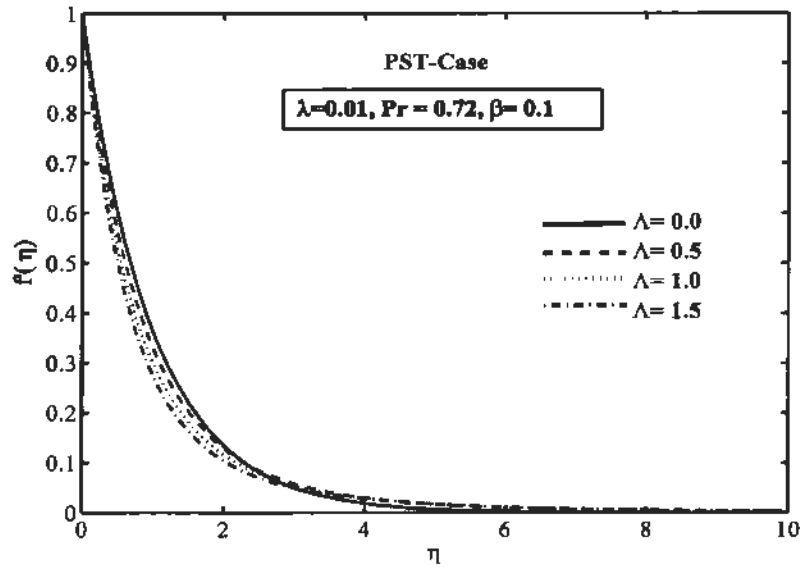

Fig. 5.5. Impact of Λ on velocity field for PST.

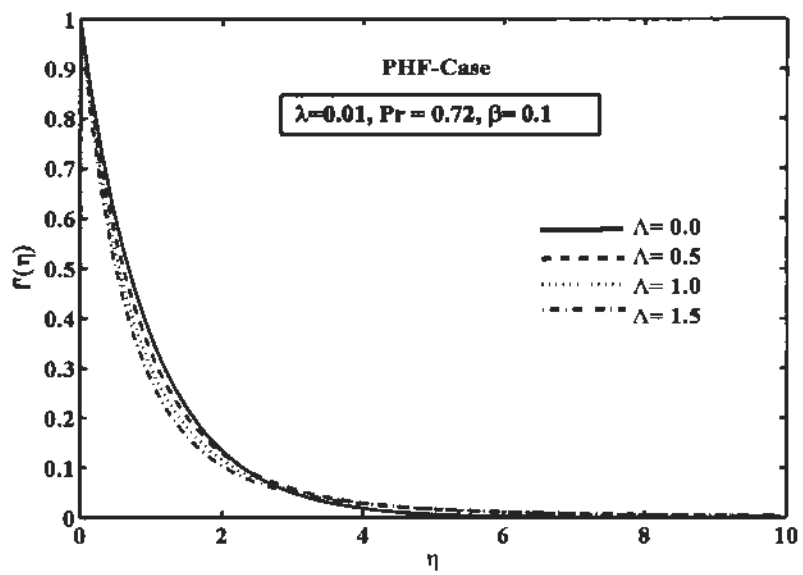

Fig. 5.6. Impact of Λ on velocity field for PHF.

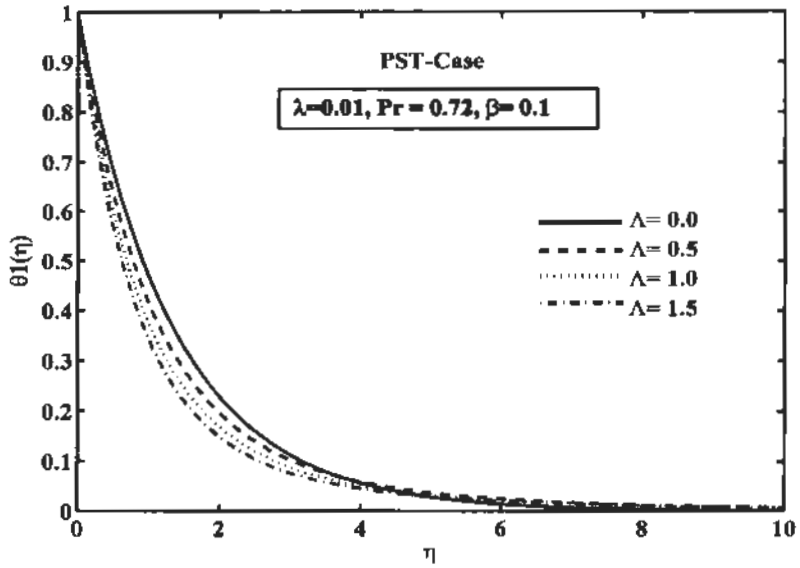

Fig. 5.7. Impact of Λ on temperature field for PST.

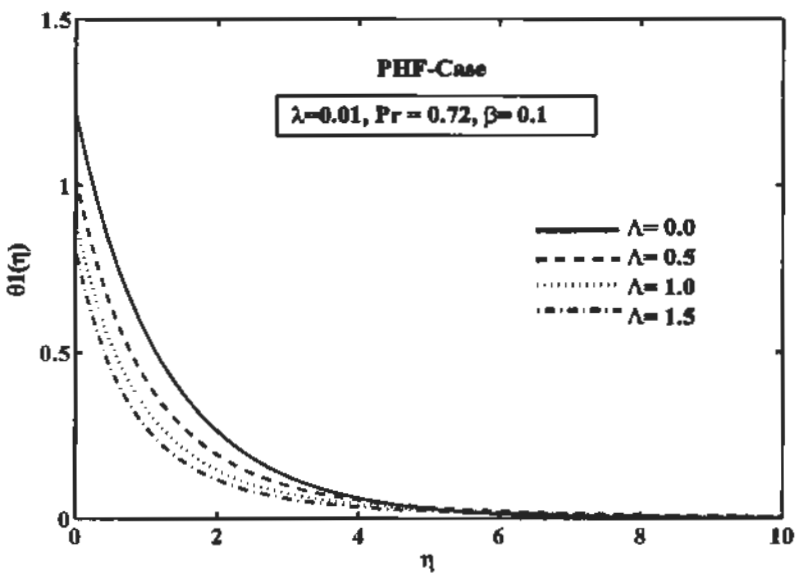

Fig. 5.8. Impact of Λ on temperature field for PHF.

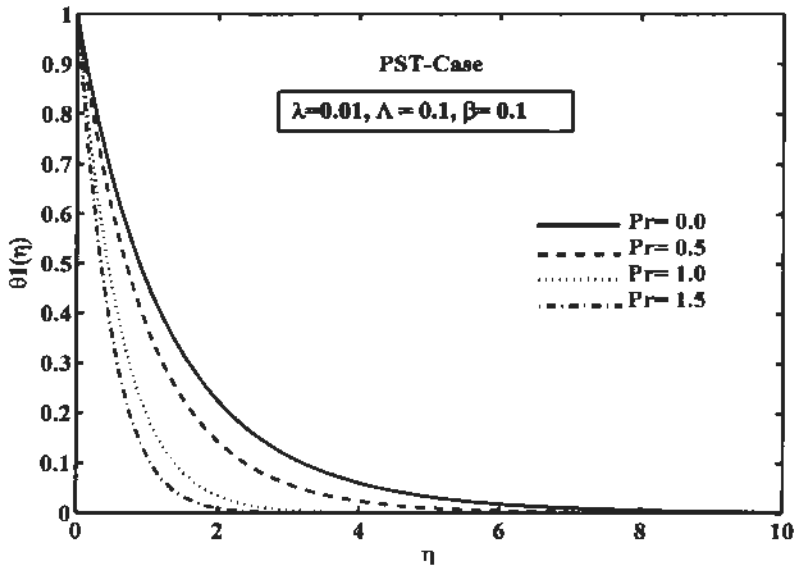

Fig. 5.9. Impact of Pr on temperature fielde for PST.

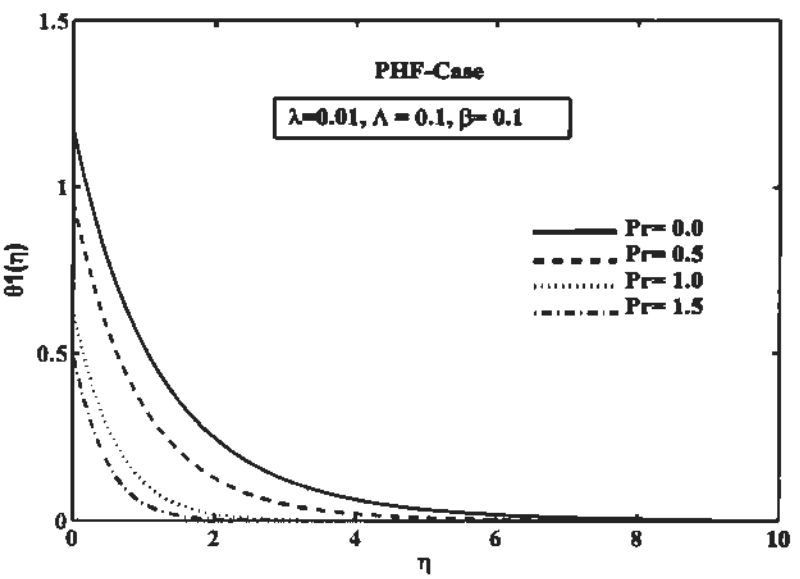

Fig. 5.10. Impact of Pr on temperature field for PHF.

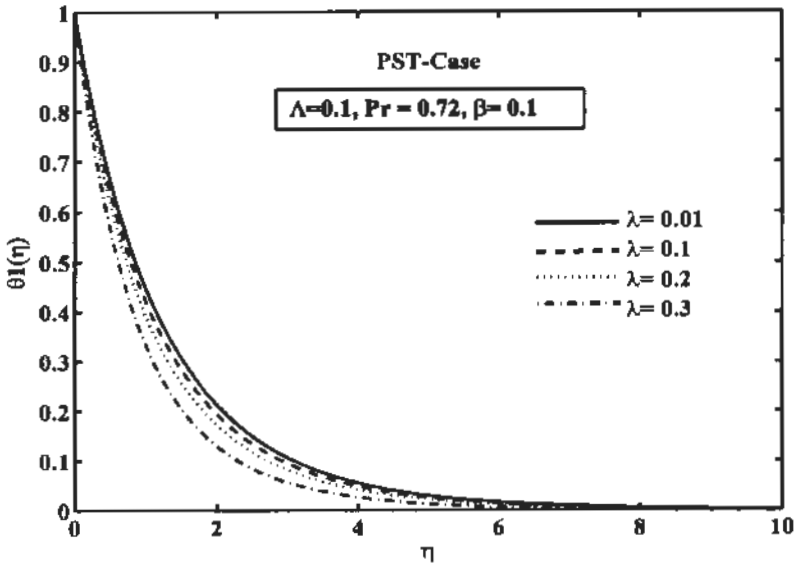

Fig. 5.11. Impact λ on temperature field for PST.

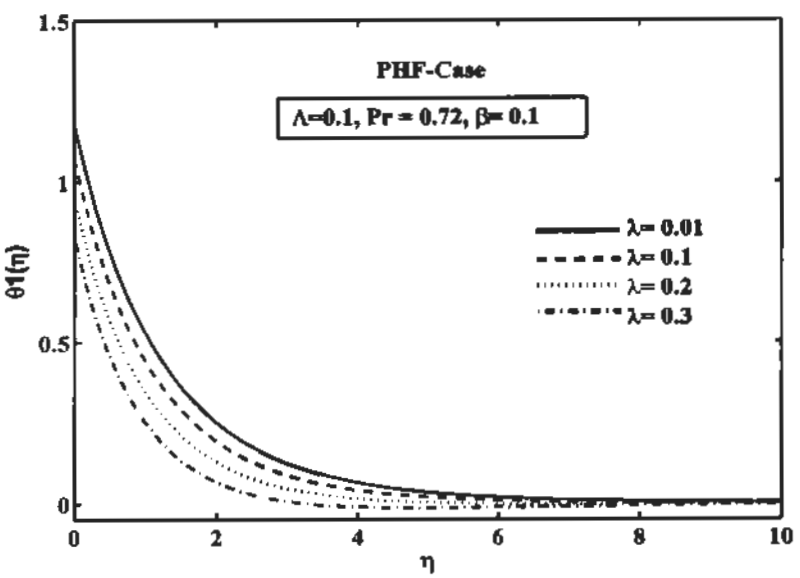

Fig. 5.12. Impact λ on temperature profile for PHF.

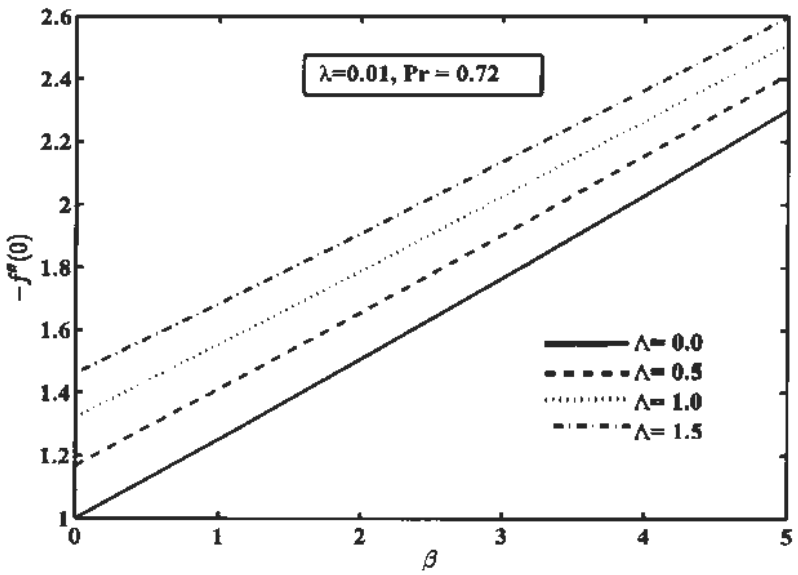

Fig. 5.13. Change of Skin friction coefficient versus β for unsteady parameter Λ.

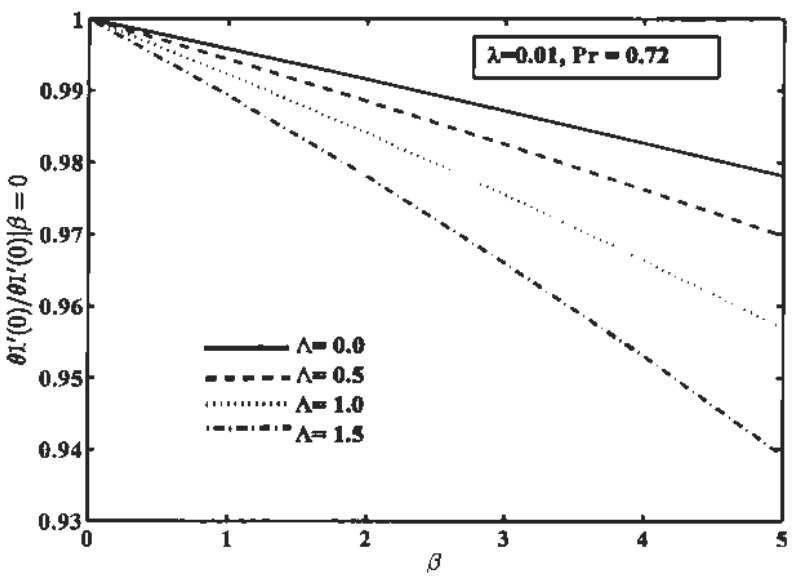

Fig. 5.14. Change of Nusselt number versus β for unsteady parameter Λ.

5.4 Conclusion

In this chapter, we considered heat transport exploration of a time dependent ferromagnetic fluid with the existence of dipole field and prescribed heat flux. The governing boundary layers problem condensed into nonlinear differential equations by means of suitable similarity approach. Velocity profile and temperature fields are also examined under two heating process, like PST and PHF. The influence of Prandtl number (Pr), ferromagnetic parameter (β), viscous dissipation parameter (λ), unsteady parameter (Λ), are displayed graphically in Figs. 5.2 to 5.15. Also the numeric values of $-f''(0)$, heat transfer rate $-\theta_1'(0)$ (PST) and wall temperature $1/\theta_1(0)$ (PHF) are presented in table 5.2. Main finding of the current problem are summarized as follows:

- Velocity is decreases by increasing the value of ferromagnetic interaction parameter β or unsteady parameter (Λ).
- The outcome of viscous dissipation (λ) is to decreases in temperature profile.
- Temperature profile increases for large value of β.
- There is enhancement in heat transfer rate for higher Λ and Pr, whereas decrement occur with the variation of β.

Chapter 6

Heat transfer analysis in ferromagnetic viscoelastic fluid flow over a stretching sheet with suction

6.1 Introduction

In this chapter, two-dimensional analysis has been performed to determine the boundary layer flow and heat transfer characteristic of ferromagnetic viscoelastic liquid flow past a stretching sheet with linear velocity under the action of dipole magnetic field and suction. The governing PDE's are rehabilitated into a system of non-linear ODE's by employing suitable similarity approach. Resulting equations are then solved by applying effective Runge-Kutta Fehlberg technique based on shooting algorithm. Physical interpretation of pertinent flow parameter like Prandtl number, viscoelastic parameter, ferromagnetic interaction parameter, and suction on flow fields, Nusselt number and skin friction coefficient inside the boundary layer are revealed pictorially and discussed, in detail.

6.2 Flow assumption and mathematical formulation

Assume two dimensional viscoelastic ferromagnetic incompressible fluid flow past a stretching surface (see geometry in section 1.17). A circular magnetic field submerge with dipole effect. The governing flow equations includes continuity equation, Naiver Stokes equation with stress tensor of viscoelastic fluid defined in Eq. (1.18) and heat transfer equation along with viscous dissipation takes the form

$$\frac{\partial u}{\partial x}+\frac{\partial v}{\partial y}=0, \tag{6.1}$$

$$\rho\left(u\frac{\partial u}{\partial x}+v\frac{\partial u}{\partial y}\right)=-\frac{\partial p}{\partial x}+\mu_0 M\frac{\partial H}{\partial x}+\mu\left(\frac{\partial^2 u}{\partial x^2}+\frac{\partial^2 u}{\partial y^2}\right)-$$
$$k_0\left[u\frac{\partial^3 u}{\partial x^3}+u\frac{\partial^3 u}{\partial x\partial y^2}+v\frac{\partial^3 u}{\partial x^2\partial y}+v\frac{\partial^3 u}{\partial y^3}-\frac{\partial u}{\partial x}\frac{\partial^2 u}{\partial y^2}-\frac{\partial u}{\partial y}\frac{\partial^2 v}{\partial y^2}-2\left(\frac{\partial u}{\partial x}\frac{\partial^2 u}{\partial x^2}+\frac{\partial v}{\partial y}\frac{\partial^2 u}{\partial y^2}\right)\right], \tag{6.2}$$

$$\rho\left(u\frac{\partial v}{\partial x}+v\frac{\partial v}{\partial y}\right)=-\frac{\partial p}{\partial y}+\mu_0 M\frac{\partial H}{\partial y}+\mu\left(\frac{\partial^2 v}{\partial x^2}+\frac{\partial^2 v}{\partial y^2}\right)-$$
$$k_0\left[u\frac{\partial^3 v}{\partial x^3}+u\frac{\partial^3 v}{\partial x\partial y^2}+v\frac{\partial^3 v}{\partial x^2\partial y}+v\frac{\partial^3 v}{\partial y^3}-\frac{\partial v}{\partial x}\frac{\partial^2 u}{\partial y^2}-\frac{\partial v}{\partial y}\frac{\partial^2 v}{\partial y^2}-2\left(\frac{\partial u}{\partial x}\frac{\partial^2 v}{\partial x^2}+\frac{\partial v}{\partial y}\frac{\partial^2 v}{\partial y^2}\right)\right], \tag{6.3}$$

$$\rho c_p\left(u\frac{\partial T}{\partial x}+v\frac{\partial T}{\partial y}\right)+\mu_0 T\frac{\partial M}{\partial T}\left(u\frac{\partial H}{\partial x}+v\frac{\partial H}{\partial y}\right)=k\left(\frac{\partial^2 T}{\partial x^2}+\frac{\partial^2 T}{\partial y^2}\right)+$$
$$\mu\left[2\left(\frac{\partial u}{\partial x}\right)^2+2\left(\frac{\partial v}{\partial y}\right)^2+\left(\frac{\partial v}{\partial x}+\frac{\partial u}{\partial y}\right)^2\right]-k_0\left(\frac{\partial u}{\partial y}\right)\frac{\partial}{\partial y}\left(u\frac{\partial u}{\partial x}+v\frac{\partial u}{\partial y}\right). \tag{6.4}$$

The corresponding boundary relation for stretching sheet and suction at the wall is specified as

$$\left.\begin{aligned} &u=u_w,\quad v=-v_w,\quad T=T_w \qquad \text{at}\ \ y=0\\ &u=0,\ \frac{\partial u}{\partial y}=0,\ T=T_c,\ p+\frac{1}{2}\rho(u^2+v^2)=\text{constant}\ \ \text{as}\ \ y\to\infty \end{aligned}\right\}. \tag{6.5}$$

By applying similarities Eqs. (1.64) and (1.65) into the Eqs. (6.2) to (6.5), we acquire the system of ordinary equations.

$$f'''+ff''-f'^2+2P_2+\frac{2\beta\theta_1}{(\eta+\alpha_1)^4}-\lambda^*\left[2ff'''-ff^{iv}+(f'')^2\right]=0, \tag{6.6}$$

$$P_1'-f''-ff'-\frac{2\beta\theta_1}{(\eta+\alpha_1)^3}-\lambda^*\left[ff'''-3ff''\right]=0, \tag{6.7}$$

$$P_2'-\frac{2\beta\theta_2}{(\eta+\alpha_1)^3}+\frac{4\beta\theta_1}{(\eta+\alpha_1)^5}=0, \tag{6.8}$$

$$\theta_1''+\Pr f\theta_1'+\frac{2\lambda\beta(\theta_1-\varepsilon)f}{(\eta+\alpha_1)^3}+2\theta_2-4\lambda(f')^2=0, \tag{6.9}$$

$$\theta_2''+\Pr\left(f\theta_2'-2f'\theta_2\right)-\lambda\beta\left(\theta_1-\varepsilon\right)\left[\frac{2f'}{(\eta+\alpha_1)^4}+\frac{4f}{(\eta+\alpha_1)^5}\right]$$
$$+\left[\frac{2\lambda\beta f\theta_2}{(\eta+\alpha_1)^3}+\lambda\left(ff''^2-ff'f'''\right)-\lambda(f'')^2\right]=0. \tag{6.10}$$

Also boundary conditions (6.5) are converted as

$$\left.\begin{aligned} &f=S,\ \ f'=1,\ \ \theta_1=1,\ \ \theta_2=0, \qquad \text{at}\ \ \eta=0\\ &f'\to 0,\ f''\to 0,\ \theta_1\to 0,\ \ \theta_2\to 0,\ \ P_1\to -P_\infty,\ \ P_2\to 0\ \ \text{as}\ \ \eta\to\infty \end{aligned}\right\}. \tag{6.11}$$

Here $\lambda^* = \frac{k_0 c}{\mu}$ is the viscoelastic parameter. Physical point of view, the supreme authoritative quantities are skin friction and rate of heat transfer are specified in Eqs. (2.14) and (2.15) using

$$\tau_w = \left(1-\lambda^*\right)\mu\left(\frac{\partial u}{\partial y}\right)_{y=0} \tag{6.12}$$

and employing similarity approach from Eqs. (1.64) and (1.65), we have

$$C_f \,\mathrm{Re}_x^{1/2} = -2\left(1-\lambda^*\right) f''(0), \qquad Nu_x / \mathrm{Re}_x^{1/2} = -\left(\theta_1'(0) + \xi^2 \theta_2'(0)\right). \tag{6.13}$$

6.3 Results and discussion

The influence of various pertinent parameter such as, viscoelastic parameter λ^*, ferromagnetic thermos-mechanical parameter β, Prandtl number Pr and suction parameter S on the flow behavior of ferromagnetic viscoelastic fluid are studied through graphs. The numerical values to the controlling physical parameter throughout the problem are taken as $Pr = 7$, $\lambda = 0.01$, $\varepsilon = 2.0$, $\alpha_1 = 1.0$. Figs. 6.1 to 6.3 has been drawn to highlights the impact of β on velocity $f'(\eta)$, temperature $\theta_1(\eta)$ and pressure profile $P_2(\eta)$. Fig. 6.1 illustrate the effect of external magnetic field generated through dipole on dynamics of fluid. So occurrence of ferromagnetic parameter β, it is simply notice that velocity of the fluid decreases for higher values of β. Infect an increment in β boosts up the Lorentz force which has a tendency to resist the fluid motion, consequently fluid velocity reduces. Fig. 6.2 pointed out the influence of β on temperature profile. It is detected that temperature of the fluid increases expressively for higher value of β. This is because of resistance among the fluid particles enhances, so that more heat is produced, so fluid temperature rises. Fig. 6.3 establishes that pressure P_2 enhances monotonically for larger values of β. It is fascinating to distinguish that for hydrodynamic case $(\beta = 0)$, the value P_2 become constant and equal to zero at infinity, so we obtained exact analytical result found by Crane [136] represented by symbols as shown in Fig. 6.3. Figs. 6.4 to 6.6 shows the influence of viscoelastic parameter λ^* on stream function $f(\eta)$, velocity $f'(\eta)$ and temperature field $\theta_1(\eta)$ against η. This graphs confirm that by increasing the values of viscoelastic parameter λ^* restrict the motion of fluid adjacent to stretching surface whereas assists fluid motion which away from the stretching surface. By rising the values of λ^* permits the fluid to flow at a faster rate, due to this there is reduction in heat transfer rate. It is

answerable for increase in momentum phenomena. So for larger values of λ^* the non-dimensional stream function and velocity increases, although temperature is reduces. Figs. 6.7 and 6.8 designate the velocity and temperature field, once $\beta = 0.1$, $Pr = 7$ and $\lambda^* = 0.1$ for innumerable values of suction parameter S. From graphs it is witnessed that velocity reduces meaningfully for increasing suction parameter. Also perceived that, boundary layer thickness decreases when wall suction $(S > 0)$ and temperature declines due to increase in suction parameter as displayed in fig. 6.8.

Fig. 6.9 represent the behavior of Prandtl number Pr on temperature field. Results clarify that the influence of Pr is to reduce the fluid temperature, which subsequently diminishes associated boundary layer thickness for higher values of Pr. For greater values of Pr means slow rate of thermal diffusion. Figs. 6.10 to 6.12 depicts the heat transfer rate, pressure profile and skin friction with the deviation of ferromagnetic parameter β for dissimilar values of viscoelastic parameter λ^*. Graphs simply clarify that coefficient of skin friction and pressure profile increases for β and reduces with an increase in λ^*. Fig. 6.11 is drawn to seen the impact of heat transfer rate diminish by varying β, along x-axis, whereas reverse effect occurs for λ^*.

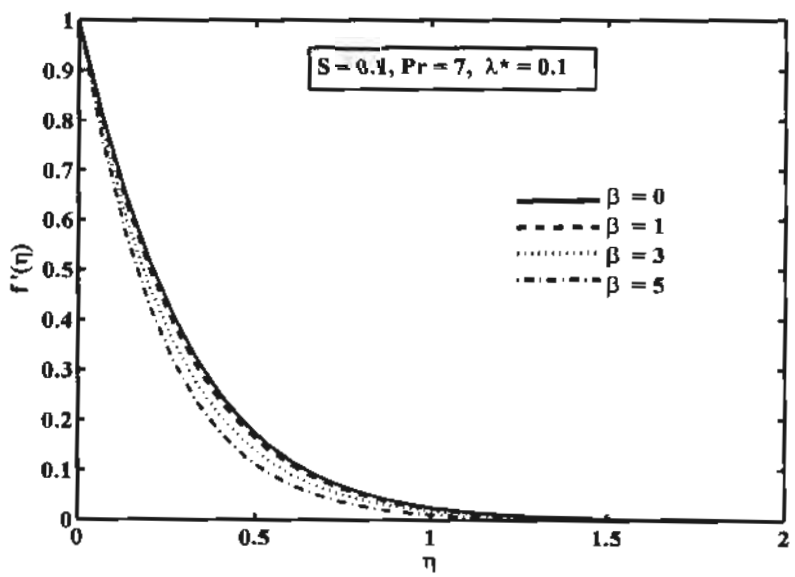

Fig. 6.1. Impact of β on velocity profile against η.

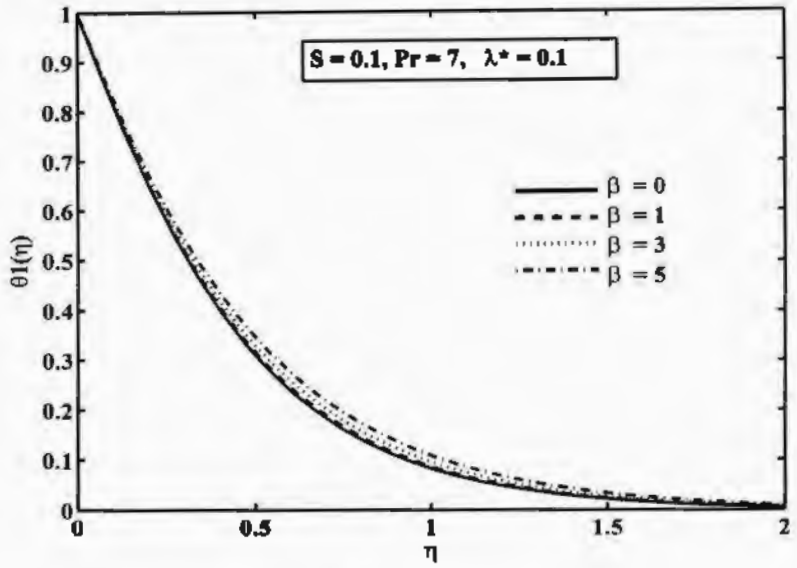

Fig. 6.2. Impact of β on temperature field versus η .

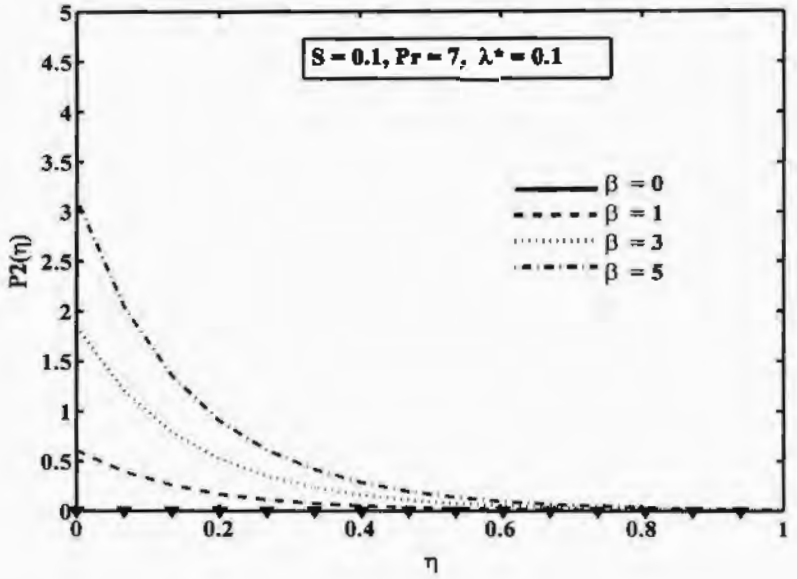

Fig. 6.3. Impact of β on pressure profile versus η .

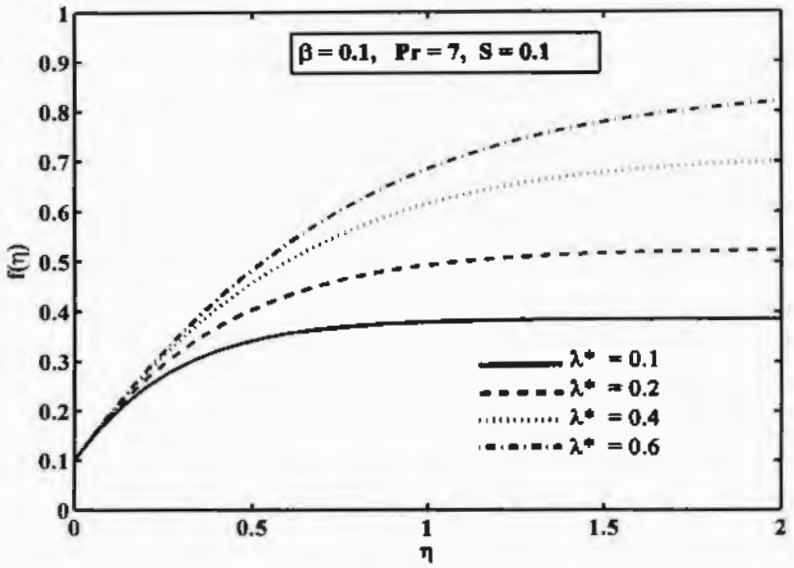

Fig. 6.4. Impact of λ^* on function f versus η.

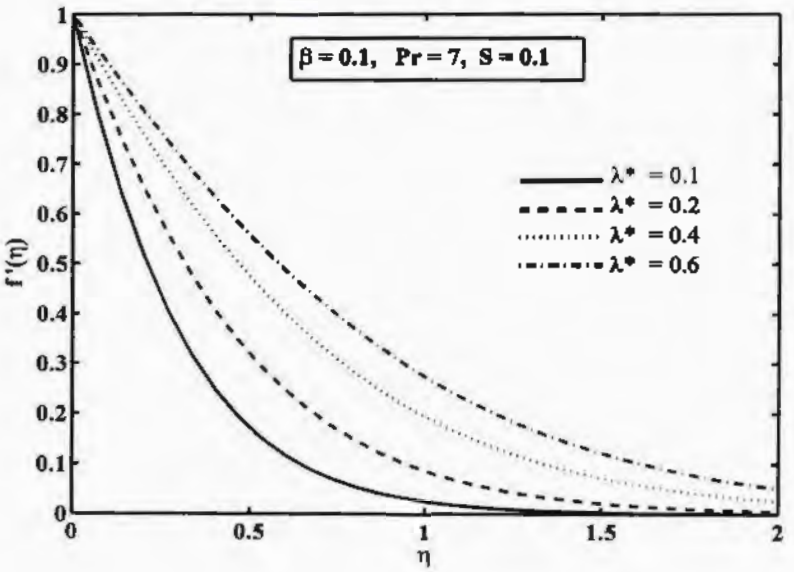

Fig. 6.5. Impact of λ^* on velocity profile versus η.

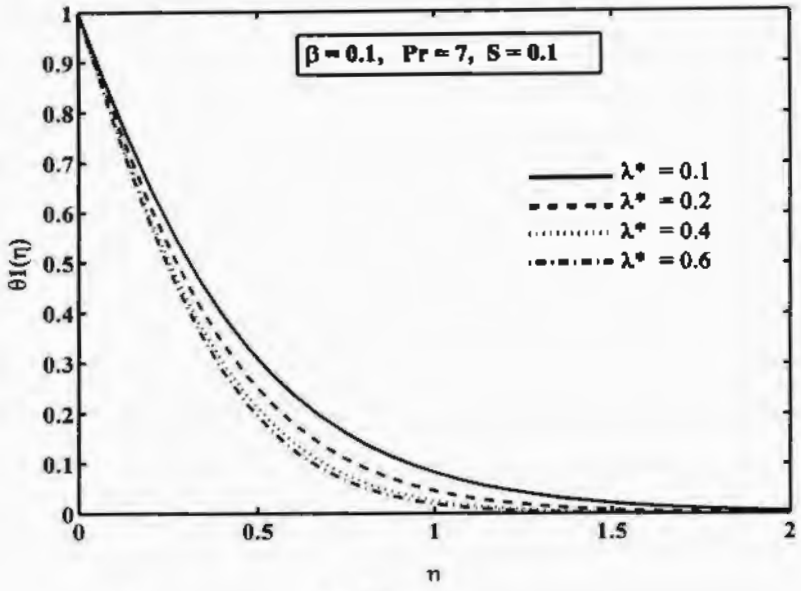

Fig. 6.6. Impact of λ^* on temperature field versus η .

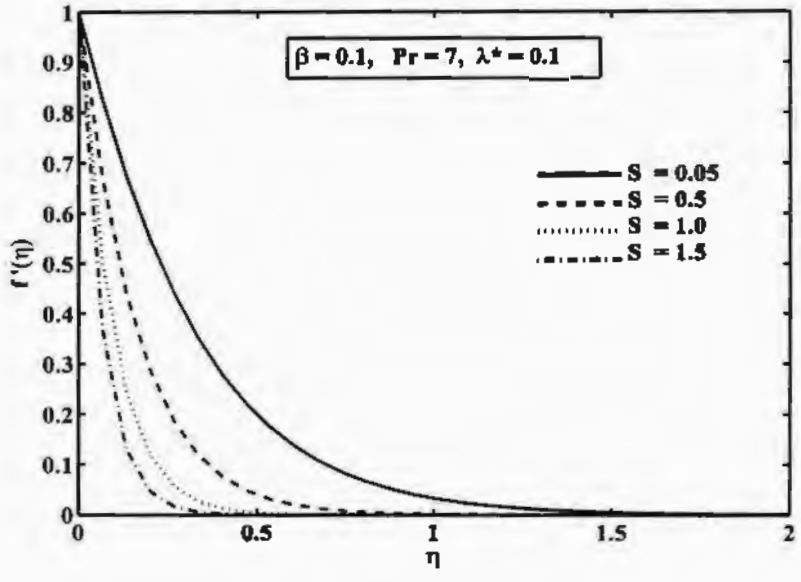

Fig. 6.7. Impact of S on velocity field versus η .

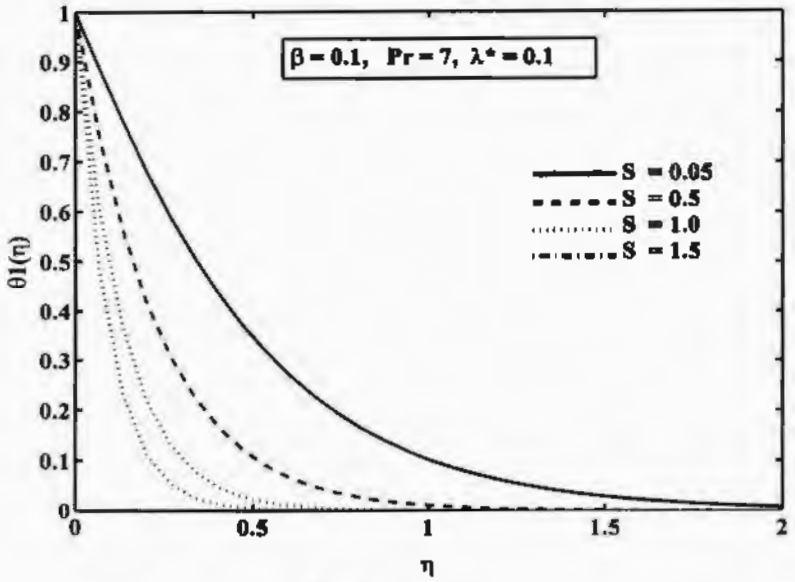

Fig. 6.8. Impact of S on temperature field versus η .

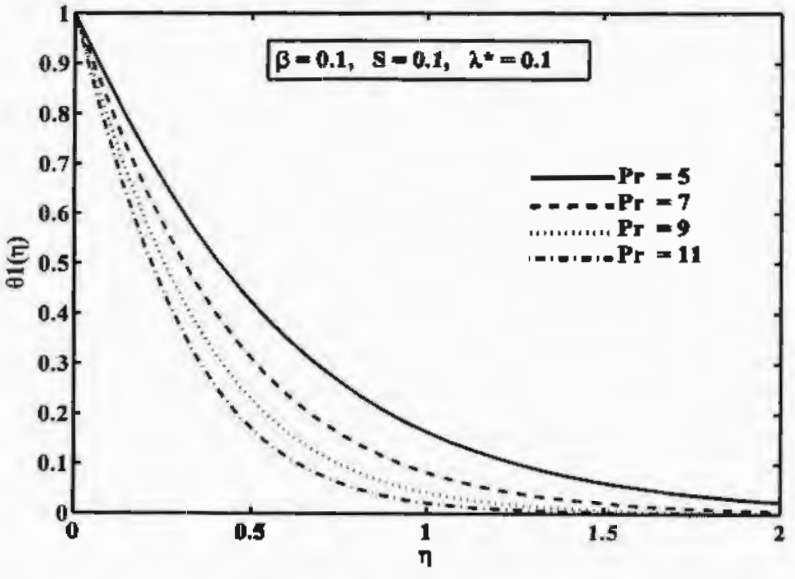

Fig. 6.9. Impact of Pr on temperature field versus η .

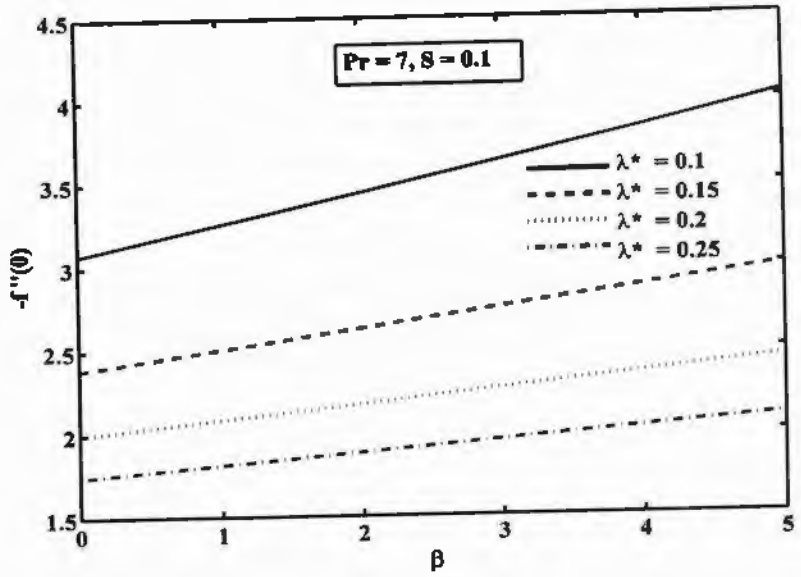

Fig. 6.10. Impact of λ^* on skin friction coefficient versus β.

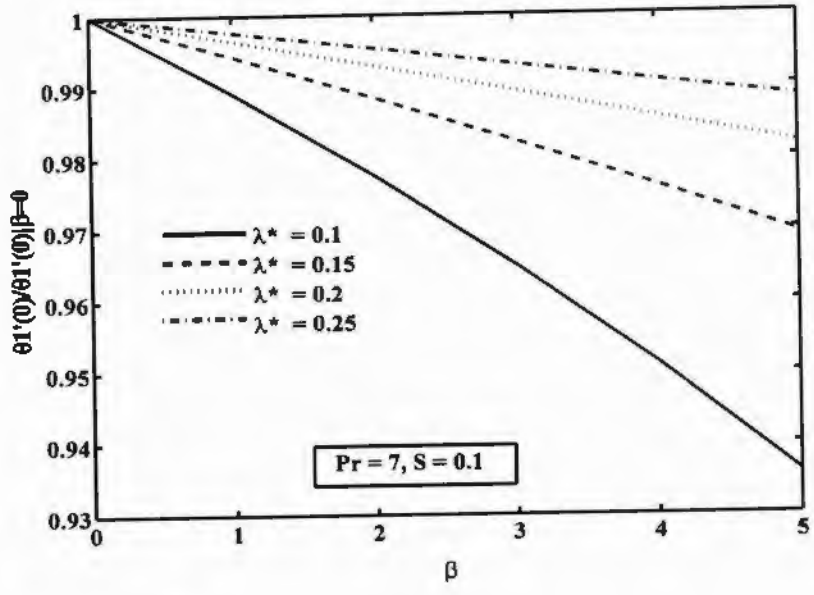

Fig. 6.11. Impact of λ^* on Nusselt number versus β.

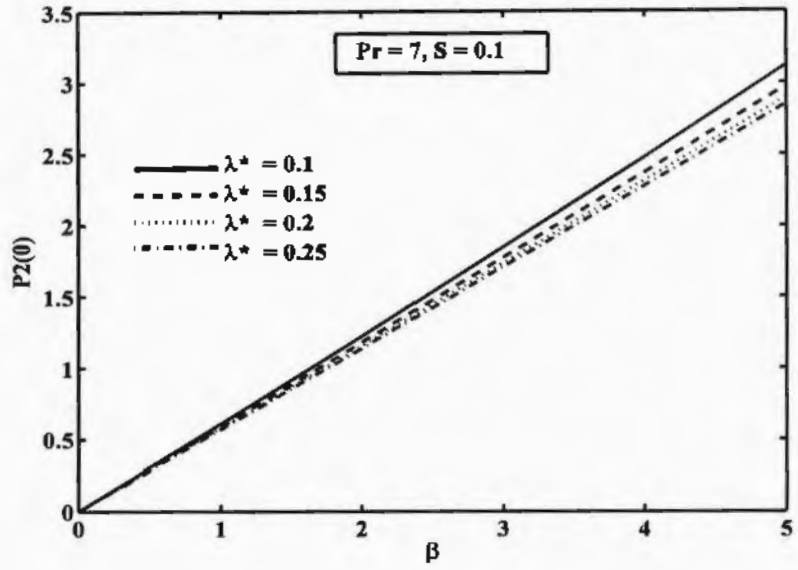

Fig. 6.12. Influence of λ^* on pressure profile versus β.

6.4 Conclusion

We have theoretically investigated two-dimensional ferromagnetic viscoelastic fluid flow embedded with dipole past a stretching surface. The governing equations for the flow problems were converted into ODE's by adopting similarity procedure. The resulting system of equations were tackled numerically by utilizing robust shooting technique along with Runga-Kutta algorithm. The impact of various values of pertinent parameters namely, viscoelastic parameter (λ^*), ferromagnetic interaction parameter (β), suction parameter (S) and Prandtl number (Pr) on common profiles are display via graphs. From the current study following outcomes are listed below:

- The function f and velocity $f'(\eta)$ increases with λ^*.
- Temperature decreases for higher values of Pr.
- Nusselt number decreases with the variation of β.
- Pressure profile and Skin friction coefficient increases against β.

Chapter 7

Chemical reaction and heat transfer on boundary layer Maxwell ferro-fluid flow under magnetic dipole with Soret and suction effects

7.1 Introduction

In this chapter, the stimulus of chemical reaction and heat transfer analysis of saturated Maxwell Ferro-fluid flow past a stretchable surface beneath the inspiration of dipole magnetic field with Soret and suction effects are investigated. The sheet is supposed to be permeable in a semi-infinite domain. Firstly, partial differential equations for the governing flow problem are modelled and rehabilitated into a system of equations by utilizing similarity approach. Then the solution of required non-linear differential equations is obtained by efficient Runge-Kutta Fehlberg technique based on shooting algorithm using MTLAB package. Effect of all appropriate parameters like Schmidt number, ferromagnetic interaction parameter, chemical reaction parameter, Deborah number, Soret number, suction parameter on dimensionless, temperature and concentration are confirmed via graphs and table. The discussion of sundry physical parameters is provided in detail along with results in pictorial and tabular form.

7.2 Flow assumption and mathematical formulation

Consider incompressible, two-dimensional chemical, reactive ferromagnetic liquid flow with heat and mass transfer under the impact of single magnetic dipole (see geometry section 1.17). By introducing Boussineq's boundary layer assumptions, the governing equation involving continuity and Navier Stokes equation employing the stress tensor of Maxwell fluid defined in Eq. (1.17) with energy and mass transport are

$$\frac{\partial u}{\partial x}+\frac{\partial v}{\partial y}=0, \tag{7.1}$$

$$u\frac{\partial u}{\partial x}+v\frac{\partial u}{\partial y}+\lambda_1\left(u^2\frac{\partial^2 u}{\partial x^2}+v^2\frac{\partial^2 u}{\partial y^2}+2uv\frac{\partial^2 u}{\partial x\partial y}\right)=\frac{\mu_0}{\rho}M\frac{\partial H}{\partial x}+\nu\frac{\partial^2 u}{\partial y^2}, \tag{7.2}$$

$$\left(u\frac{\partial T}{\partial x}+v\frac{\partial T}{\partial y}\right)+\frac{\mu_0 T}{\rho c_p}\frac{\partial M}{\partial T}\left(u\frac{\partial H}{\partial x}+v\frac{\partial H}{\partial y}\right)=\frac{k}{\rho c_p}\frac{\partial^2 T}{\partial y^2}$$
$$+\frac{Dk_T}{c_s c_p}\frac{\partial^2 C}{\partial y^2}+\frac{k}{\rho c_p}\left[\mu\left(\frac{\partial u}{\partial y}\right)^2+2\mu\left(\frac{\partial v}{\partial y}\right)^2\right], \tag{7.3}$$

$$u\frac{\partial C}{\partial x}+v\frac{\partial C}{\partial y}=D\frac{\partial^2 C}{\partial y^2}-k_0(C-C_\infty)+\frac{Dk_T}{T_m}\frac{\partial^2 T}{\partial y^2}, \tag{7.4}$$

$$\begin{aligned} &u=u_w=cx,\quad v=v_w,\quad C=C_w \quad \text{at} \quad y=0,\\ &u\to 0,\quad \frac{\partial u}{\partial y}\to 0,\quad C\to C_\infty \quad \text{as} \quad y\to\infty, \end{aligned} \tag{7.5}$$

along with PST for temperature (1.59). Using similarity transformation Eqs. (1.64) and (1.65) into the Eqs. (7.2) to (7.5), and comparing coefficients up to ξ^2, we get

$$f'''\left(1-\gamma_1 f^2\right)-\left(f''^2-ff''\right)+2\gamma_1 ff'f''-\frac{2\beta\theta_1}{\left(\eta+\alpha_1\right)^4}=0, \tag{7.6}$$

$$\theta_1''+\Pr(f\theta_1'-2f'\theta_1)+\frac{2\lambda\beta(\theta_1-\varepsilon)f}{\left(\eta+\alpha_1\right)^3}-2\lambda f'^2-D_r\phi''=0, \tag{7.7}$$

$$\theta_2''-\Pr\left(4f'\theta_2-f\theta_2'\right)+\frac{2\lambda\beta\theta_2 f}{\left(\eta+\alpha_1\right)^3}-\lambda\beta\left(\theta_1-\varepsilon\right)\left[\frac{2f'}{\left(\eta+\alpha_1\right)^4}+\frac{4f}{\left(\eta+\alpha_1\right)^5}\right]-\lambda f''^2=0, \tag{7.8}$$

$$\phi''+S_c\left(f\phi'-k_1\phi+S_r\theta_1''\right) \tag{7.9}$$

The initial and boundary conditions (7.5) are renovated as

$$\left.\begin{aligned} &f=S,\quad f'=1,\quad \theta_1=1,\quad \theta_2=0,\quad \phi=1,\quad \text{at } \eta=0\\ &f'\to 0,\quad \theta_1\to 0,\quad \theta_2\to 0,\quad \phi\to 0\quad \text{as } \eta\to\infty \end{aligned}\right\}. \tag{7.10}$$

The new non-dimension quantities occur in Eqs. (7.6) to (7.9) are

$$\left.\begin{aligned} &\gamma_1=\lambda_1 c,\quad S_r=\frac{Dk_T\left(T_c-T_w\right)}{T_m\nu\left(C_\infty-C_w\right)},\quad K_r=\frac{k_0}{c},\quad S_c=\frac{\nu}{D^*}, \end{aligned}\right\}, \tag{7.11}$$

where γ_1 is Deborah number, λ is viscous dissipation parameter, S_c is Schmidt number, S_r in Soret number, κ_r is chemical reaction parameter. Concerning capacities of practical concern are friction of skin, rate of heat transfer, and Sherwood number, which can be expressed as:

$$C_{fx} = \frac{-\tau_w}{\rho(cx)^2}, \quad Nu_x = \frac{xq_w}{-k(T_c - T_w)}, \quad Sh_x = \frac{xJ_w}{D_e(C_w - C_\infty)}, \tag{7.12}$$

where

$$\tau_w = \mu(1+\gamma_1)\left(\frac{\partial u}{\partial y}\right)_{y=0}, q_w = -k\left(\frac{\partial T}{\partial y}\right)_{y=0}, J_w = -D_e\left(\frac{\partial C}{\partial y}\right)_{y=0}. \tag{7.13}$$

Using the relation from Eqs. (1.64) to (1.65), we obtain

$$\left.\begin{aligned} C_f Re_x^{1/2} &= -(1+\gamma_1) f''(0) \\ Nu_x / Re_x^{1/2} &= -\left(\theta_1'(0) + \xi^2 \theta_2'(0)\right) \\ Sh_x / Re_x^{1/2} &= -\phi'(0) \end{aligned}\right\}. \tag{7.14}$$

7.3. Results and discussion

In this section, comprehensive numerical experiments are conducted for several pertinent governing constraints that designate the flow pattern and results are demonstrated through pictorially and tabular form. Figures are drawn for velocity, temperature, and concentration profiles against ferromagnetic interaction parameter, Soret number, chemical reaction parameter, Deborah number, suction parameter and Schmidt number. The values of the emerging parameter throughout the problem are taken as $Pr = 7$, $\beta = 0.1$, $\gamma_1 = 0.1$, $\lambda = 0.01$, $S = 0.1$, $S_r = 0.5$, $S_c = 0.5$, $K_r = 0.2$, $\varepsilon = 2.0$, $\alpha_1 = 1.0$. The comparison is given in table 7.1, showing a marvellous agreement with the published data. Fig. 7.1. illustrate the concentration profile for some values of the Soret number. From the figure it is perceived that increase in *Sr*, concentration of fluid is growing boundary layer region because of involvement of temperature gradients in species diffusion escalations the concentration. The impact of Schmidt number *Sc* on dimensionless concentration profiles is pointed out in fig. 7.2. It is simply apparent from the figure that concentration in boundary layer thickness suppressed by enlarging the Schmidt number. By definition, *Sc* is inversely varied to the diffusion coefficient D^*. Also observed that *Sc* defined electiveness of the momentum diffusion in hydrodynamic flow to the species diffusion in concentration field. So higher values of *Sc* causes reduction in concentration field. Chemical reaction parameter shows similar behavior as the Schmidt number on concentration profile. By analyzing the influence of a destructive chemical reaction parameter ($K_r > 0$) caused a reduction in the concentration diffusion species. Physical point of view chemical reaction for destructive case is very large. Because of this fact molecular motion is quite higher which enhances the transport phenomenon, thus suppressing the concentration field in the fluid

flow as display in fig. 7.3. Figs. 7.4 to 7.6 classify the impact of ferromagnetic interaction parameter on dimensionless velocity, temperature and concentration fields. The outcome of the magnetic field due to magnetic dipole demonstrates through a ferromagnetic parameter β. The existence of magnetic effects acts as retarding force on fluid velocity and thereby as rises, so does retarding force and hereafter the results in suppressing the velocity profile $f'(\eta)$ as seen in fig. 7.4. Because, this occurs owing to the effect of Lorentz force which opposes the flow and produces more resistance to the transport phenomena. Because there is an interference among fluid motion and the action of external magnetic field. This kind of interference decreases the velocity and rising the frictional heating involving within the fluid layers which are accountable for increment in concentration and heat profiles as cleared in fig. 7.5 and fig. 7.6.

Figs. 7.7 to 7.9 inaugurate the consequence of Deborah number γ_1 on dimensionless velocity, temperature and concentration fields. It is perceived that when Deborah number increases, then the fluid velocity is declined at any point above the sheet and reduction in boundary layer for large value of γ_1. From a physical point of view, when shear stress is eliminated, fluid will come to rest. This sort of phenomena is shown in many polymeric liquids that cannot be defined in the Newtonian fluid model. A large value of Deborah number will produce a retarding force between two adjacent layers in the flow. Due to this, there is a reduction in the velocity as seen in fig. 7.7. Also observed that temperature and concentration profile enhances by enlarging the Deborah number, because the thickening of the thermal and solute boundary layer happens for increasing the elasticity stress parameter as confirmed in figs. 7.8 and 7.9. The impact of suction constraint S on temperature and concentration profile explained through figs. 7.10 and 7.11. It is detected that both velocity and concentration decreases expressively by rising suction parameter. This behavior occurs due to appearance of suction at the surface, which is the result to draw the quantity of fluid on the surface and therefore boundary layer flow becomes thinner and both thermal, and species boundary layer gets slowed down by enlarging S. figs. 7.12 and 7.13 shows the impact of Deborah number on skin friction and Sherwood number for versus β. Graphs clarify that increasing the values of Deborah number causes enhancement in the skin friction, whereas decrement in Sherwood number. Physical point of view, at greater Deborah number, the material performance converted to non-Newtonian regime, gradually controlled by elasticity, signifying solid-like response, hence high skin friction.

Table 7.1. Comparison of Nusselt number for the case of $\beta = \lambda = \gamma_1 = S = K_r = S_r = S_c$

Pr	Abel et al. [128]	Chen [126]	Present results
0.72	1.0885	1.0885	1.088527
1	1.3333	1.3333	1.333333
3	----	2.5097	2.509725
10	4.7968	4.7968	4.796873

Table 7.2. Skin friction $-f''(0)$, Nusselt number $-\theta'_1$ and Sherwood number $-\emptyset'(0)$ for β, $\gamma_1, S_r, Sc, K_r, S$

β	γ_1	S_r	Sc	K_r	S	$-(1+\gamma_1)f''(0)$	$-\theta_1'(0)$	$-\emptyset'(0)$
0.5	0.1	0.5	0.5	0.2	0.1	0.1336	2.0799	0.5449
0.7						0.1920	2.0733	0.5422
1.2						0.3391	2.0564	0.5352
0.5	0.1	0.5	1.0	0.2	0.1		--	0.7482
			1.5				--	0.8821
			2.0				--	0.9830
0.5	0.5	0.5	0.5	0.2	0.1	0.1301	2.0345	0.5108
	0.7					0.2663	2.0131	0.4962
	1.2					0.6154	1.9620	0.4650
0.5	0.1	0.5	0.5	0.2	0.1		--	0.5449
				0.4			--	0.6250
				0.6			--	0.6950
0.5	0.1	0.5	0.5	0.2	0.2	0.1997	2.1852	0.5324
					0.4	0.3474	2.4095	0.5047
					0.6	0.5189	2.6514	0.4737
0.5	0.1	0.5	0.5	0.2	0.1		--	0.5449
		0.7					--	0.3880
		1.2					--	-0.0044

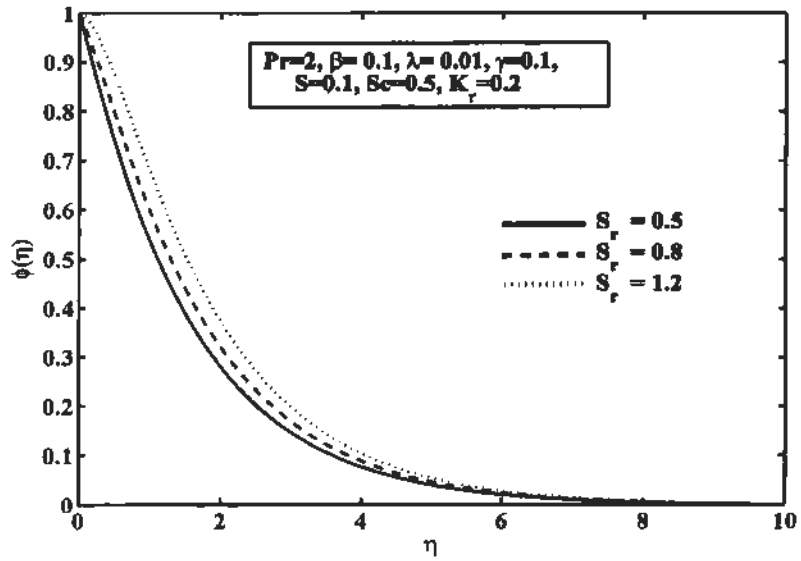

Fig. 7.1. Impact of S_r on concentration profile.

.

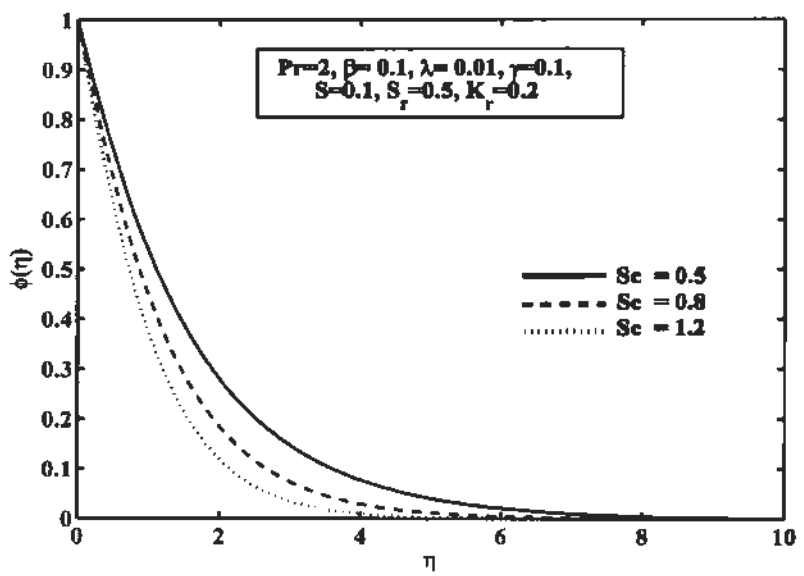

Fig. 7.2. Impact of *Sc* on concentration profile.

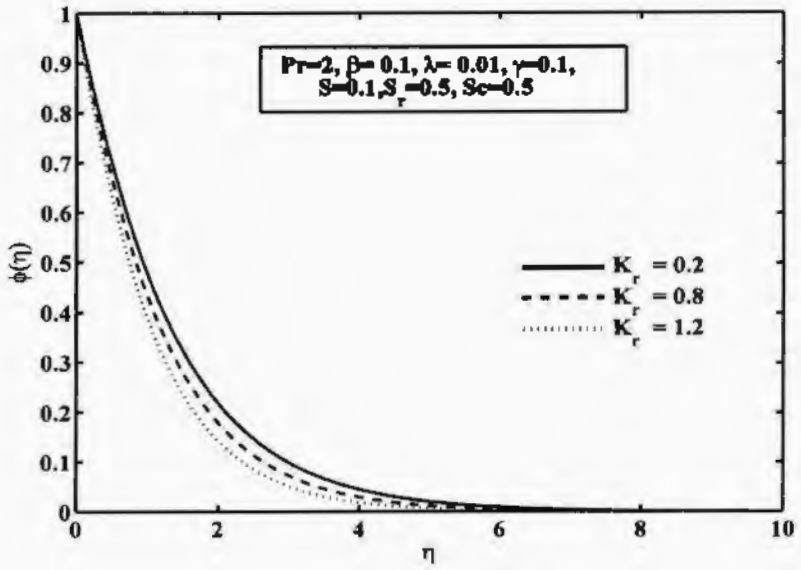

Fig. 7.3. Impact of K_r on concentration profile.

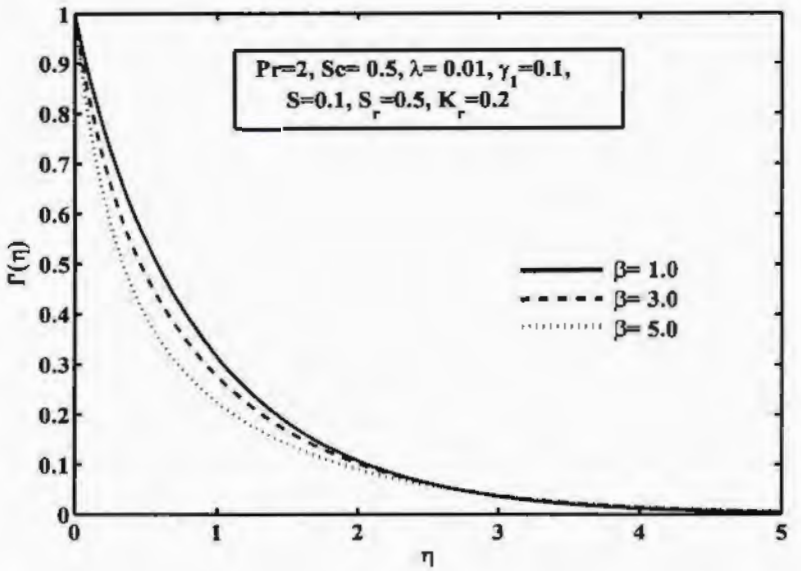

Fig. 7.4. Impact of β on velocity profile.

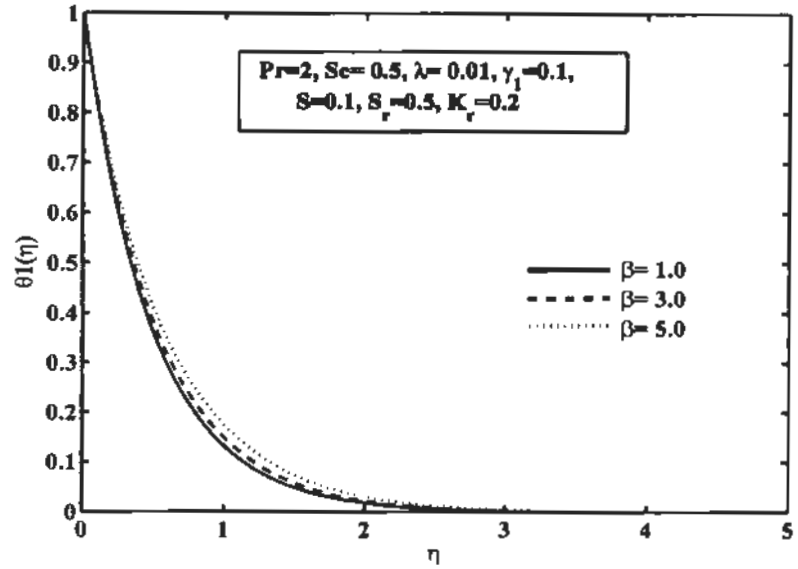

Fig. 7.5. Impact of β on temperature field.

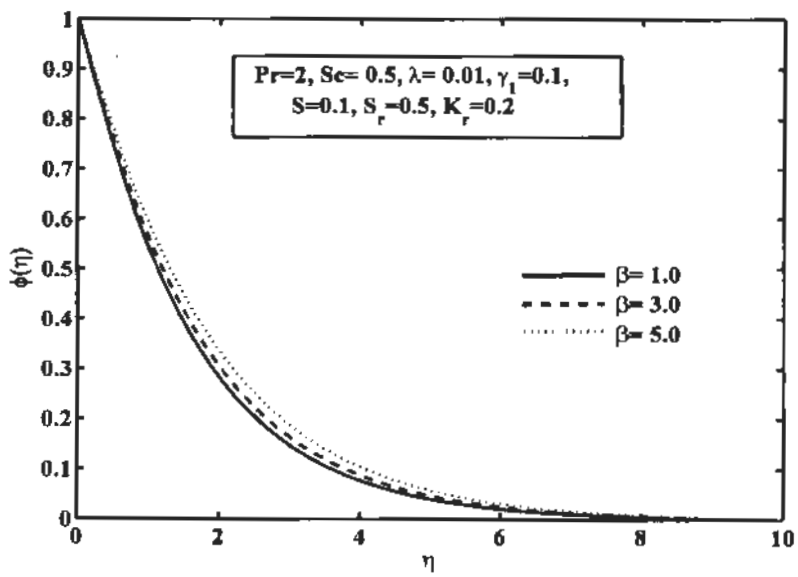

Fig. 7.6. Impact of β on temperature field.

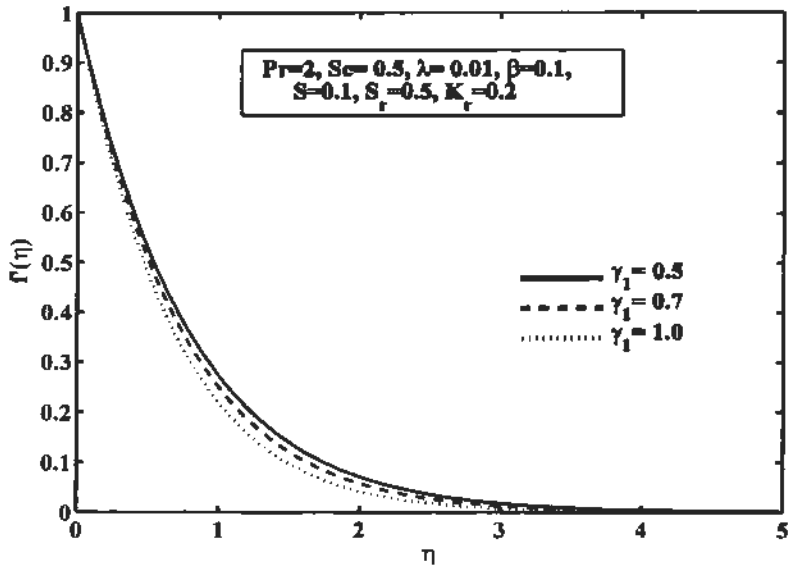

Fig. 7.7. Impact of γ_1 on velocity field.

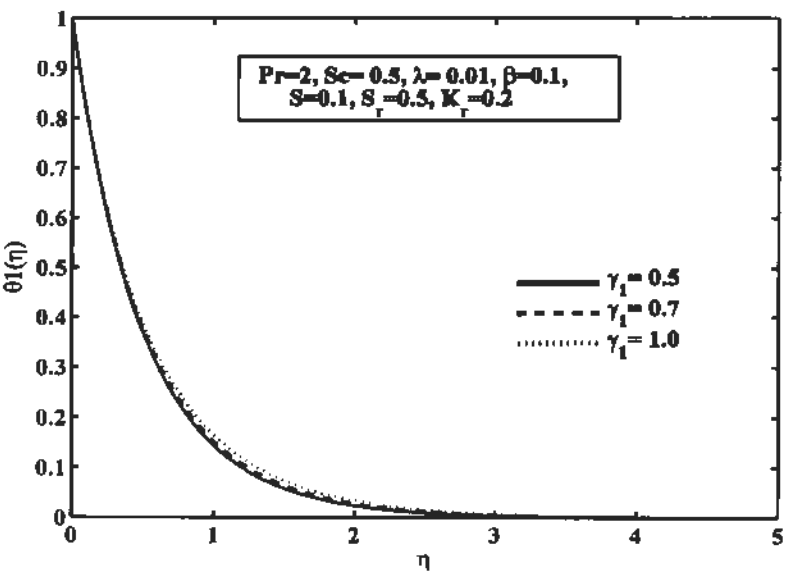

Fig. 7.8. Impact of γ_1 on temperature field.

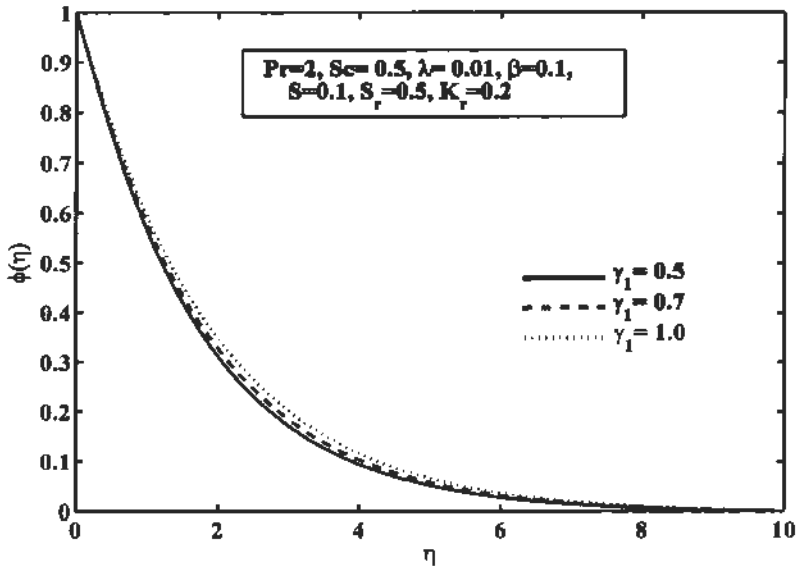

Fig. 7.9. Impact of γ_1 on concentration field.

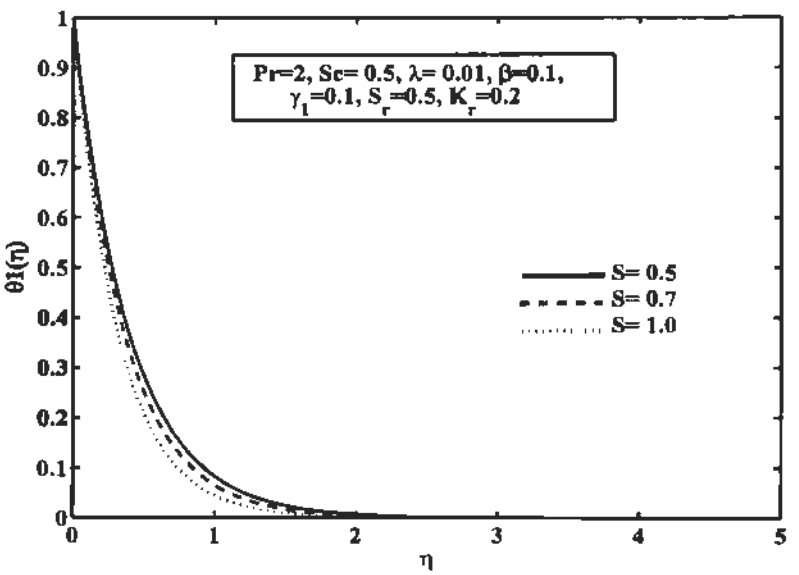

Fig. 7.10. Impact of S on temperature field.

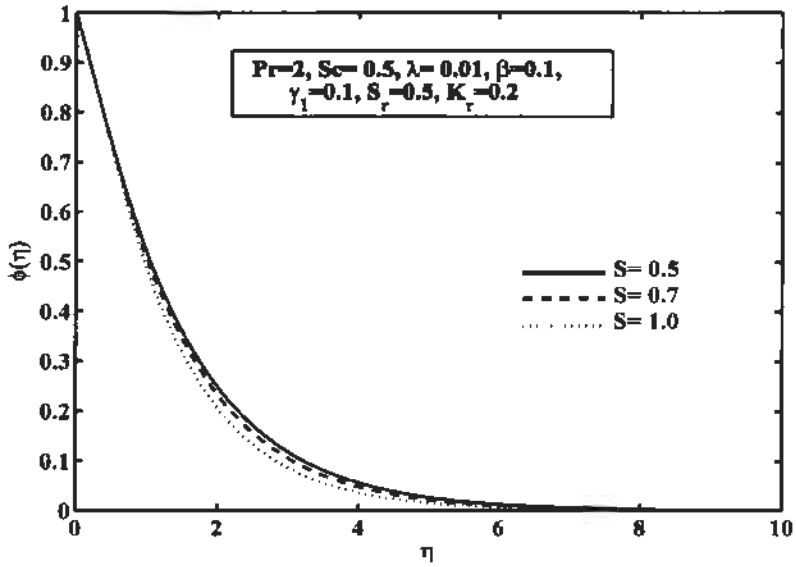

Fig. 7.11. Impact of S on concentration field.

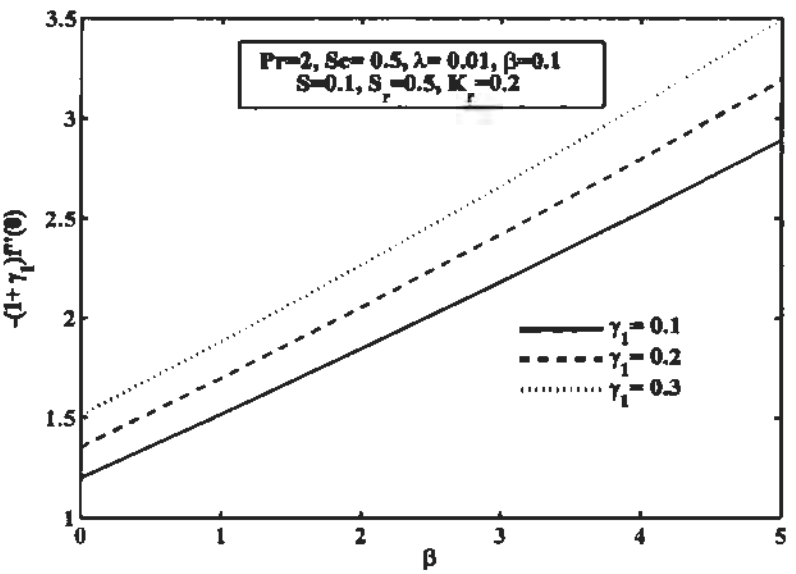

Fig. 7.12. Impact of γ_1 on Skin friction coefficient versus β.

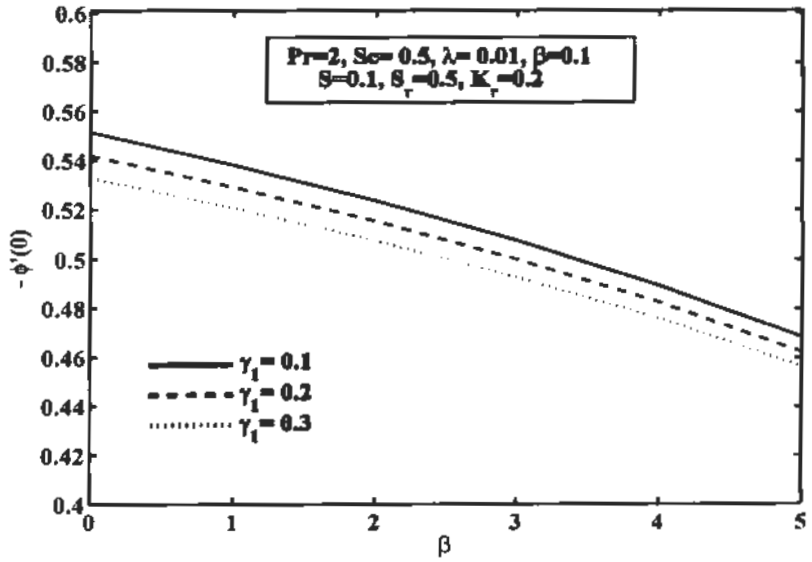

Fig. 7.13. Influence of γ_1 on Sherwood number versus β.

7.4 Conclusion

In this investigation, the problem of boundary layer heat and mass transfer with chemically reactive Maxwell Ferro-fluid flow over a stretching sheet under the influence of single dipole have studied. Mathematical equations are modelled and converted into ODE's, then solved numerically by adopting Runge-Kutta based shooting technique with MATLAB package. Some effective governing parameter on the flow problem like chemical reaction parameter (K_r), Deborah number (γ_1), ferromagnetic interaction parameter (β), suction parameter (S), Soret number (S_r), Schmidt number (S_c) on velocity profile, temperature profile, concentration filed, skin friction, heat transfer rate and Sherwood number are sketched graphically and elucidated in detail. Heat transfer rate is taken against Pr which is increased approximately 18%, 56.6% and 77% at Prandtl number 1.0, 3.0 and 10. Some of the major observations of the current flow problem are elaborated as follows:

- Fluid velocity is flattening for larger values of suction and ferromagnetic parameter.
- Nusselt number and Sherwood number decreases by increasing chemical reaction and ferromagnetic interaction parameter, whereas reverse effect in noted for Skin friction coefficient as seen in table 7.2.
- Both concentration and temperature field enhances with increasing Deborah number.
- Rising the values of Schmidt number is to reduce the concentration profile and reverse nature is found for Sort number.

Chapter 8

Impact of Cattaneo-Christov heat flux model on the flow of Maxwell ferromagnetic liquid along a cold flat plate embedded with two equally magnetic dipole

8.1 Introduction

The target of this chapter is to inspect theoretically two-dimensional boundary layer Maxwell ferromagnetic liquid flow toward a flat surface with the occurrence of external magnetic field because of the fact that two equally line dipole which are equidistant from the wall and perpendicular to the flow plane. Cattaneo-Christov heat flux model is utilized in modified form of Fourier's Law to disclose the heat transfer characteristic. Governing flow problems are normalized into ordinary differential equation by adopting transformation procedure. The solution of resulting non-linear ODE's are solved numerically using MATLAB. Characteristic of sundry parameter like magneto-thermomechanical (ferrohydrodynamic) interaction parameter, dimensionless thermal relaxation, Prandtl and Deborah numbers on velocity and temperature fields are displayed via graphics and tables. It is also pointed out that temperature profile suppresses by varying values of the thermal relaxation time and Prandtl number and increasing behaviour is seen against ferrohydrodynamic interaction. Present numerical results are matched with those published previously in the literature for the case of Newtonian fluid $(\alpha_1 \to 0)$ and found an excellent agreement.

8.2 Flow assumption and mathematical formulation

Consider an incompressible flow of Maxwell ferromagnetic liquid over a flat plate with two equally line dipole as shown in fig.1.7. Temperature of the wall is assumed $T_w = T_\theta\left(1 - x/l\right)$, where l represent plate length $(l \gg d)$. Heat transfer analysis are deliberate, because the impact of applied force on the flow field is restricted to a tinny region which in very near to the wall where temperature T of the fluid is reasonably less from Curie temperature $(T < T_\theta)$

.

The governing equations reporting the physical situation of the flow problem in term of Maxwell ferromagnetic fluid communicated as

$$\frac{\partial u}{\partial x}+\frac{\partial v}{\partial y}=0, \tag{8.1}$$

$$u\frac{\partial u}{\partial x}+v\frac{\partial u}{\partial y}+\lambda_1\left(u^2\frac{\partial^2 u}{\partial x^2}+v^2\frac{\partial^2 u}{\partial y^2}+2uv\frac{\partial^2 u}{\partial x\partial y}\right)=\frac{\mu_0}{\rho}M\frac{\partial H}{\partial x}+\nu\frac{\partial^2 u}{\partial y^2}, \tag{8.2}$$

$$\rho c_p\left(u\frac{\partial T}{\partial x}+v\frac{\partial T}{\partial y}\right)=-\nabla.\mathbf{q}. \tag{8.3}$$

C-C model [137] is taken as

$$\mathbf{q}+\lambda_1\left(\frac{\partial \mathbf{q}}{\partial t}+(\mathbf{V}.\nabla)\mathbf{q}-(\mathbf{q}.\nabla)\mathbf{V}+(\nabla.\mathbf{V})\mathbf{q}\right)=-k\nabla T, \tag{8.4}$$

where $\mathbf{q}$ is heat flux, when $\lambda_1=0$, Eq. (8.4) is reduced to Fourier's law. By assuming incompressible fluid, Eq. (8.4) can be written easily in the form:

$$\mathbf{q}+\lambda_1\left(\frac{\partial \mathbf{q}}{\partial t}+(\mathbf{V}.\nabla)\mathbf{q}-(\mathbf{q}.\nabla)\mathbf{V}\right)=-k\nabla T. \tag{8.5}$$

By eliminating '$\mathbf{q}$' between Eqs. (8.3) and (8.5), the transformed equation for temperature is specified by

$$u\frac{\partial T}{\partial x}+v\frac{\partial T}{\partial y}+\lambda_1\left(\begin{array}{l}u\dfrac{\partial u}{\partial x}\dfrac{\partial T}{\partial x}+v\dfrac{\partial v}{\partial y}\dfrac{\partial T}{\partial y}+u\dfrac{\partial v}{\partial x}\dfrac{\partial T}{\partial y}\\ +v\dfrac{\partial u}{\partial y}\dfrac{\partial T}{\partial x}+2uv\dfrac{\partial^2 T}{\partial x\partial y}+u^2\dfrac{\partial^2 T}{\partial x^2}+v^2\dfrac{\partial^2 T}{\partial y^2}\end{array}\right)=\frac{k}{\rho c_p}\frac{\partial^2 T}{\partial y^2}. \tag{8.6}$$

The corresponding boundary relations imposed to the cold flat plate are given by

$$\left.\begin{array}{ll}u=v=0, & T=T_\theta\left(1-\dfrac{x}{l}\right) \quad \text{at } y=0\\ u=u_0, & T=T_\theta \quad \text{at } y=\infty\end{array}\right\}. \tag{8.7}$$

Using the following similarity transformation [92]

$$\eta=\left(\frac{u_0}{\nu x}\right)^{\frac{1}{2}}y,\ u=u_0 f'(\eta),\ v=\left(\frac{\nu u_0}{x}\right)^{\frac{1}{2}}\left[\frac{\eta f'(\eta)}{2}-\frac{f(\eta)}{2}\right],\ T=T_\theta\left[1-\frac{x}{l}\theta(\eta)\right]. \tag{8.8}$$

Substituting Eq. (8.8) into the Eqs. (8.2) to (8.6), we obtained the consequential equations:

$$f'''\left(1-\frac{\alpha_1 f^2}{2}\right)+\frac{ff''}{2}-\frac{\gamma_1}{4}\left(f''^2 f''\eta+2ff'f''\right)-\beta\theta=0, \tag{8.9}$$

$$\frac{1}{\Pr}\theta''+\frac{f\theta'}{2}-f'\theta+\frac{\alpha_2}{4}\left(2ff''+2ff'\theta'-f^2\theta''\right)=0. \tag{8.10}$$

The corresponding transformed boundary relation given in Eq. (8.7) taken as

$$\left.\begin{array}{ll} f=f'=0, & \theta=1, \quad \text{at} \quad \eta=0 \\ f'\to 1, & \theta\to 0, \quad \text{as} \quad \eta\to\infty \end{array}\right\}, \tag{8.11}$$

where $\beta=\frac{\gamma\mu_0 KT_\theta}{\pi\rho l u_0^2}$ is the ferrohydrodynamic interaction parameter, $\gamma_1=\lambda_1 u_0 x^{-1}$ is the dimensionless Deborah number and $\alpha_2=\lambda_2 u_0 x^{-1}$ is the dimensionless thermal relaxation time. In view of many industrial applications, we have also computed the friction factor and Nusselt number is computed as

Using Eqs. (2.14) and (2.15) along with similarity transformation, the Skin friction and heat transfer rate are acquired as

$$C_f \mathrm{Re}_x^{1/2}=f''(0), \quad Nu_x \mathrm{Re}_x^{-1/2}=\theta'(0). \tag{8.12}$$

8.3. Results and discussion

In this segment, we have explore the different rheological aspects of the problem, the behavior of numerous governing parameters involved in velocity and temperature profile are illustrated in figs. 8.1 to 8.7. For verification and efficiency of the numerical procedure, evaluation of our present results corresponding to local Nusselt number $\theta'(0)$ in case of Newtonian fluid $(\alpha_1=0)$ are compared with those reported by [92] for several values of β are presented in table 8.1 and found an dazzling agreement with the available data which shows the legitimacy of our numerical scheme.

Fig.8.1 is displayed to highlight impact of ferromagnetic interaction parameter β on velocity field. It is simply perceived that in the occurrence of magnetic dipole velocity profile reduces for large values of β, because this happen owing to the existence of resistive force (Lorentz force), which restarted the flow and this force has tendency to develop more resistance to enhance the temperature field and consequently flattening the axial velocity $f'(\eta)$. It is more stimulating to observe that the occurrence of applied magnetic field, the velocity profile is less as compared with the hydrodynamic case $(\beta=0)$, because due to interference among fluid

motion and the stroke of applied dipole field. This kind of interference decreases velocity and rising the frictional heating involving within the layers of fluid which are accountable for the increment in the thickness of thermal boundary layer as cleared in fig. 8.2.

Fig. 8.3 illustrate the outcome of thermal relaxation parameter α_2 on temperature field. It is obviously noticeable that fluid temperature decreases by enlarging α_2. The physical thinking behind it, is the case that by rising the value of α_2, material particles need additional time to exchange energy to their neighbouring particles. Thus for larger value of α_2 causes decrement in temperature field and opposite trend is noted for velocity profile as illustrated in fig. 8.4.

Fig. 8.5 disclose the behavior of Deborah number regarding to relaxation time γ_1 on velocity profile. It is prominent that velocity profile indicate decreasing result corresponding to higher values of Deborah number. This is because of the fact that ratio of relaxation to observation times represent the Deborah number. So relaxation time is upshot by increasing Deborah number which gives extra imperviousness to the motion of the fluid. Hence, boundary layer thickness also decreases. Fig. 8.6 illustrate the physical characteristics of Deborah number γ_1 on temperature field $\theta(\eta)$. One can observe that larger values of Deborah number leads to increases fluid temperature. As greatest values of Deborah number relates to larger relaxation time which conveys opposition to the fluid motion and consequently heat is generated and therefore increases thermal boundary layer thickness. Therefore fluid temperature is rises.

Fig. 8.7 is outlined to discuss the behavior of Pr on temperature field. It is concluded that higher Pr lead to decline in temperature distribution. From physical point of view Pr is the proportion of momentum diffusivity to thermal diffusivity. Reduction in thermal diffusivity consequently decreases the temperature field. In addition it is seen that for greater Pr, heat diffuses bit by bit, so thinning the thermal boundary layer as contrasted to low Pr. Outcome of low Pr marks a denser thermal boundary layer which diffuses heat rapidly than bigger Pr. Fig. 8.8 shows the impact of Deborah number γ_1 on Nusselt number with the change of Prandtl number. It is evident that rate of heat transfer increases by rising Prandtl number while reverse trend is detected for higher values of γ_1.

Table 8.1. Comparing Nusselt number and Skin friction when $Pr = 10, \gamma_1 = 0, \alpha_2 = 0$.

	$f''(0)$		$\theta'(0)$	
β	Neuringer [92]	Present result	Neuringer [92]	Present result
0.0	0.3320	0.3321	1.1756	1.1757
0.05	0.3058	0.3058	1.1557	1.1552
0.10	0.2782	0.2777	1.1338	1.1333
0.15	0.2497	0.2491	1.1102	1.1096
0.20	0.2199	0.2193	1.0845	1.0837
0.25	0.1887	0.1880	1.0561	1.0553
0.30	0.1556	0.1548	1.0244	1.0233
0.35	0.1201	0.1191	0.9881	0.9866
0.40	0.0811	0.0798	0.9449	0.9429

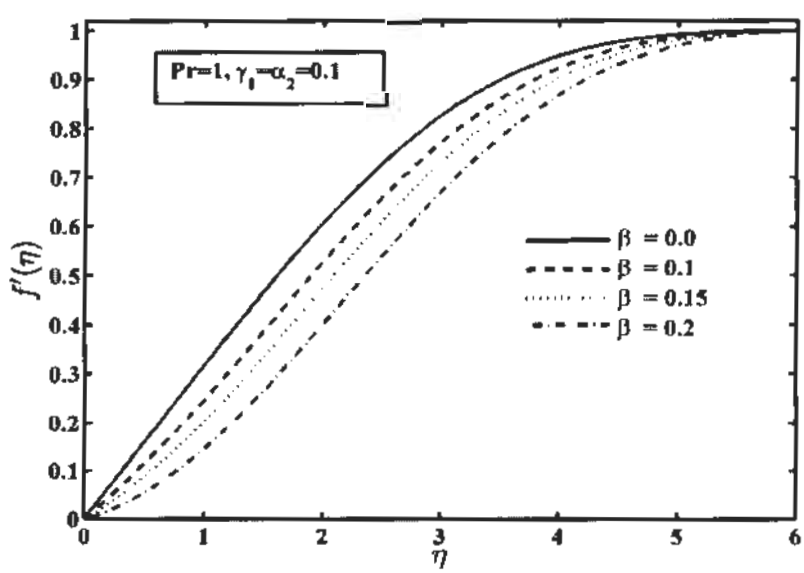

Fig. 8.1. Impact of β on $f'(\eta)$.

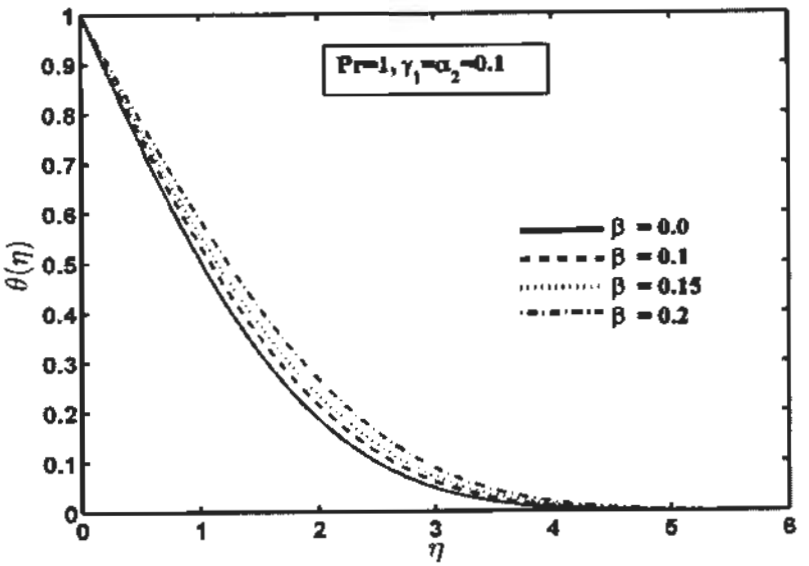

Fig. 8.2. Impact of β on $\theta(\eta)$.

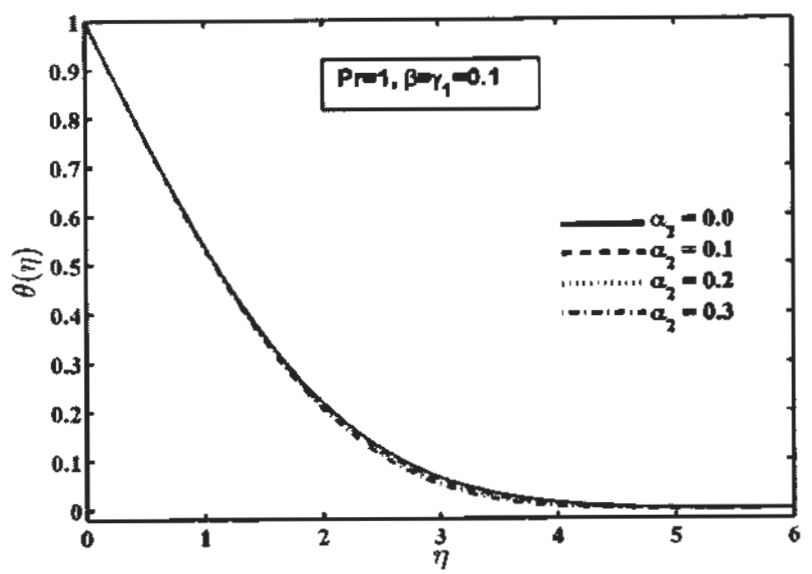

Fig. 8.3. Impact of α_2 on $\theta(\eta)$.

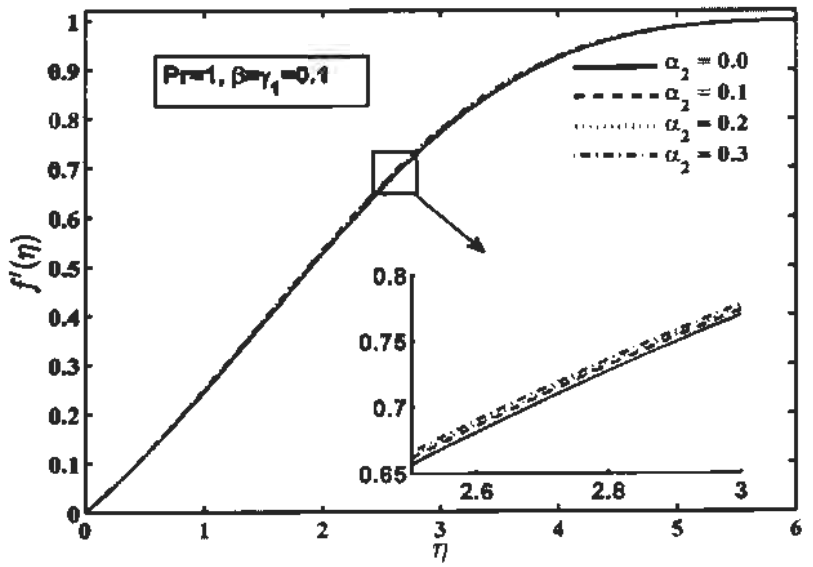

Fig. 8.4. Impact of α_2 on $f'(\eta)$.

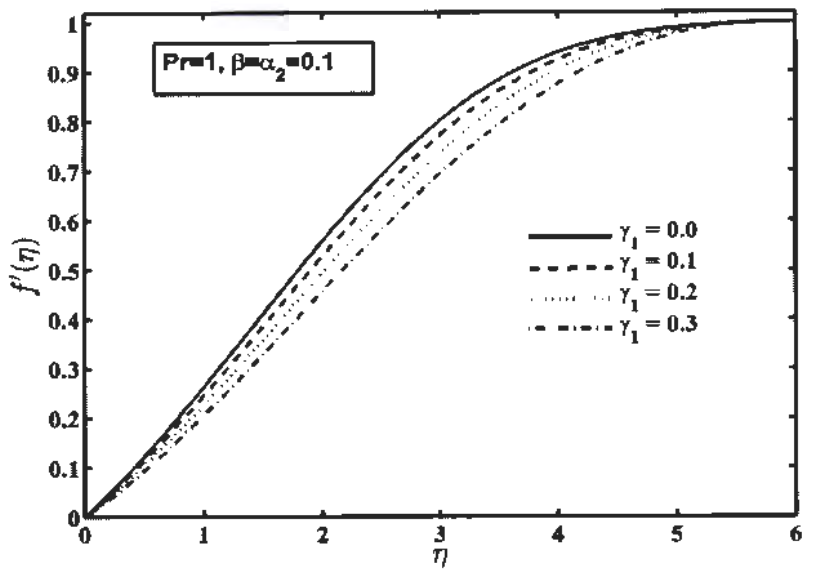

Fig. 8.5. Impact of γ_1 on $f'(\eta)$.

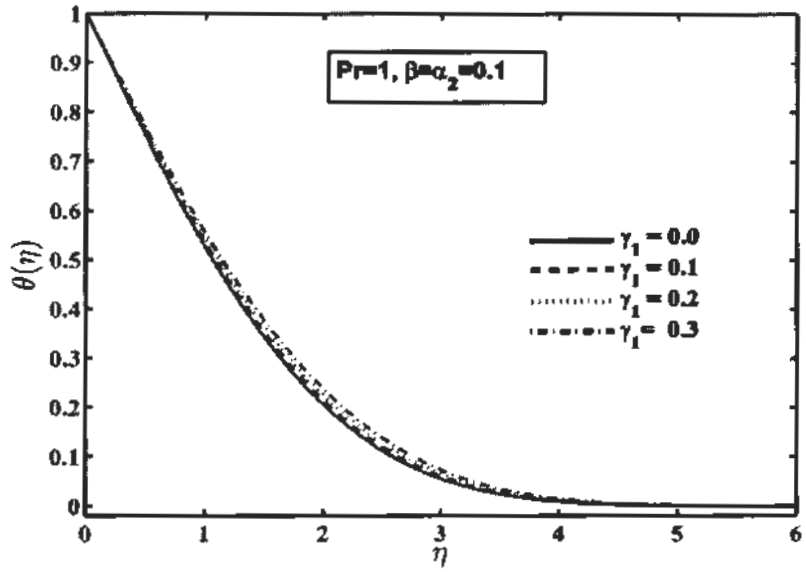

Fig. 8.6. Impact of γ_1 on $\theta(\eta)$.

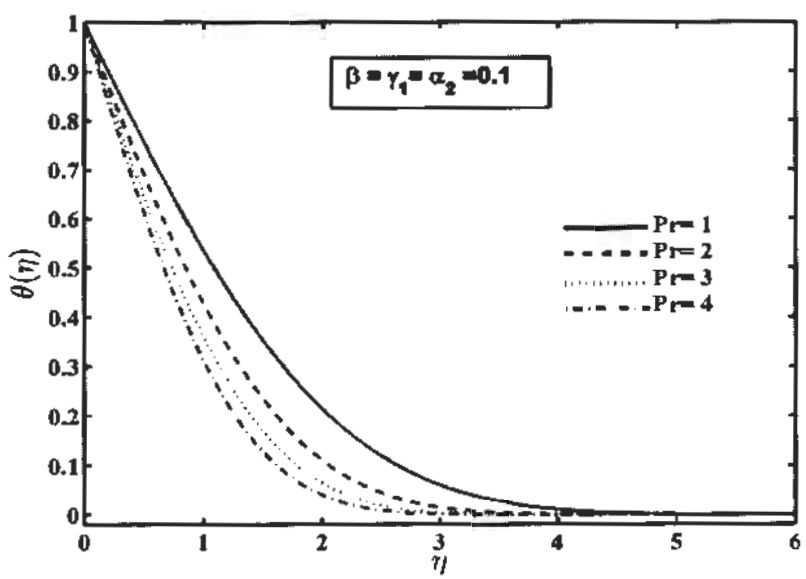

Fig. 8.7. Impact of Pr on $\theta(\eta)$.

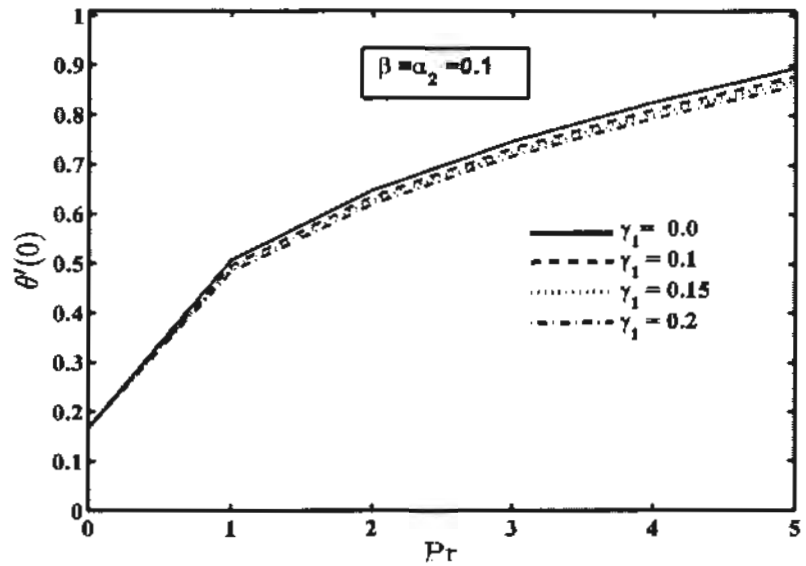

Fig. 8.8. Impact of γ_1 on $\theta'(\eta)$.

8.4 Conclusion

In this chapter, we investigate two dimensional incompressible parallel flow of Maxwell fluid saturated with ferromagnetic liquid over a flat surface under the influence of two dipole current. The mathematical model of the flow problems are converted into ODE's and then solved numerically by adopting R-K based shooting method using MATLAB package. Influence of some pertinent parameter on the flow problem like ferromagnetic interaction parameter β, Deborah number γ_1, thermal relaxation time α_2, Prandtl number Pr on velocity, temperature, and local Nusselt number are deliberated through sketchily in detail. Important judgements of the present problem are as follows:

- Velocity of the fluid reduces, while temperature increases by enlarging the values of ferromagnetic interaction parameter β.
- Temperature profile indicate falling behavior of Cattaneo-Christov model [112] as compared with Fourier's law.
- For large values of Deborah number γ_1 velocity profile decreases.
- Nusselt number is enhances against Pr and reverse trend is examined for γ_1.

Chapter 9

Study of boundary layer slip flow of heat transfer ferrofluid comprising nanoparticle in porous medium under the influence of magnetic dipole

9.1 Introduction

This chapter, characterizes the heat transfer and velocity slip flow of magnetic nanofluid (ferromagnetic liquid) through porous medium over a stretching sheet. Cogitate a three different sort of conventional fluids like kerosene, water and refrigerant-134a with magnetite as a nanoparticle is taken into account. The partial differential equations are first mended into nonlinear system of ordinary differential equations by implementing appropriate transformations and then evaluated by using R-K Fehlberg scheme depend on shooting algorithm. Impact of emerging parameters are discussed through graphs and tables in details. . Graph reveals that influence of thermo-mechanical (ferrohydrodynamic) parameter in to diminish the velocity profile whereas temperature profile demonstrate the opposite behavior for larger values of nanoparticle volume fraction. Also noted that heat transfer rate is greater in case of refrigerant-134a than water and kerosene base fluid with snowballing nanoparticle volume fraction.

9.2 Flow assumption and mathematical formulation

Consider a viscous two-dimensional, incompressible magnetic nanofluid. Taking water (H_2O) , Refrigerant-134a $(C_2H_2F_4)$ and kerosene $(C_{10}H_{22})$ as conventional fluid with the suspension of magnetite (Fe_3O_4) nanoparticle flow over a stretching sheet (as shown is section 1.17) The boundary layer equations of ferromagnetic liquid flow and heat transport are stated as

$$\frac{\partial u}{\partial x}+\frac{\partial v}{\partial y}=0, \tag{9.1}$$

$$u\frac{\partial u}{\partial x}+v\frac{\partial u}{\partial y}=\frac{\mu_{nf}}{\rho_{nf}}\left(\frac{\partial^2 u}{\partial x^2}\right)+\frac{\mu_0}{\rho_{nf}}M\frac{\partial H}{\partial x}-\frac{\mu_{nf}}{\rho_{nf}K}u, \tag{9.2}$$

$$\left(u\frac{\partial T}{\partial x}+v\frac{\partial T}{\partial y}\right)+\frac{\mu_0}{(\rho c_p)_{nf}}T\frac{\partial M}{\partial T}\left(u\frac{\partial H}{\partial x}+v\frac{\partial H}{\partial y}\right)$$
$$=\alpha_{nf}\frac{\partial^2 T}{\partial y^2}+\frac{\mu_{nf}}{(\rho c_p)_{nf}}\left[\left(\frac{\partial u}{\partial y}\right)^2+2\left(\frac{\partial v}{\partial y}\right)^2\right], \tag{9.3}$$

subject to substantial boundary equations with slip and suction at wall are

$$\left.\begin{aligned} &u=u_w+A\frac{\partial u}{\partial y},\quad v=v_w \text{ at } y=0\\ &u\to 0,\quad \text{as } y\to\infty \end{aligned}\right\}. \tag{9.4}$$

Along with PST temperature on the surface Eq. (1.59). The thermo-physical parameters are specified as follow [138]

$$\mu_{nf}=\frac{\mu_f}{(1-\phi)^{2.5}},\quad \rho_{nf}=\rho_f(1-\phi)+\rho_s\phi, \tag{9.5}$$

$$\alpha_{nf}=\frac{k_{nf}}{(\rho c_p)_{nf}},\quad (\rho c_p)_{nf}=(1-\phi)(\rho c_p)_f+(\rho c_p)\phi, \tag{9.6}$$

$$k_{nf}=k_f\left\{\frac{2k_f+k_s-2(k_f-k_s)\phi}{2k_f+k_s+(k_f-k_s)\phi}\right\}. \tag{9.7}$$

Applying Eqs. (1.64) and (1.65) into the Eqs. (9.2) to (9.4) reduces to following system of equations of order ξ^2

$$f'''-(1-\phi)^{2.5}\left\{\left((1-\phi)+\phi\frac{\rho_s}{\rho_f}\right)(f'^2-ff'')+\frac{2\beta\theta_1}{(\eta+\alpha_1)^4}\right\}-K_1f'=0, \tag{9.8}$$

$$\frac{k_{nf}}{k_f}\theta_1''+\left[(1-\phi)+\phi\frac{(\rho c_p)_s}{(\rho c_p)_f}\right]\Pr(f\theta_1'-2f'\theta)+\frac{2\lambda\beta(\theta_1-\varepsilon)f}{(\eta+\alpha_1)^3}-\frac{2\lambda}{(1-\phi)^{2.5}}f''^2=0, \tag{9.9}$$

$$\frac{k_{nf}}{k_f}\theta_2''+\left[(1-\phi)+\phi\frac{(\rho c_p)_s}{(\rho c_p)_f}\right]\Pr\left(f\theta_2'-4f'\theta_2\right)+\frac{2\lambda\beta\theta_2 f}{(\eta+\alpha_1)^3}-\lambda\beta(\theta_1-\varepsilon)$$
$$\times\left[\frac{2f'}{(\eta+\alpha_1)^4}+\frac{4f}{(\eta+\alpha_1)^5}\right]-\frac{\lambda}{(1-\phi)^{2.5}}f''^2=0. \tag{9.10}$$

Also, the boundary conditions (9.4) are of the form

$$\left.\begin{array}{l} f = S,\ f' = 1 + \delta f'',\ \theta_1 = 1,\ \theta_2 = 0,\ \text{at}\ \ \eta = 0 \\ f' \to 0,\ \ \theta_1 \to 0,\ \ \theta_2 \to 0,\ \ \ \text{as}\ \eta \to \infty \end{array}\right\}. \tag{9.11}$$

Expression for skin friction, and Nusselt number stated in Eqs. (2.14) and (2.15), after utilizing the Eqs. (1.64) and (1.65), we get

$$C_f Re_x^{1/2} = -\frac{2}{(1-\phi)^{2.5}} f''(0),\quad Nu_x / Re_x^{1/2} = -\frac{k_{nf}}{k_f}\left(\theta_1'(0) + \xi^2 \theta_2'(0)\right). \tag{9.12}$$

9.3. Results and discussion

The evaluated numerical fallouts are achieved for a some sundry dimensionless parameter alike β, Pr, ϕ, δ, K_1 and S on temperature and velocity fields are discussed via graphs in Figs. 9.1-9.7. Thermal characteristic of conventional fluid (H_2O, $C_2H_2F_4$, $C_{10}H_{22}$) with magnetite (Fe_3O_4) particle are described in table 9.1. Fixed values of pertinent parameters for the present problem are taken as $\lambda = 0.01$, $\varepsilon = 2.0$, $\alpha_1 = 1.0$. The values of Nusselt number and skin friction coefficient against volume fraction of nanoparticle ϕ with three sort of conventional fluid water (H_2O), Refrigerant-134a ($C_2H_2F_4$) and kerosene ($C_{10}H_{22}$) for numerous values of ferrohydrodynamic (ferromagnetic) parameter β are presented in table 9.2. From results it is clear that the that both the values of Nusselt number and skin friction remains lesser without β and greater with the occurrence of β. This is due to the fact that alignment of ferroparticle in definite order. Similarly witnessed that Nusselt number and skin friction coefficient have larger values for Refrigerant-134a based ferrofluid rather than the others.

Influence of nanoparticle volnme fraction $0 \le \phi \le 1$ on velocity and temperature profiles of magnetite (Fe_3O_4) with three different conventional fluid like water (H_2O), Refrigerant-134a ($C_2H_2F_4$), and kerosene ($C_{10}H_{22}$) for relevant parameters β, K_1, S and Pr are displayed pictorially. Figs. 9.1 and 9.2 elucidate that for higher values of volume fraction of nanoparticles velocity profile decreases gradually and reverse impact is prominent for temperature field. Fig. 9.2 exhibited physical response with the variation of nanoparticles volume fraction indicate enhancement in thermal conductivity and thickness of boundary layer. Further fig. 9.1 shows that Fe_3O_4 nanoparticle based on kerosene fluid has more impact on velocity field rather than others, on the other hand temperature profile gain maximum enhancement for Fe_3O_4

nanoparticle based on Refrigerant-134a fluid followed by kerosene and water as perceived in fig. 9.2.

Figs. 9.3 and 9.4 depicts the impact of porosity parameter $K_1 = 0.0, 0.4, 0.8$ on velocity and temperature fields. From the given fallouts that velocity reduces for larger porosity parameter. This is owing to the fact that, increment in permeability parameter, enhances the permeable media resistance, which is the reason for slow down the motion of fluid and reverse behavior is noted for temperature as seen in fig. 9.4. Moreover inspected that boundary layer thickness and velocity field of Fe_3O_4 nanoparticle based on kerosene are higher than Refrigerant-134a and water, whereas temperature field is maximum for Refrigerant-134a based nanoparticle as compared to the remaining ones. Figs. 9.5 and 9.6 elaborate the influence of velocity slip parameter $\delta = 0.0, 0.4, 0.8$ on velocity and temperature distribution. Fig. 9.5 reveal that wall velocity reduces for larger slip parameter and approaches to zero on the edge of the boundary at η equal to 5 .For no-slip case (δ equal to 0), then $f'(0)$ equal to 1. It is because of the fact that greater value of δ comes to acceleration lubrication and slipperiness of the surface. Diversely, fig. 9.6 shows that surface slipperiness disturbs the fluid temperature reversely; so increment in δ goes to enhances the temperature and thickness of thermal boundary layer. Also observed that velocity is larger for kerosene based magnetic nanofluid as compared to the other conventional fluids, although temperature field achieve maximum increment in Fe_3O_4 nanoparticle based on Refrigerant-134a fluid followed by kerosene and water based magnetic nanofluid. Figs. 9.7 and 9.8 describes the influence of thermo-mechanical (ferromagnetic) parameter β due to dipole field on temperature and velocity distribution by considering different fluids such as water (H_2O), Refrigerant-134a ($C_2H_2F_4$) and kerosene ($C_{10}H_{22}$). Since magnetic dipole field play as a retarding force which opposes the fluid motion, therefore for increase in β, produce more retarding force, hence outcomes shows decrease in velocity profile as displayed in fig. 9.7. Since there exist a collaboration among motion of fluid and the impact of applied field. This relation increasing the frictional heating and declines velocity profile, which accordingly enhances heat transport as displayed in fig. 9.8. Also noticed that in case of Fe_3O_4-Refrigerant-134a temperature distribution have increasing impact than other base fluids.

Fig. 9.9 describes the deviation of skin friction under the impact of slip parameter δ for dissimilar base fluids with the suspension of magnetite nanoparticle. The fallout confirm that skin friction coefficient rises against volume fraction ϕ and reduces for higher values of slip

parameter. Furthermore perceived that coefficient of skin friction gain maximum increase for Fe_3O_4 nanoparticle based on Refrigerant-134a fluid. This is due to minimum Prandtl number and specific heat of Refrigerant-134a as compared to water and kerosene. Fig. 9.10 describe the influence of porosity parameter K_1 on skin friction coefficient with horizontal variation of volume concentration ϕ of nanoparticle. The graph exemplifies that skin friction boost up for both ϕ and K_1. Also noted that the numeric results of nanoparticle with kerosene base fluid are lower than Refrigerant-134a and water base fluid.

Table 9.1. Thermo-physical characteristics of base fluid and nanoparticle

Material properties	Base fluids			nanoparticle
	Water	Kerosene	Refrigerant-143a	Fe_3O_4
ρ	997	783	1199.7	5180
C_p	4179	2090	1432.0	670
k	0.613	0.15	0.0803	9.7
Pr	6.2	21	3.4	---

Table 9.2. Calculated results of skin friction and Nusselt number.

Magnetite Fe_3O_4 Nanoparticle							
		Presence of Ferromagnetic Parameter $\beta = 2$			Absence of Ferromagnetic Parameter $\beta = 0$		
	ϕ	Water base	Kerosene base	Refrigerant -134a base	Water base	Kerosene base	Refrigerant -134a base
$C_f Re_x^{1/2}$	0.02	1.4489	1.3099	1.5189	1.0606	1.0727	1.0531
	0.05	1.5593	1.4336	1.6154	1.1626	1.1921	1.1440
	0.1	1.7563	1.6523	1.7895	1.3454	1.4032	1.3083
$Nu_x Re_x^{-1/2}$	0.02	0.2647	0.1183	0.3896	0.2565	0.1169	0.3718
	0.05	0.2991	0.1333	0.4385	0.2902	0.1317	0.4194
	0.1	0.3643	0.1614	0.5302	0.3540	0.1596	0.5091

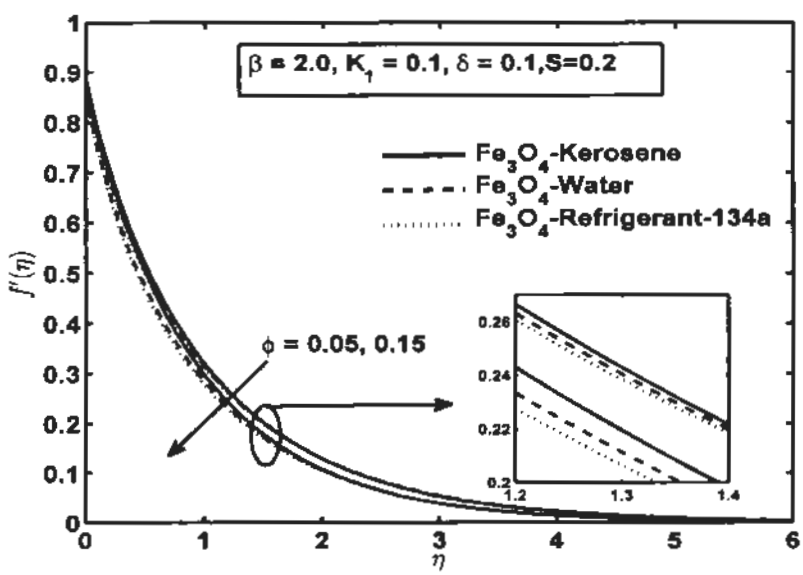

Fig. 9.1. Influence of ϕ on f'.

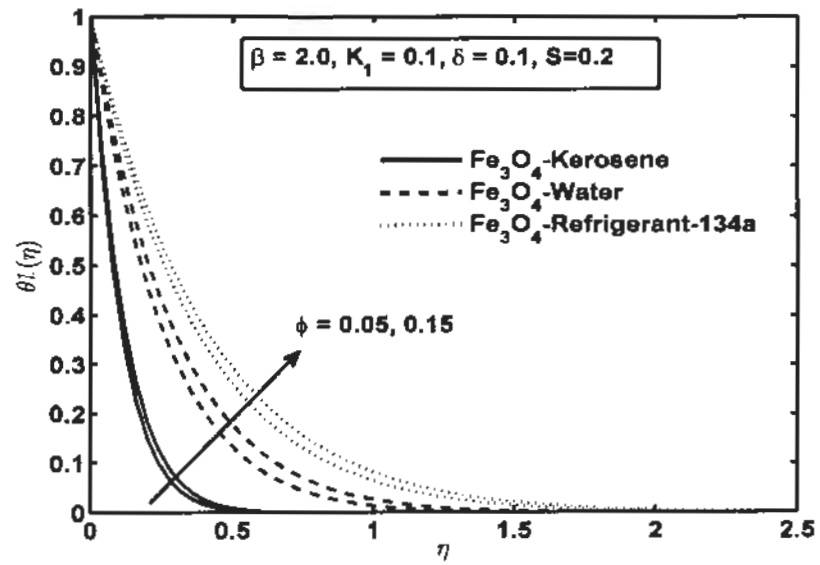

Fig. 9.2. Influence of ϕ on θ_1.

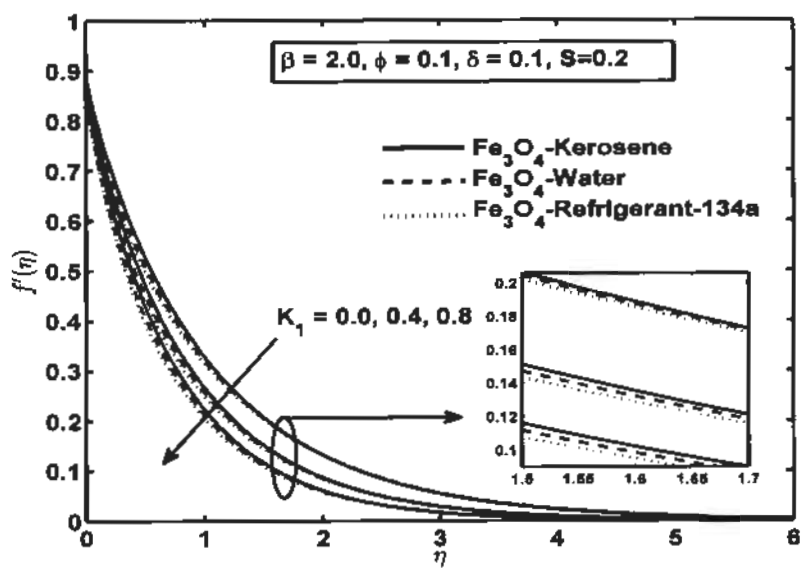

Fig. 9.3. Influence of K_1 on f'.

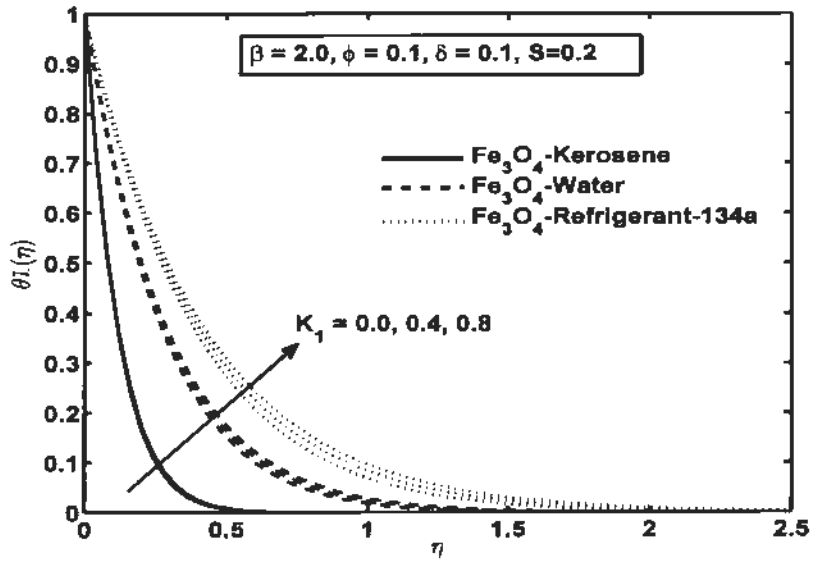

Fig. 9.4. Influence of K_1 on θ_1.

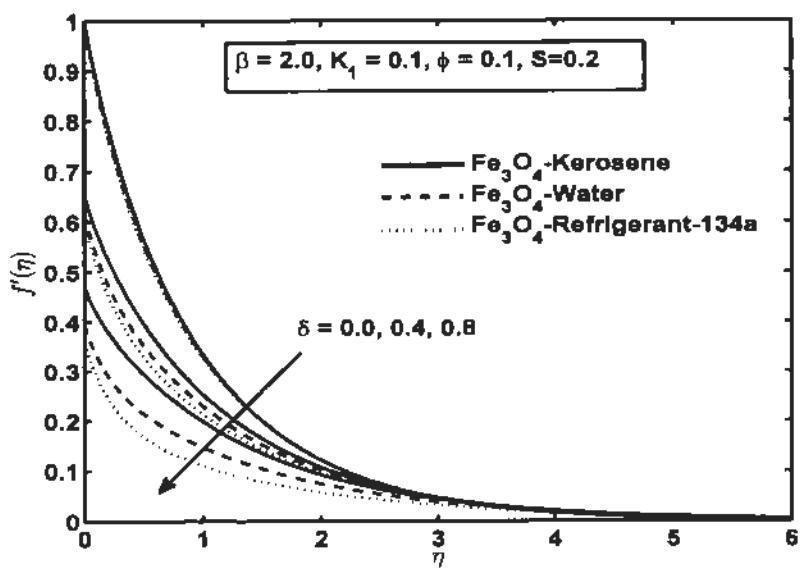

Fig. 9.5. Influence of δ on f'.

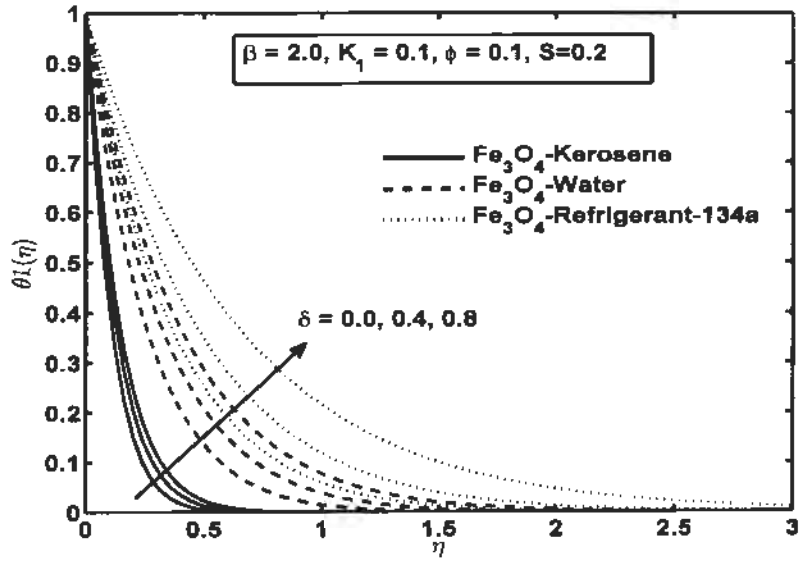

Fig. 9.6. Influence of δ on θ_1.

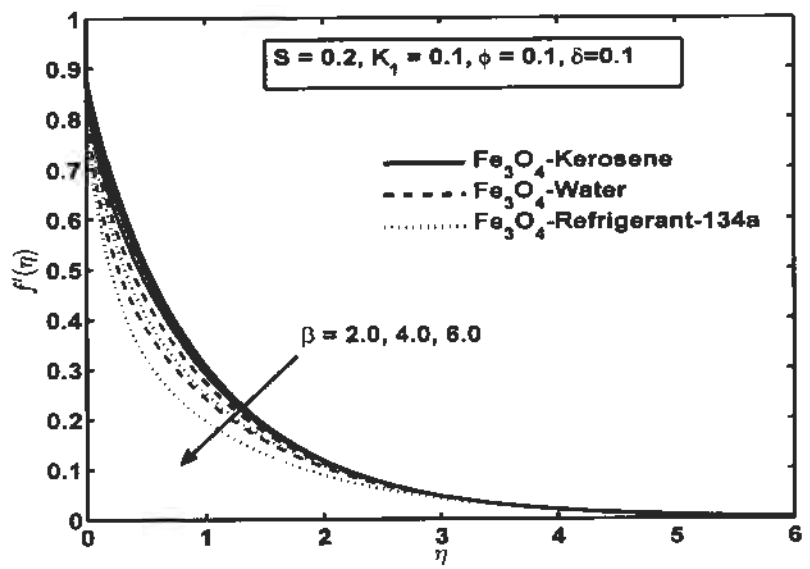

Fig. 9.7. Influence of β on f'.

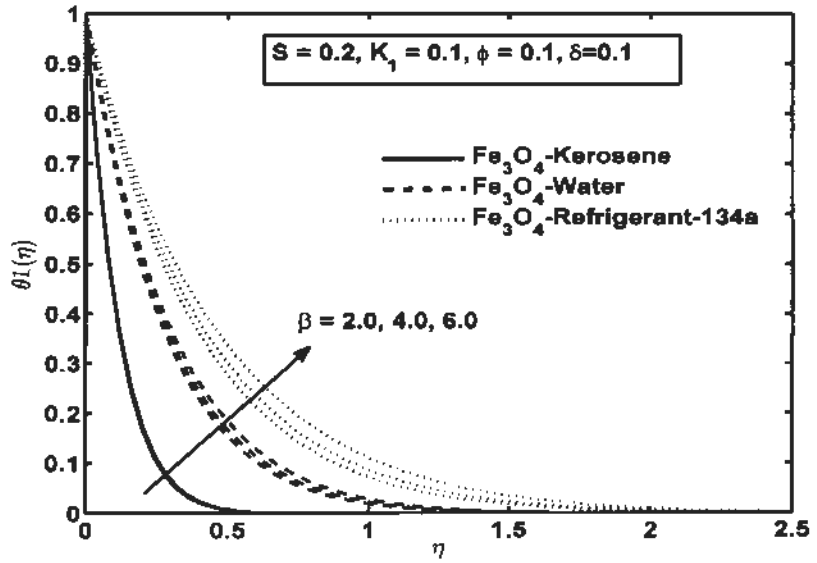

Fig. 9.8. Influence of β on θ_1.

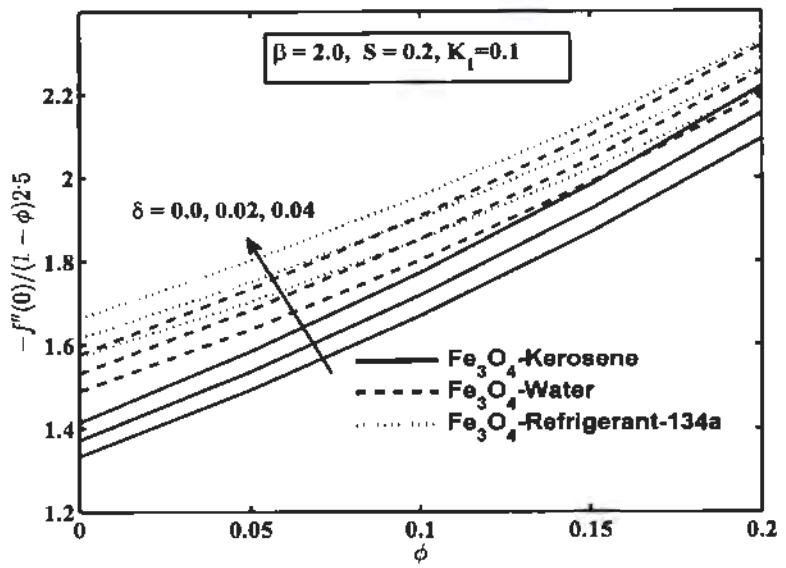

Fig. 9.9. Influence of δ and ϕ on skin friction coefficient.

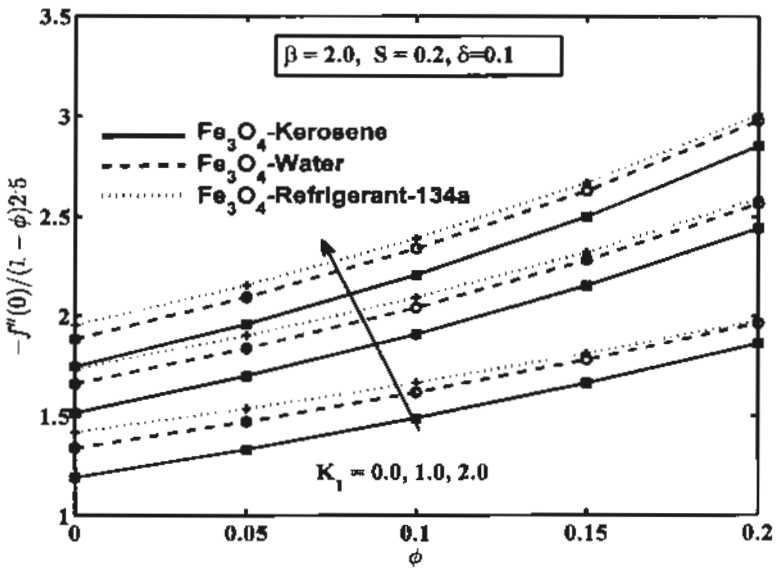

Fig. 9.11. Influence of K_1 and ϕ on skin friction coefficient.

9.4 Conclusion

In current discussion, we have examined the characteristic of nanofluid and transfer of heat by stretched surface. Water (H_2O), refrigerant-134a $(C_2H_2F_4)$, and kerosene $(C_{10}H_{22})$ are considered as base fluid with the insertion of Fe_3O_4 nanoparticle. The main key points are condensed as:

- Skin friction increases for larger values of concentration of nanoparticle whereas it reduces against slip.
- Fe_3O_4-Refrigerant-134a based nanoparticle has attained supreme value as compared to water and kerosene based magnetic nanofluid.
- Nusselt number Fe_3O_4-Refrigerant-134a based nanofluid is superior than base fluid like water and kerosene for higher values of ϕ, due to higher thermal conductivity enhancement in refrigerant-134a based nanofluid rather than others.

Chapter 10

Analysis of magnetic nano particles due to applied magnetic dipole in aqueous medium with momentum slip condition

10.1 Introduction

In this chapter, flow of magnetic nanoparticles and dipole effect past a stretchable surface toward velocity slip condition have been investigated. Water is chosen as a base fluid while ferromagnetic, diamagnetic, paramagnetic, antiferromagnetic and ferrimagnetic particles are considered as nanoparticles. The flow and heat transfer process can be control with the help of external magnetic nanofluid. Obtained system of boundary layer problems are renovated into ordinary differential equations which are then elucidated via shooting algorithm. Influence of some emerging constraints on flow field (velocity, temperature), Nusselt number and skin friction are clarified pictorially. We notice that diamagnetic particle has larger thermal conductivity to the others. Furthermore, the values of Nusselt number and skin friction have minimum value for ferrimagnetic particle (Fe_3O_4).

10.2 Flow assumption and mathematical formulation

Let us contemplate incompressible, two dimensional viscous flow of ferro and non-ferro nano fluid due to stretched surface embedded with dipole field define in geometry under section (1.17). Under boundary layer assumption, the governing flow equations over current problem take the form.

$$\frac{\partial u}{\partial x}+\frac{\partial v}{\partial y}=0, \tag{10.1}$$

$$u\frac{\partial u}{\partial x}+v\frac{\partial u}{\partial y}=\frac{\mu_{nf}}{\rho_{nf}}\left(\frac{\partial^2 u}{\partial y^2}\right)+\frac{\mu_0}{\rho_{nf}}M\frac{\partial H}{\partial x}-\frac{\mu_{nf}}{\rho_{nf}K}u, \tag{10.2}$$

$$\left(u\frac{\partial T}{\partial x}+v\frac{\partial T}{\partial y}\right)+\frac{\mu_0}{(\rho c_p)_{nf}}T\frac{\partial M}{\partial T}\left(u\frac{\partial H}{\partial x}+v\frac{\partial H}{\partial y}\right)=\alpha_{nf}$$
$$\times\frac{\partial^2 T}{\partial y^2}+\frac{\mu_{nf}}{(\rho c_p)_{nf}}\left(\frac{\partial u}{\partial y}\right)^2. \tag{10.3}$$

Corresponding boundary condition for stretching sheet and velocity slip at the wall are

$$\left.\begin{aligned} &u=u_w+A\frac{\partial u}{\partial y},\quad v=0,\ \text{at}\ y=0\\ &u\to 0,\quad \text{as}\quad y\to\infty \end{aligned}\right\}, \tag{10.4}$$

along with prescribed surface condition (PST) in Eq. (1.59). The thermophysical parameters are specified as [138]

$$\rho_{nf}=(1-\phi)\rho_f+\phi\rho_s,\quad \mu_{nf}=\frac{\mu_f}{(1-\phi)^{2.5}}, \tag{10.5}$$

$$(\rho c_p)_{nf}=(1-\phi)(\rho c_p)_f+\phi(\rho c_p),\quad \alpha_{nf}=\frac{k_{nf}}{(\rho c_p)_{nf}}, \tag{10.6}$$

$$k_{nf}=k_f\left\{\frac{k_s+2k_f-2\phi(k_f-k_s)}{k_s+2k_f+\phi(k_f-k_s)}\right\}. \tag{10.7}$$

Employing transformation Eqs. (1.64) and (1.65) into the Eqs. (10.2) to (10.4) reduces into the following system of equations

$$f'''-(1-\phi)^{2.5}\left\{\left((1-\phi)+\phi\frac{\rho_s}{\rho_f}\right)(f'^2-ff'')+\frac{2\beta\theta_1}{(\eta+\alpha_1)^4}\right\}-K_1 f'=0, \tag{10.8}$$

$$\frac{k_{nf}}{k_f}\theta_1''+\left[(1-\phi)+\phi\frac{(\rho c_p)_s}{(\rho c_p)_f}\right]\Pr(f\theta_1'-2f'\theta)+\frac{2\lambda\beta(\theta_1-\varepsilon)f}{(\eta+\alpha_1)^3}-\frac{2\lambda}{(1-\phi)^{2.5}}f'^2=0, \tag{10.9}$$

$$\frac{k_{nf}}{k_f}\theta_2''+\left[(1-\phi)+\phi\frac{(\rho c_p)_s}{(\rho c_p)_f}\right]\Pr\left(f\theta_2'-4f'\theta_2\right)+\frac{2\lambda\beta\theta_2 f}{(\eta+\alpha_1)^3}$$
$$-\lambda\beta(\theta_1-\varepsilon)\left[\frac{2f'}{(\eta+\alpha_1)^4}+\frac{4f}{(\eta+\alpha_1)^5}\right]-\frac{\lambda}{(1-\phi)^{2.5}}f''^2=0. \tag{10.10}$$

Boundary equations are

$$\left.\begin{array}{l} f=0,\ f'=1+\delta f'',\ \theta_1=1,\ \theta_2=0, \quad \text{at} \quad \eta=0 \\ f'\to 0,\ \theta_1\to 0,\ \theta_2\to 0, \quad \text{as} \quad \eta\to\infty \end{array}\right\}. \tag{10.11}$$

The non-dimensional form of skin friction and heat transfer rate are defined in Eq. (9.12).

10.3. Results and discussion

We have taken different kinds of nanoparticles like ferromagnetic (Fe), ferrimagnetic (Fe_3O_4), paramagnetic (Ta), diamagnetic (Cu), and anti-ferromagnetic (CuO) on velocity and temperature profiles, Nusselt number and skin friction coefficient. Graphs are drawn for numerous controlling parameters to check the efficiency of the particles in different situation like β, ϕ, K_1, δ. Physical parameters of base fluid (H_2O) and nanoparticles are presented in Table 10.1. Throughout the problem fixed values of sundry constraints are $Pr=6.2$, $\beta=1.0$, $\phi=0.1$, $K_1=0.2$, $\delta=0.1$, $\lambda=0.01$, $\varepsilon=2.0$, $\alpha_1=1.0$. The influence of magnetic nanoparticles like ferromagnetic, ferrimagnetic, diamagnetic, paramagnetic, and anti-ferromagnetic on velocity profile $f'(\eta)$ and temperature profile $\theta_1(\eta)$ are portrayed in figs. 10.1 to 10.2. It is fascinating to point out that velocity arrangement enhances in direction Ta, Cu, Fe, CuO, and Fe_3O_4. From results we determine that boundary layer thickness and velocity for ferrimagnetic particle (Fe_3O_4) is greater than the remaining ones. Also we infer that reverse trend is noted for temperature field and thickness of thermal boundary layer has maximum value for paramagnetic particle (Ta) followed by Cu, Fe, CuO and Fe_3O_4 in fig. 10.2.

Figs. 10.3 and 10.4 display the different type of magnetic nanoparticles on skin friction and Nusselt number versus ferromagnetic interaction parameter β. Results pointed out that skin friction coefficient accelerate monotonically for higher values of β. Physically, because in fact that increment in β produces a resistance force in the flow field, called Lorentz force which has ability to suppress the velocity profile and rising skin friction, and reduces the heat transfer rate. Also establish that paramagnetic particle gain maximum values of skin frication and ferrimagnetic has minimum values of Nusselt number as compared with the others as shown in figs. 10.3 and 10.4. The principles of skin friction against slip parameter δ are exhibited in fig. 10.5. For higher values of slip parameter, there is decay in flow resistance and consequently magnitude of skin friction coefficient reduces in each case. We accomplish due to sufficiently smooth surface, skin friction coefficient at wall diminishes significantly. The

effect of porosity parameter K_1 on skin friction coefficient and heat transfer rate are provided in figs. 10.6 and 10.7. Fig. 10.7 disclose that skin friction coefficient enhances very rapidly for higher value of K_1 for all sort of nanoparticles comprising Tu, Cu, Fe, CuO, and Fe_3O_4. Additional, it is witnessed that Nusselt number and skin friction and have smallest value for ferrimagnetic (Fe_3O_4) while compared with the others. Fig. 10.7 depict that Nusselt decays for largest porous medium parameters. Fig. 10.8 demonstrates thermal conductivities k_{nf}/k_f of dissimilar kind of nanoparticles with the insertion of water (H_2O), describe the ratio of thermal conductivity of solid particles to thermal conductivity of conventional fluid with the deviation of particle fraction ϕ. From graph it infer that thermal conductivity of nanoparticle enhances linearly by increasing the concentration of volume fraction. Though highest thermal conductivity is noticed for diamagnetic case tailed by paramagnetic, ferromagnetic, anti-ferromagnetic, and ferrimagnetic. The reason is that diamagnetic have maximum thermal conductivity rather than the other nanoparticles as displayed in table 10.2.

Table 10.1. Material properties of base fluid and nanoparticle [139]

Physical properties	Magnetic Nanoparticles					Base fluid
	Paramagnetic (Tu)	Diamagnetic (Cu)	Ferromagnetic (Fe)	Anti-ferromagnetic (CuO)	Ferrimagnetic (Fe_3O_4)	Water (H_2O)
$\rho(kg/m^3)$	16600	8933	7870	6320	5180	997
$c_p(j/Kg.k)$	140	385	447	531.8	670	4179
$k(W/m.k)$	57.5	401	80.2	76.5	9.7	0.613
Pr					---	6.2

Table 10.2. Thermal conductivities of nanoparticles and volume concentration.

Volume concentration	Thermal conductivities of magnetic particles k_{nf} / k_f				
ϕ	Paramagnetic	Diamagnetic	Ferromagnetic	Anti-ferromagnetic	Ferrimagnetic
0.25%	1.0073	1.0075	1.0073	1.0073	1.0063
0.50%	1.0146	1.0150	1.0147	1.0147	1.0125
0.75%	1.0220	1.0226	1.0222	1.0221	1.0188
1.00%	1.0293	1.0302	1.0296	1.0296	1.0252
1.25%	1.0368	1.0378	1.0371	1.0371	1.0315
1.50%	1.0442	1.0455	1.0446	1.0446	1.0379
1.75%	1.0517	1.0532	1.0522	1.0521	1.0443
2.00%	1.0593	1.0609	1.0598	1.0597	1.0507
3.00%	1.0898	1.0923	1.0906	1.0905	1.0768
4.00%	1.1209	1.1244	1.1221	1.1219	1.1032
5.00%	1.1527	1.1571	1.1541	1.1540	1.1302

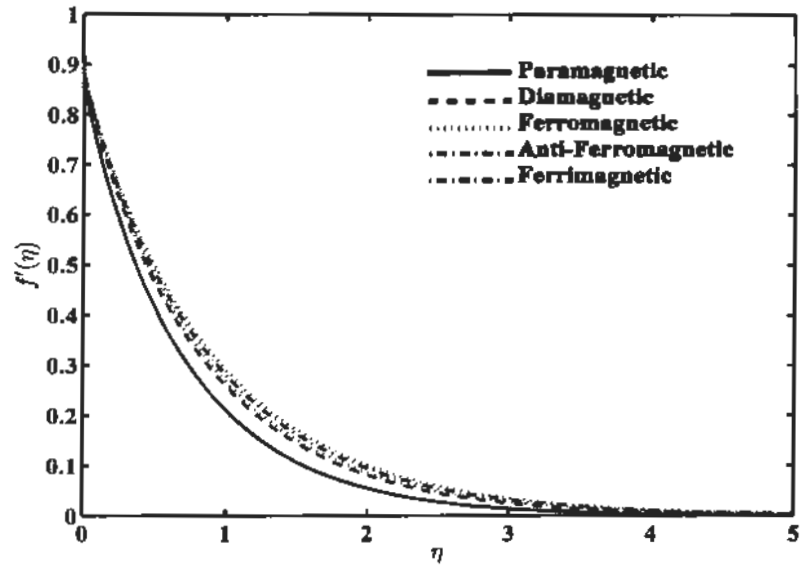

Fig. 10.1. Impact of different nanoparticles particles on velocity profile.

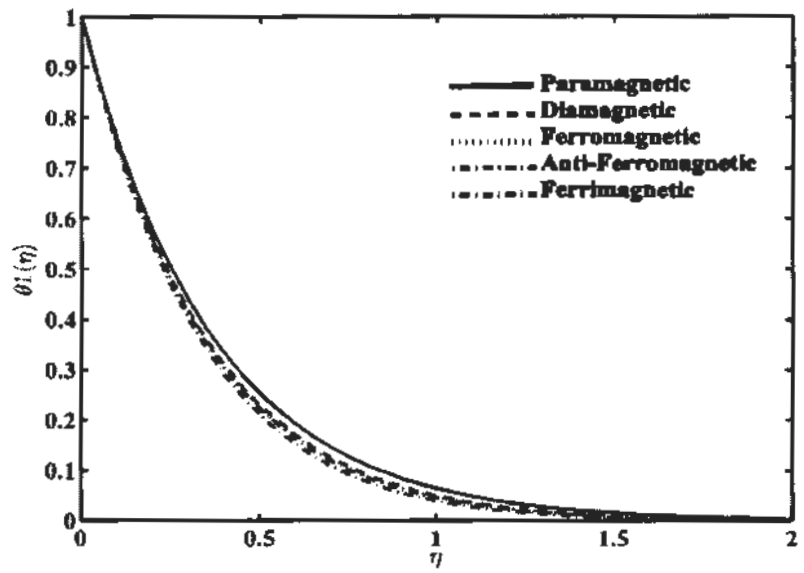

Fig. 10.2. Impact of different nanoparticle on temperature profiles.

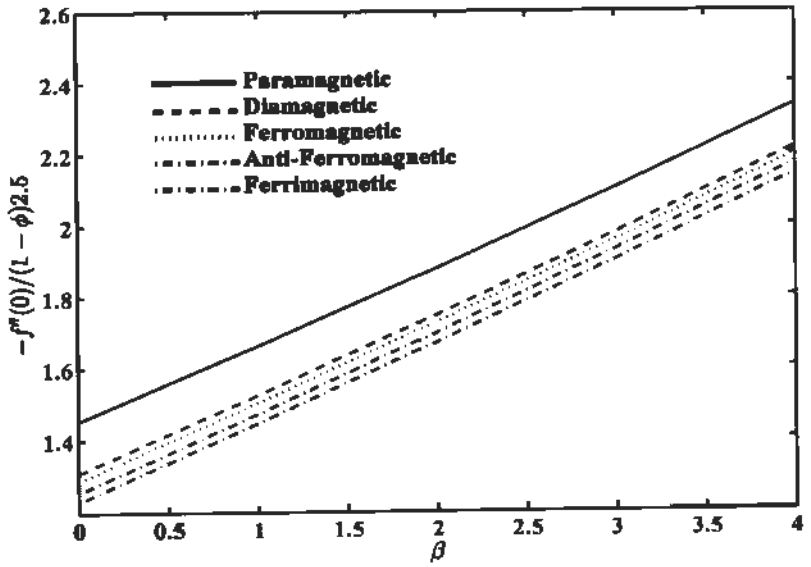

Fig. 10.3. Change of Skin friction coefficient versus β .

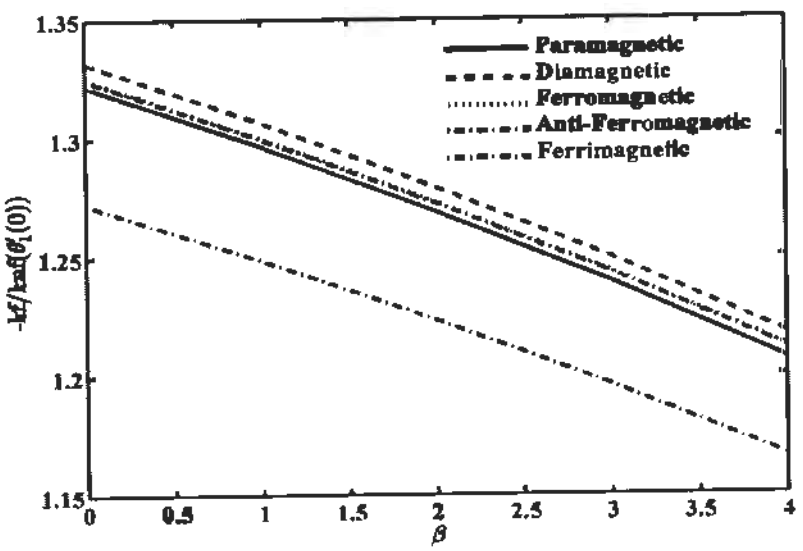

Fig. 10.4. Change of Nusselt number versus β .

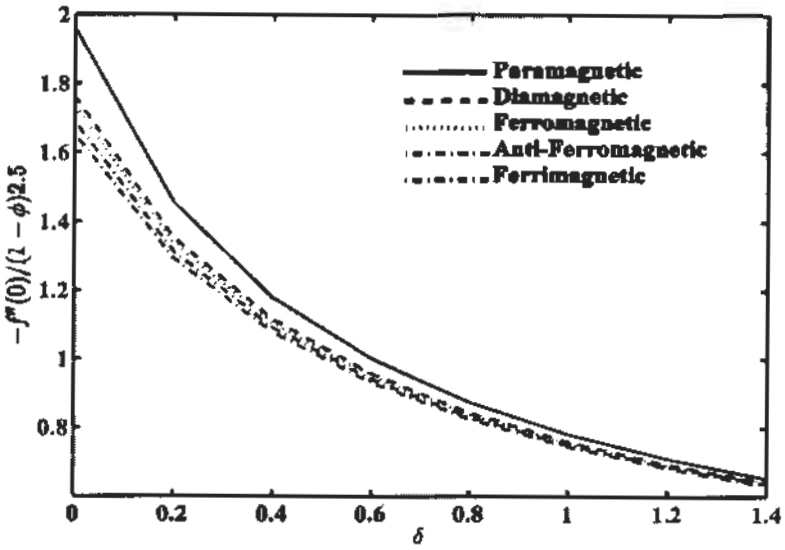

Fig. 10.5. Change of Skin friction coefficient versus δ.

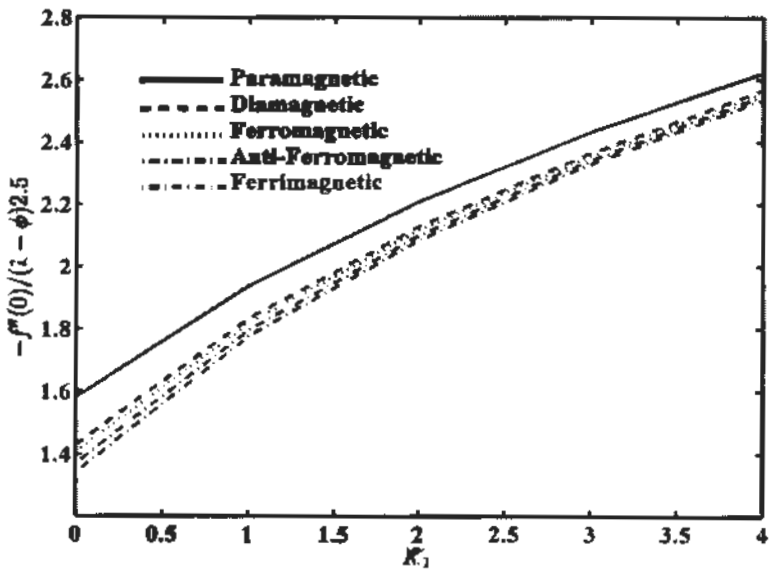

Fig. 10.6. Change of Skin friction coefficient versus K_1.

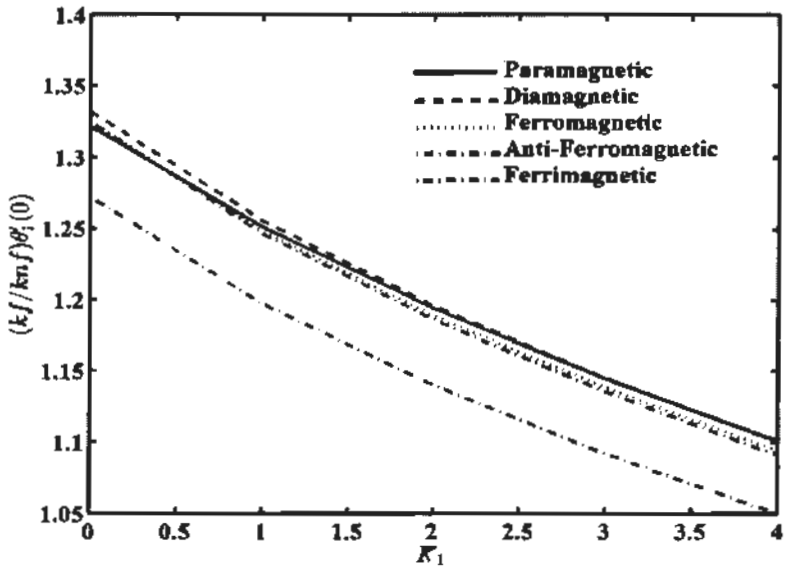

Fig. 10.7. Change of Nusselt number versus K_1.

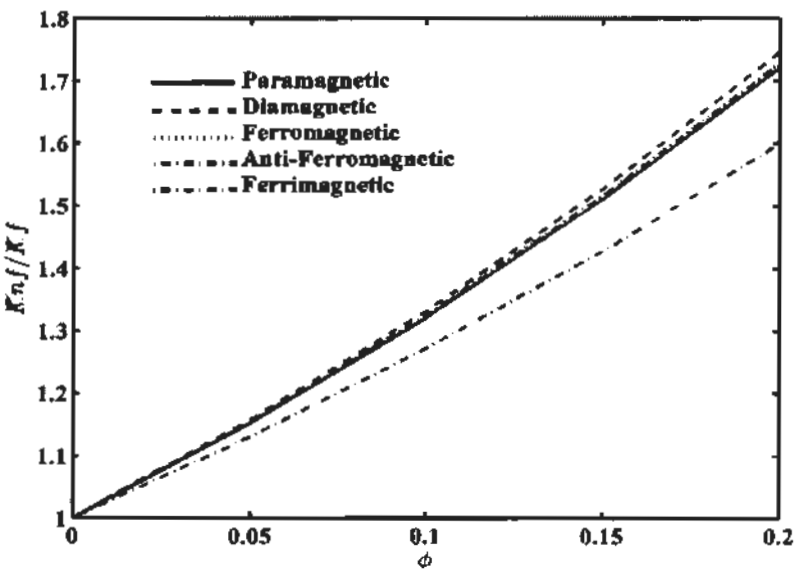

Fig. 10.8. Thermal conductivity versus volume fraction ϕ.

10.4 Conclusion

Here we explored behavior of different magnetic nanoparticles over a stretching sheet. The following points are summarized as follow.

- The velocity for paramagnetic nanoparticles is highest whereas it has lowest in temperature profile.
- Skin friction coefficient increases versus ferromagnetic parameter as well as porosity parameter while it declines for slip parameter.
- Nusselt number declines by increasing ferromagnetic interaction parameter and porous medium parameter.
- Both Nusselt number and skin friction have lowest value for ferrimagnetic particle(Fe_3O_4) case as compared with the others.
- Thermal conductivity of nanoparticles enhances with the deviation of volume fraction.

Chapter 11

Particle shape effects on ferrofluids flow and heat transfer under influence of low oscillating magnetic field disk

11.1 Introduction

This chapter investigate the shapes effect of magnetic nanoparticle on boundary layer flow of ferrofluid over a rotating disk with the existence of low oscillating magnetic field. The disk is rotate about z-axis with uniform angular velocity. Water is considered as a base fluid while magnetite as nanoparticle with three different shapes like platelet, cylinder and brick, which is based on Hamilton-Crosser model. Ferrofluid is electrically non-conducting. Transformation procedure is adopted to change the governing equations of motions into nonlinear ODE's which are then tackle numerically by employing robust R-k method. A tremendous agreement is viewed among the present results and earlier published in the literature for limiting case. Shape effects on radial, tangential, and axial velocity along with temperature fields are demonstrated through graphically while computational values of shear stress and heat transfer characteristics are elaborated in tabular form against ferromagnetic (ferro-hydrodynamic) parameter and volume fraction of magnetic nanoparticle.

11.2 Flow assumption and mathematical formulation

Consider an incompressible axially symmetric laminar and non-conducting ferromagnetic liquid flow over rotating disk with speed $\Omega_* r/|1-a_3 t|$ as displayed in section (1.17). The basic governing flow equations containing continuity, momentum with rotating effects, temperature, magnetization and rotational motion equations takes the form

$$\nabla.\mathbf{V} = 0, \tag{11.1}$$

$$\rho_{nf}\frac{d\mathbf{V}}{dt} - \mu_0(\boldsymbol{M}.\nabla)\boldsymbol{H} = -\nabla p + \mu_{nf}\nabla^2\mathbf{V} + \frac{1}{2\lambda_1}\nabla\times(\boldsymbol{\omega}_p - \boldsymbol{\Omega}), \tag{11.2}$$

$$(\rho C_p)_{nf}\frac{dT}{dt} = k_{nf}\nabla^2 T, \tag{11.3}$$

$$\frac{dM}{dt}+\frac{1}{\tau_B}\left(M-M_0\right)=\omega_p\times M, \tag{11.4}$$

$$I\frac{d\omega_p}{dt}+\frac{1}{\lambda_3}\left(\omega_p-\Omega\right)=M\times H. \tag{11.5}$$

Here, $\mathbf{V}=\left(u_r,u_\theta,u_z\right)$ is velocity, ω_p is angular moment of particles, I is total moments of inertia , μ_0 is permeability of free space , τ_w is Brownian relaxation time, , Ω is vorticity of the flow. For small λ_3, the inertial term i.e., $I\frac{d\omega_p}{dt}\ll I\frac{\omega_p}{\lambda_3}$, hence, Eq. (11.5) lead to the expression

$$\omega_p=\Omega+\frac{\lambda_3}{I}\left(M\times H\right). \tag{11.6}$$

Now, Eqs. (11.2) and (11.4) with involving Eq. (11.6) takes the form

$$\rho_{nf}\frac{d\mathbf{V}}{dt}+\left(M.\nabla\right)H=-\nabla p+\mu_{nf}\nabla^2\mathbf{V}-\frac{1}{2}\nabla\times\left(M\times H\right) \tag{11.7}$$

$$\frac{dM}{dt}-\frac{1}{\tau_B}\left(M-M_0\right)=\frac{\lambda_3}{I}M\times\left(M\times H\right)+\Omega\times M, \tag{11.8}$$

where $M\times H$ is magnetic torques. When both torques, magnetic and viscous are be in balance form, then rotation of particle is inscribed as

$$M\times H=-6\left(\Omega-\omega_p\right)\mu_{nf}\phi, \tag{11.9}$$

and at equilibrium

$$M=\frac{L(\lambda_e)M_s\lambda_e\phi}{\lambda}, \tag{11.10}$$

where λ_e effective magnetic parameter and ϕ designates the concentration of nanoparticle. Under the stimulus of sluggish vacillating magnetic field Eq. (11.8) is stated as [140-142]

$$\frac{d}{dt}\left(L_e\frac{\lambda_e}{\lambda}\right)=\Omega\times\left(L_e\frac{\lambda_e}{\lambda}\right)-\frac{1}{\tau_B}\frac{L_e}{\lambda_e}\left(\lambda_e-\lambda\right)-\frac{L_e^{\,2}}{2\tau_B\lambda_e^{\,3}}\lambda_e\times\left(\lambda_e-\lambda\right). \tag{11.11}$$

So, from Eq. (11.11) effective field can be stated in term of zero approximation equation as

$$\tau_B\frac{d\lambda_e}{dt}=-\left(\frac{d\log L_e}{d\lambda_e}\right)^{-1}\left(1-\frac{\lambda_o}{\lambda_e}\cos\omega_o t\right). \tag{11.12}$$

Above, the parameters ω_o and λ_o are frequency and amplitude of magnetic field, whereas the active Langevin function is donated as parameter L_e. From [143], applying linear estimations in $\Omega\tau_B$ and the statement

$$M^{(1)} = (\lambda_e)\tau_B R M^{(0)}\,\Omega \times \boldsymbol{h}. \tag{11.13}$$

Here $M^{(0)} = L(\lambda_e)\phi M_s$ and $\boldsymbol{h}$ is unit vector toward the applied field, Eq. (11.11) reduces to

$$\frac{dR(\lambda_e)}{dt} = \frac{1}{\tau_B}\left(1 - \frac{1}{2}\left(\frac{\lambda_e - L_e}{\lambda_e L_e}\right)\cos\omega_0 t \times \lambda_o R(\lambda_e)\right). \tag{11.14}$$

Subsequently torque is not zero, so from Eqs. (11.9) and (11.11), the statement for magnetic torque turn out to be

$$\overline{\boldsymbol{M}\times\boldsymbol{H}} = -6\beta\mu\phi\Omega,\ \ \beta = \frac{1}{2}\lambda_0\overline{\cos\omega_0 t L(\lambda_e)R(\lambda_e)}. \tag{11.15}$$

Here, $\beta(\lambda_0, \omega_0\tau_B)$ represent effective magnetization parameter.

$$\frac{1}{2}\nabla\times\overline{\boldsymbol{M}\times\boldsymbol{H}} = \frac{1}{2}\nabla\times -6(\mu_f)\phi\beta\Omega = -\frac{3}{2}\mu_f\beta\phi\nabla(\nabla.\mathbf{V}) = \frac{3}{2}\mu_f\beta\phi\nabla^2\mathbf{V}. \tag{11.16}$$

In view of Eq. (11.16), Eq. (11.7) takes the form

$$\rho_{nf}\frac{d\mathbf{V}}{dt} - \left(\mu_{nf} + \frac{3}{2}\mu_f\phi\beta\right)\nabla^2\mathbf{V} = -\nabla p + (\boldsymbol{M}.\nabla)\boldsymbol{H}, \tag{11.17}$$

$$\rho\frac{d\mathbf{V}}{dt} - \left(\mu_{nf} + \frac{3}{2}\mu_f\phi\beta\right)\nabla^2\mathbf{V} = -\nabla\tilde{p}. \tag{11.18}$$

Here $-\nabla\tilde{p}$ is condensed pressure, transformed equations of motion and energy with pressure in cylindrical coordinates along with boundary conditions are

$$\frac{\partial u_r}{\partial r} + \frac{u_r}{r} + \frac{\partial u_z}{\partial z} = 0, \tag{11.19}$$

$$\begin{aligned} -\frac{\partial\tilde{p}}{\partial r} + \left(\mu_{nf} + \frac{3}{2}\mu_f\phi\beta\right)\left[\frac{\partial^2 u_r}{\partial r^2} + \frac{\partial}{\partial r}\left(\frac{u_r}{r}\right) + \frac{\partial^2 u_r}{\partial z^2}\right] + g(\rho\beta_1)_{nf}(T - T_\infty) \\ = \rho_{nf}\left[\frac{\partial u_r}{\partial t} + u_r\frac{\partial u_r}{\partial r} + u_z\frac{\partial u_r}{\partial z} - \frac{u_\theta^{\,2}}{r}\right], \end{aligned} \tag{11.20}$$

$$\begin{aligned} \left(\mu_{nf} + \frac{3}{2}\mu_f\phi\beta\right)\left[\frac{\partial^2 u_\theta}{\partial r^2} + \frac{\partial}{\partial r}\left(\frac{u_\theta}{r}\right) + \frac{\partial^2 u_\theta}{\partial z^2}\right] + g(\rho\beta_1)_{nf}(T - T_\infty) \\ = \rho_{nf}\left[\frac{\partial u_\theta}{\partial t} + u_r\frac{\partial u_\theta}{\partial r} + u_z\frac{\partial u_\theta}{\partial z} + \frac{u_r u_\theta}{r}\right], \end{aligned} \tag{11.21}$$

$$-\frac{\partial \tilde{p}}{\partial z}+\left(\mu_{nf}+\frac{3}{2}\mu_f\phi\beta\right)\left[\frac{\partial^2 u_z}{\partial r^2}+\frac{1}{r}\frac{\partial u_z}{\partial r}+\frac{\partial^2 u_z}{\partial z^2}\right]+g(\rho\beta_1)_{nf}(T-T_r)$$
$$=\rho_{nf}\left[\frac{\partial u_z}{\partial t}+u_r\frac{\partial u_z}{\partial r}+u_z\frac{\partial u_z}{\partial z}\right], \tag{11.22}$$

$$\left(\rho C_p\right)_{nf}\left[\frac{\partial T}{\partial t}+u_r\frac{\partial T}{\partial r}+u_z\frac{\partial T}{\partial z}\right]=k_{nf}\left[\frac{\partial^2 T}{\partial r^2}+\frac{1}{r}\frac{\partial T}{\partial r}+\frac{\partial^2 T}{\partial z^2}\right], \tag{11.23}$$

$$\left.\begin{aligned} &at\ \ z=0;\quad u_r=\frac{\Omega_u r}{1-a_3 t},\ u_\theta=\frac{\Omega_u r}{1-a_3 t},\ u_z=0,\ T=T_w \\ &at\ \ z=\infty;\quad u_r=0,\ u_\theta=0,\ T=T_\infty \end{aligned}\right\}. \tag{11.24}$$

Employing following transformation

$$\left.\begin{aligned} &\eta=\sqrt{\Omega/\nu_f}\,\frac{z}{\sqrt{1-a_3 t}},\ u_r(r,\theta,z)=\frac{\Omega r}{1-a_3 t}F(\eta),\ u_\theta(r,\theta,z)=\frac{\Omega r}{1-a_3 t}G(\eta), \\ &u_z(r,\theta,z)=\sqrt{\frac{\Omega\nu_f}{1-a_3 t}}E(\eta),\ \ \frac{p}{\rho_f}=-\frac{\Omega\nu_f}{1-a_3 t}P(\eta),\ \ \theta(\eta)=\frac{T-T_\infty}{T_w-T_\infty}, \end{aligned}\right\}. \tag{11.25}$$

By using Eqs. (11.25) into Eq. (11.19) to (11.23) and obtained non-dimension system of equations in ordinary form

$$2F(\eta)+E'(\eta)=0, \tag{11.26}$$

$$\frac{\rho_{nf}}{\rho_f}\left[F^2-G^2+EF'+S\left(F+\frac{\eta}{2}F'\right)\right]=\left(\frac{\mu_{nf}}{\mu_f}+\frac{3}{2}\phi\beta\right)F''+\lambda\frac{(\rho\beta_1)_{nf}}{(\rho\beta_1)_f}\theta, \tag{11.27}$$

$$\frac{\rho_{nf}}{\rho_f}\left[EG'+2FG+S\left(G+\frac{\eta}{2}G'\right)\right]=\left(\frac{\mu_{nf}}{\mu_f}+\frac{3}{2}\phi\beta\right)G''+\lambda\frac{(\rho\beta_1)_{nf}}{(\rho\beta_1)_f}\theta, \tag{11.28}$$

$$\frac{\rho_{nf}}{\rho_f}\left[EE'+\frac{S}{2}\left(E+\eta E'\right)\right]=-\frac{\partial P}{\partial\eta}+\left(\frac{\mu_{nf}}{\mu_f}+\frac{3}{2}\phi\beta\right)E''+\lambda\frac{(\rho\beta_1)_{nf}}{(\rho\beta_1)_f}\theta, \tag{11.29}$$

$$\frac{\left(\rho C_p\right)_{nf}}{\left(\rho C_p\right)_f}\Pr\left[E\theta'+S\frac{\eta}{2}\theta'\right]=\left(\frac{k_{nf}}{k_f}+R_d\right)\theta'' \tag{11.30}$$

with suitable boundary conditions

$$\left.\begin{aligned} &G(0)=1,\ F(0)=0,\ E(0)=0,\ \theta(0)=1, \\ &G(\infty)=0,\quad F(\infty)=0,\quad \theta(\infty)=0 \end{aligned}\right\}, \tag{11.31}$$

where, $A=a_3/\Omega$ is unsteadiness parameter, and $Pr=\mu_f C_{pf}/k_f$ is modified Prandtl number. For magnetite (Fe_3O_4), ρ_{nf} the expression of density, μ_{nf} dynamic viscosity, and heat capacitance $(\rho C_p)_{nf}$, and thermal expansion coefficient $(\rho\beta_1)_{nf}$ are described as

$$\rho_{nf}=(1-\phi)\rho_f+\phi\rho_s,\ \mu_{nf}=\frac{\mu_f}{(1-\phi)^{2.5}}, \tag{11.32}$$

$$(\rho C_p)_{nf}=\phi(\rho C_p)_s+(1-\phi)(\rho C_p)_f, \tag{11.33}$$

$$(\rho\beta_1)_{nf}=(1-\phi)(\rho\beta_1)_f+\phi(\rho\beta_1)_s, \tag{11.34}$$

where ϕ is symbolized as volume concentration of solid particle, μ_f is viscosity of the conventional fluid, ρ_f and ρ_s are effective densities of base fluid and nanoparticle, k_f and k_s are signify energy conductivities for pure fluid and solid particle. Thermal conductivity k_{nf} of the nanoparticles specified by Hamilton and Crosser [144] is defined as

$$k_{nf}=k_f\left\{\frac{k_s+(m+1)k_f-(m+1)\phi(k_f-k_s)}{k_s+(m+1)k_f+\phi(k_f-k_s)}\right\}. \tag{11.35}$$

Here, "m" represent the empirical shape factor specified by $3/\psi^*$. When we take shape factor m=3, Hamilton-Crosser model becomes Maxwell model. The values of nanoparticles for different sphericity and shapes are given in table 11.1. Skin friction and Nusselt number are describe as

$$C_f=\frac{\sqrt{\tau_{wr}^2+\tau_{w\phi}^2}}{\rho_f\left(\dfrac{\Omega r}{1-a_3 t}\right)^2},\quad Nu=\frac{rq_w}{k_f\left(T_w-T_\infty\right)}. \tag{11.36}$$

Here τ_{wr} is radial and $\tau_{w\phi}$ is transversal skin friction coefficient of rotating disk, q_w is temperature flux are presented as

$$\tau_{wr}=\left(\mu_{nf}+\frac{3}{2}\mu_f\phi\beta\right)\left(\frac{\partial u_r}{\partial z}+\frac{\partial u_z}{\partial\theta}\right)_{z=0},\quad \tau_{w\phi}=\left(\mu_{nf}+\frac{3}{2}\mu_f\phi\beta\right)\left(\frac{\partial u_\theta}{\partial z}+\frac{1}{r}\frac{\partial u_z}{\partial\theta}\right)_{z=0},$$
$$q_w=-k_{nf}\left(\frac{\partial T}{\partial z}\right)_{z=0}. \tag{11.37}$$

After replacing Eqs. (11.25) and (11.37) in to Eq. (11.36), we get

$$C_f \,\mathrm{Re}^{\frac{1}{2}} = \sqrt{F'(0)^2 + G'(0)^2}\left(\frac{\mu_{nf}}{\mu_f} + \frac{3}{2}\phi\beta\right), \qquad Nu/\mathrm{Re}^{\frac{1}{2}} = -\frac{k_{nf}}{k_f}\theta'(0), \qquad (11.38)$$

where, $\mathrm{Re} = r^2\Omega_v/(1-a_3t)\nu_f$ is the rotational Reynolds number.

11.3. Results and discussion

In this section, interpretation of controlling quantities involved in velocity and temperature profiles are inspected via Figs. 11.1 to 11.8. Ferrofluid contained magnetite- Fe_3O_4 nanoparticle with different shapes with water is taken as a base fluid. The influence of low isolating magnetic field is also accounted. The values of the governing constraints throughout the problem are considered $Pr = 6.2$, $\beta = 0.1$, $\lambda = 0.01$, $\Lambda = 0.1$ to perceive the influence of volume fraction and ferro-magnetization effects on velocities and temperature profiles along with three shapes of magnetic nanoparticles. Some thermo-mechanical properties of magnetite (Fe_3O_4) and water are enumerated in table 11.2. In table 11.3 we compared the results of $F'(0)$, $G'(0)$, $E'(\infty)$ and $\theta'(0)$ with available literature and obtained good agreement.

The numerical values of different dimensionless physical parameter are of practical interest. The influence of volume fraction on shear stress and heat transfer rate are displayed in table 11.4. Skin friction increases when the fluid has interaction with the surface of the body. It is perceived that when volume fraction of magnetite (Fe_3O_4) increases, then skin friction at wall is increases. The skin friction depends on acceleration and dynamic viscosity. It is establish that when the concentration of particles is enhanced, then dynamic viscosity and gradient of the velocity rises that are reason for enhancement in skin friction. In table 11.4, it is also perceived that there is enhancement in heat transfer rate against ϕ. In heat transfer process the role of thermal conductivity is imperative. For specimen, if increment in thermal conductivity is noted 35% and 70.3% at 5% and 10% volume fraction of magnetic nanoparticles. Then by similar tendency, increment in Nusselt number at surface is noted 11.4% and 21.7% at 5% and 10% concentration. The consequence of ferromagnetic parameter on skin friction coefficient and Nusselt are exposed in table 11.5. It is declared that with the decrement of ferromagnetic parameter, there is depression in shear stress and heat transfer rate. In addition, results indicate that for higher value of β skin friction and Nusselt number gain maximum decrease in brick case when compared with cylinder and platelet.

The impact of volume fraction of magnetite (Fe_3O_4) nanoparticles of different shapes on radial, tangential, and axial component of velocity are shown in figs. 11.1 to 11.3. The results indicate that velocity components reduces by increasing volume fraction of magnetite (Fe_3O_4) nanoparticle ϕ. Because increment in volume fraction of magnetic nanoparticle ϕ, the viscosity of ferromagnetic liquid increases and thinning the velocity boundary layer as suggested by Brinkman [143].

It is further comprehended that different shapes of magnetite (Fe_3O_4) nanoparticles like platelets, cylinders and bricks also affect the velocity profiles due to their dissimilar orientation and physical properties. The ferromagnetic nanofluid that consist of platelets and cylinder shape particle has gain maximum velocity in radial and tangential direction when compared to other shapes whereas opposite behavior is noted for axial velocity case as shown in fig. 11.3.

Fig. 11.4. demonstrate the influence of magnetic nanoparticle concentration ϕ on temperature circulation. It is prominent that the temperature of magnetite (Fe_3O_4) nanofluid is increases by intensifying volume fraction. When the amount of volume fraction is increases, then thermal conductivity enhances and hence produce enhancement in thermal boundary layer. Additionally, impact of ferromagnetic particle shapes also affect the temperature profile. It is perceived that fluid temperature has gained ultimate increment due to platelets followed by cylinder and brick respectively.

Figs. 11.5 to 11.7. fascinates the velocity profiles along radial, tangential and axial direction for numerous values of low oscillating ferromagnetic parameter. Form the figures we observed that the impact of ferromagnetic parameter in is not so conspicuous on axial, radial and tangential directions. Because under the action of low oscillating applied magnetic field angular velocity of magnetite (Fe_3O_4) nanoparticle become lesser when compared to the angular velocity of fluid. So influence of ferromagnetic parameter is not so prevailing. Also noticed that velocity components are suppressed in all direction when ferromagnetic parameter is decreased. This is because of the fact that increase in angular velocity of the magnetic nanoparticle, which correspond to reduction in magnetization effects and created an extra opposition in ferromagnetic fluid. Fig. 11.8. portrays the temperature field under the effect of ferromagnetic parameter. Results shows that temperature is boost up by enlarging the magnetization impact. The outcome of magnetization is the signs of increment in turning viscosity that develop a foundation of temperature enrichment.

Table 11.1 The values of different shapes factor and sphericity of nanoparticles [145].

Shape of Nanoparticles	Phase ratio	Sphericity	Shape factor (m)
Cylinder	1:8	0.62	4.9
Brick	1:1:1	0.81	3.7
Platelet	1:1/8	0.52	5.7

Table 11.2 Physical properties of water and magnetic nanoparticle.

	$\rho(\text{kg/ m}^3)$	$c_p(\text{j/ Kg.k})$	$k(\text{W/ m.k})$	$\beta\times10^{-5}(\text{k}^{-1})$
water	997	4179	0.613	21
Fe_3O_4	5180	670	9.7	0.5

Table 11.3 Comparison of current results with previously published work when $Pr = 6.2$, $\lambda = \beta = \Lambda = 0$.

	Present result	Kelson and Desseaux [146]	Rashidi et al. [147]
$F'(0)$	0.5102327	0.510233	0.50186
$-G'(0)$	0.6159220	0.615922	0.61589
$-E'(\infty)$	0.8844681	0.884474	---------
$-\theta'(0)$	0.3258625	---------	0.3276

Table 11.4 Effect of volume fraction magnetite (Fe_3O_4) nanoparticle on Skin friction and Nusselt number when $Pr = 6.2, \beta = 0.1, \lambda = 0.01, \Lambda = 0.0$.

	ϕ	Platelet	Cylinder	Bricks
$C_f \mathrm{Re}^{1/2}$	0.0	0.8042	0.8042	0.8042
	0.05	1.0864	1.0863	1.0863
	0.10	1.3699	1.3698	1.3697
	0.15	1.6599	1.6597	1.6595
$Nu\,\mathrm{Re}^{-1/2}$	0.0	0.3319	0.3319	0.3319
	0.05	0.3696	0.3669	0.3633
	0.10	0.4038	0.3991	0.3925
	0.15	0.4356	0.4292	0.4203

Table 11.5 Effect of ferromagnetic parameter on Skin friction and Nusselt number when $Pr = 6.2, \phi = 0.1, \lambda = 0.01, \Lambda = 0.0$.

	β	Platelet	Cylinder	Bricks
$C_f \mathrm{Re}^{1/2}$	0	1.0925	1.0924	1.0923
	0.5	1.1234	1.1233	1.1231
	1.0	1.1534	1.1533	1.1532
	1.5	1.1826	1.1825	1.1824
	2.0	1.2112	1.2111	1.2109
	3.0	1.2663	1.2662	1.2661
	5.0	1.3699	1.3698	1.3697
$Nu\,\mathrm{Re}^{-1/2}$	0	0.3842	0.3802	0.3745
	0.5	0.3869	0.3828	0.3771
	1.0	0.3895	0.3853	0.3795
	1.5	0.3918	0.3875	0.3816
	2.0	0.3940	0.3896	0.3836
	3.0	0.3978	0.3933	0.3871
	5.0	0.4038	0.3991	0.3925

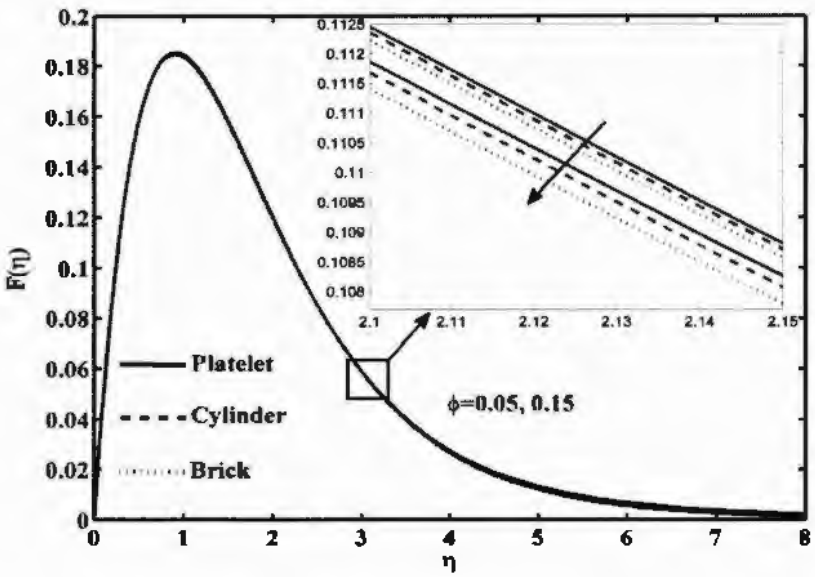

Fig. 11.1. Impact of volume fraction of magnetite- Fe_3O_4 nanoparticle on radial velocity profile with different shapes

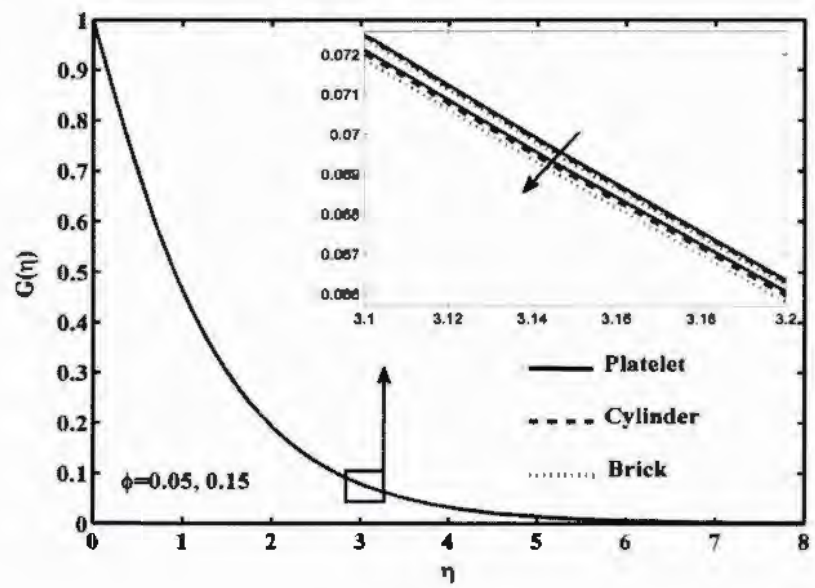

Fig. 11.2. Impact of volume fraction of magnetite- Fe_3O_4 nanoparticle on tangential velocity profile with different shapes.

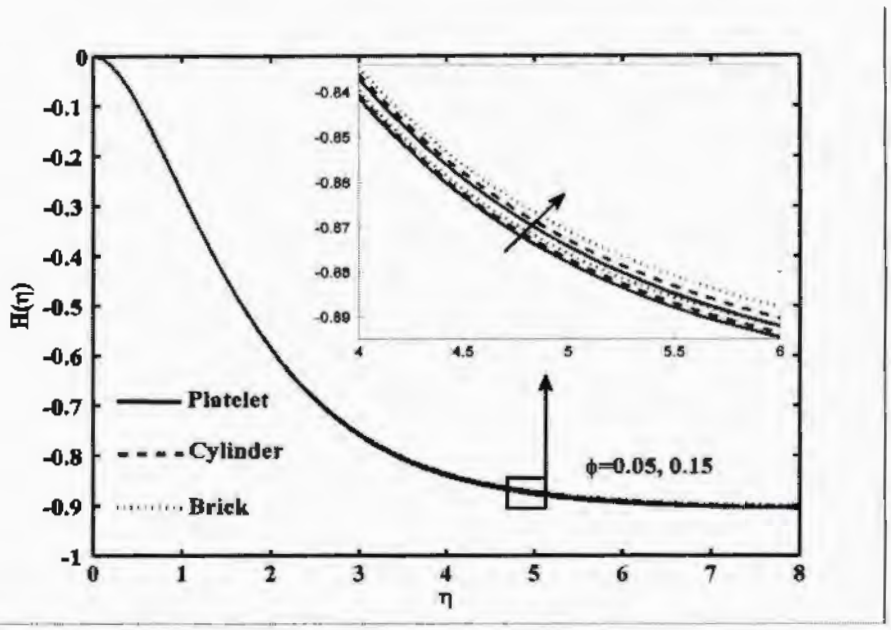

Fig. 11.3. Impact of volume fraction of magnetite- Fe_3O_4 nanoparticle on axial velocity profile with different shapes.

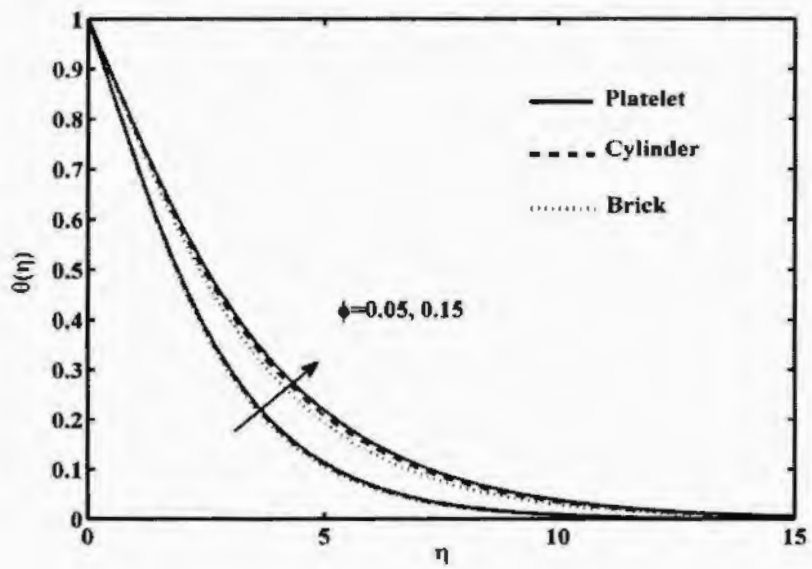

Fig. 11.4. Impact volume fraction of magnetite- Fe_3O_4 nanoparticle on temperature profile with different shapes.

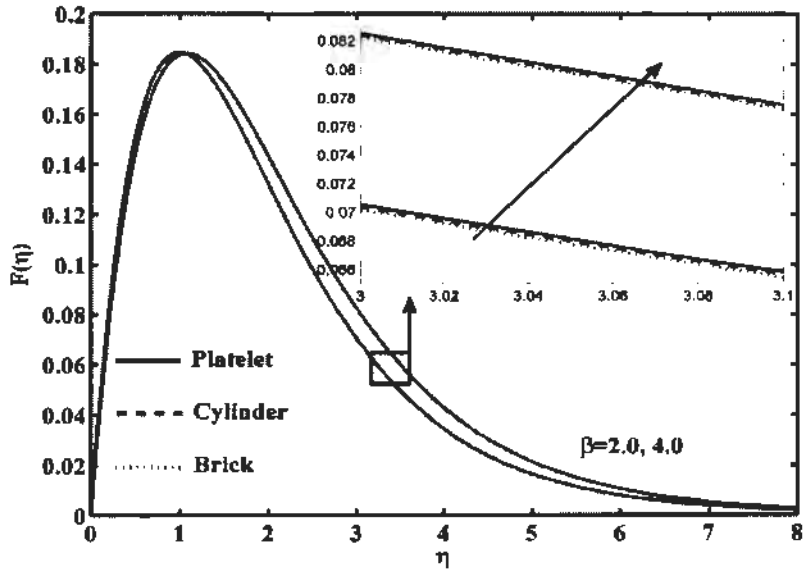

Fig. 11.5. Impact of ferromagnetic parameter on radial velocity field.

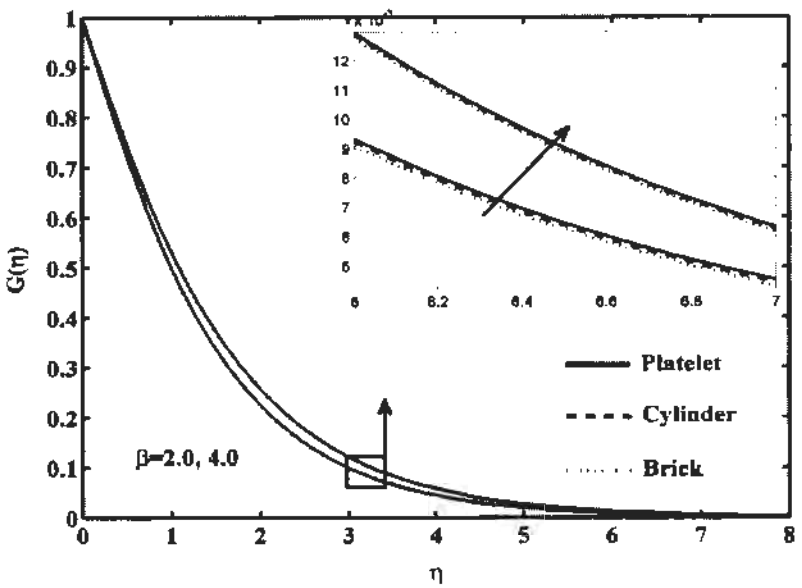

Fig. 11.6. Impact of ferromagnetic parameter on tangential velocity field.

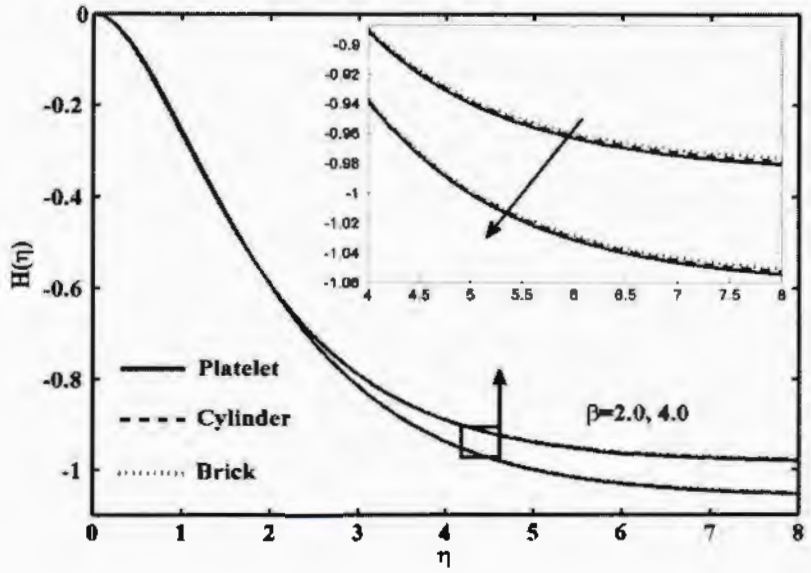

Fig. 11.7. Impact of ferromagnetic parameter on axial velocity field.

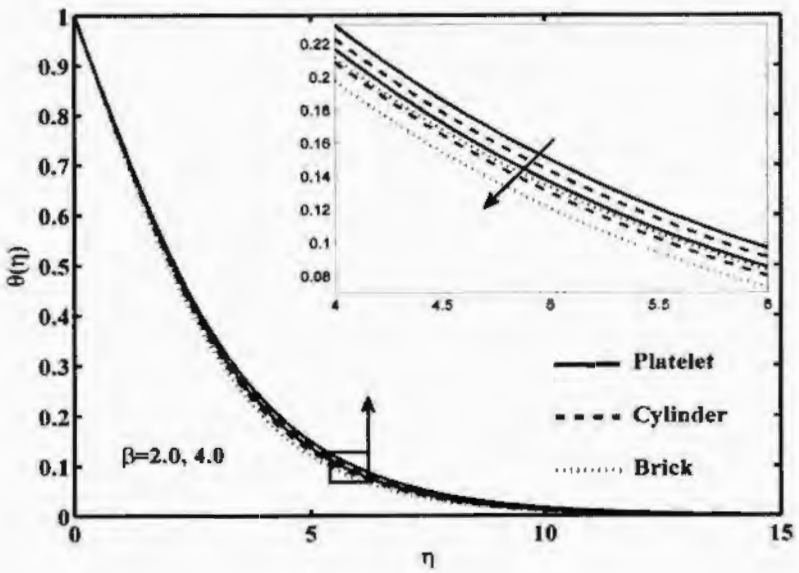

Fig. 11.8. Impact of ferromagnetic parameter on temperature field.

11.4 Conclusion

In this paper, shape effect of ferromagnetic particles like platelet, cylinder and brick over a rotating disk under low oscillating magnetic field is discussed. Water is considered as a base fluid while magnetite- Fe_3O_4 as nanoparticle. Similarity approach is used to obtain the highly non-linear coupled differential equation which are then solved numerically. The major finding of present problem are as follow

- Velocity components decreases by increasing volume fraction of nanoparticles.
- Platelets and cylindrical shape nanoparticles gain maximum velocity in radian and tangential direction.
- It is perceived that fluid temperature has gain ultimate increment due to platelets followed by cylinder and brick respectively.
- Both Skin friction and Nusselt number gain maximum decrease in brick case when compared with cylinder and platelet for higher value of β .

References

[1] Gazeau, F., Baravian, C., Bacri, J. C., Perzynski, R., & Shliomis, M. I. (1997). Energy conversion in ferrofluids magnetic nanoparticles as motors or generators. *Physical Review E, 56(1), 614.*

[2] Vales-Pinzón, C., Alvarado-Gil, J. J., Medina-Esquivel, R., & Martínez-Torres, P. (2014). Polarized light transmission in ferrofluids loaded with carbon nanotubes in the presence of a uniform magnetic field. *Journal of Magnetism and Magnetic Materials, 369, 114-121.*

[3] Yellen, B. B., Fridman, G., & Friedman, G. (2004). Ferrofluid lithography. *Nanotechnology, 15(10), S562.*

[4] Hathway, D. B. (1979) Use of ferrofluid in moving coil loudspeakers. *DB-Sound Engineering Magazine. 13*(2), 42-44.

[5] Feynman, R. P., Leighton, R. B., & Sands, M. (1965). The feynman lectures on physics. *American Journal of Physics*, *33*(9), 750-752.

[6] Shliomis, M. I. (2004). Comment on ferrofluids as thermal ratchets. *Physical Review Letters*, *92*(18), 188901.

[7] Maruno, S., Yubakami, K., & Soga, M. (1983). Plain paper recording process using magnetic fluids magneto-fluid-graphy. *Journal of Magnetism and Magnetic Materials*, *39*(1-2), 187-189.

[8] Rosensweig, R. E., Nestor, J. W., & Timmins, R. S. (1965). Ferrohydrodynamic fluids for direct conversion of heat energy. *In Materials associated with direct energy conversion.*

[9] Neuringer, J. L. (1966). Some viscous flows of a saturated ferro-fluid under the combined influence of thermal and magnetic field gradients. *International Journal of Non-Linear Mechanics*, *1*(2), 123-137.

[10] Tangthieng, C., Finlayson, B. A., Maulbetsch, J., & Cader, T. (1999). Heat transfer enhancement in ferrofluids subjected to steady magnetic fields. *Journal of Magnetism and Magnetic Materials*, *201*(1), 252-255.

[11] Yamaguchi, H., Zhang, Z., Shuchi, S., & Shimada, K. (2002). Heat transfer characteristics of magnetic fluid in a partitioned rectangular box. *Journal of Magnetism and Magnetic Materials*, *252*, 203-205.

[12] Snyder, S. M., Cader, T., & Finlayson, B. A. (2003). Finite element model of magnetoconvection of a ferrofluid. *Journal of Magnetism and Magnetic Materials*, *262*(2), 269-279.

[13] Ramanathan, A., & Suresh, G. (2004). Effect of magnetic field dependent viscosity and anisotropy of porous medium on ferroconvection. *International Journal of Engineering Science*, *42*(3), 411-425.

[14] Finlayson, B. A. (1970). Convective instability of ferromagnetic fluids. *Journal of Fluid Mechanics*, *40*(04), 753-767.

[15] Ganguly, R., Sen, S., & Puri, I. K. (2004). Heat transfer augmentation using a magnetic fluid under the influence of a line dipole. *Journal of Magnetism and Magnetic Materials*, *271*(1), 63-73.

[16] Aminfar, H., Mohammadpourfard, M., & Mohseni, F. (2012). Two-phase mixture model simulation of the hydro-thermal behavior of an electrical conductive ferrofluid in the presence of magnetic fields. *Journal of Magnetism and Magnetic Materials*, *324*(5), 830-842.

[17] Aminfar, H., Mohammadpourfard, M., & Kahnamouei, Y. N. (2011). A 3D numerical simulation of mixed convection of a magnetic nanofluid in the presence of non-uniform magnetic field in a vertical tube using two phase mixture model. *Journal of Magnetism and Magnetic Materials*, *323*(15), 1963-1972.

[18] Aminfar, H., Mohammadpourfard, M., & Zonouzi, S. A. (2013). Numerical study of the ferrofluid flow and heat transfer through a rectangular duct in the presence of a non-uniform transverse magnetic field. *Journal of Magnetism and Magnetic materials*, *327*, 31-42.

[19] Strek, T., & Jopek, H. (2007). Computer simulation of heat transfer through a ferrofluid. *Physica Status Solidi (b)*, *244*(3), 1027-1037.

[20] Sheikholeslami, M., & Rashidi, M. M. (2015). Ferrofluid heat transfer treatment in the presence of variable magnetic field. *The European Physical Journal Plus*, *130*(6), 115.

[21] Ghofrani, A., Dibaei, M. H., Sima, A. H., & Shafii, M. B. (2013). Experimental investigation on laminar forced convection heat transfer of ferrofluids under an alternating magnetic field. *Experimental Thermal and Fluid Science*, *49*, 193-200.

[22] Selimefendigil, F., & Öztop, H. F. (2014). Effect of a rotating cylinder in forced convection of ferrofluid over a backward facing step. *International Journal of Heat and Mass Transfer*, *71*, 142-148.

[23] Jafari, A., Tynjälä, T., Mousavi, S. M., & Sarkomaa, P. (2008). Simulation of heat transfer in a ferrofluid using computational fluid dynamics technique. *International Journal of Heat and Fluid Flow*, *29*(4), 1197-1202.

[24] Sekar, R., & Vaidyanathan, G. (1993). Convective instability of a magnetized ferrofluid in a rotating porous medium. *International Journal of Engineering Science*, *31*(8), 1139-1150.

[25] Zahn, M., & Rosensweig, R. (1980). Stability of magnetic fluid penetration through a porous medium with uniform magnetic field oblique to the interface. *IEEE Transactions on Magnetics*, *16*(2), 275-282.

[26] Jue, T. C. (2006). Analysis of combined thermal and magnetic convection ferrofluid flow in a cavity. *International Communications in Heat and Mass Transfer*, *33*(7), 846-852.

[27] Narayana, M., Titus, L. R., Abraham, A., & Sibanda, P. (2014). Modelling micropolar ferromagnetic fluid flow due to stretching of an elastic sheet. *Afrika Matematika*, *25*(3), 667-679.

[28] Bashtovoi, V., Berkovski, B., & Bashtovol, V. (1996). Magnetic fluids and applications handbook. *Series of Learning Materials, New York: Begell house*.

[29] Gazeau, F., Baravian, C., Bacri, J. C., Perzynski, R., & Shliomis, M. I. (1997). Energy conversion in ferrofluids: Magnetic nanoparticles as motors or generators. *Physical Review E*, *56*(1), 614.

[30] Zahn, M., & Pioch, L. L. (1998). Magnetizable fluid behaviour with effective positive, zero or negative dynamic viscosity. *India Journal of Engineering and Materials Sciences, 5*, 400-410.

[31] Zahn, M., & Pioch, L. L. (1999). Ferrofluid flows in AC and traveling wave magnetic fields with effective positive, zero or negative dynamic viscosity. *Journal of Magnetism and Magnetic Materials*, *201*(1), 144-148.

[32] Zakinyan, A., Nechaeva, O., & Dikansky, Y. (2012). Motion of a deformable drop of magnetic fluid on a solid surface in a rotating magnetic field. *Experimental Thermal and Fluid Science*, *39*, 265-268.

[33] Buzduga, C., Vlad, V., & Ciufudean, C., Experimenting the stability of ferrofluids. *Mathematical Models in Engineering and Computer Science*.

[34] Shliomis, M. I., & Morozov, K. I. (1994). Negative viscosity of ferrofluid under alternating magnetic field. *Physics of Fluids*, *6*(8), 2855-2861.

[35] Oliveira, R. M., Miranda, J. A., & Leandro, E. S. (2008). Ferrofluid patterns in a radial magnetic field: Linear stability, nonlinear dynamics, and exact solutions. *Physical Review E*, *77*(1), 016304.

[36] Vieru, D., Fetecau, C., Athar, M., & Fetecau, C. (2009). Flow of a generalized Maxwell fluid induced by a constantly accelerating plate between two side walls. *Zeitschrift für angewandte Mathematik und Physik*, *60*(2), 334-343.

[37] Fetecau, C., Rana, M., & Fetecau, C. (2013). Radiative and porous effects on free convection flow near a vertical plate that applies shear stress to the fluid. *Zeitschrift für Naturforschung A*, *68*(1-2), 130-138.

[38] Bég, O. A., Bég, T. A., Bakier, A. Y., & Prasad, V. R. (2009). Chemically-reacting mixed convective heat and mass transfer along inclined and vertical plates with Soret and Dufour effects: Numerical solutions. *Internal Journal of Applied Mathematics and Mechanics*, *5*(2), 39-57.

[39] Vafai, K. (1984). Convective flow and heat transfer in variable-porosity media. *Journal of Fluid Mechanics*, *147*, 233-259.

[40] Jothimani, S., & Devi, S. A. (2000). Oblique magnetic field effects over stability in superposed viscous ferrofluids. *Journal of Magnetism and Magnetic materials*, *222*(1), 1-7.

[41] Chol, S. U. S. (1995). Enhancing thermal conductivity of fluids with nanoparticles. *ASME-Publications-Fed*, *231*, 99-106.

[42] Saidur, R., Leong, K. Y., & Mohammad, H. (2011). A review on applications and challenges of nanofluids. *Renewable and Sustainable Energy Reviews*, *15*(3), 1646-1668.

[43] Choi, S. U. S., Zhang, Z. G., Yu, W., Lockwood, F. E., & Grulke, E. A. (2001). Anomalous thermal conductivity enhancement in nanotube suspensions. *Applied Physics Letters*, *79*(14), 2252-2254.

[44] Buongiorno, J., Venerus, D. C., Prabhat, N., McKrell, T., Townsend, J., Christianson, R., & Bang, I. C. (2009). A benchmark study on the thermal conductivity of nanofluids. *Journal of Applied Physics*, *106*(9), 094312.

[45] Masuda, H., Ebata, A., & Teramae, K. (1993). Alteration of thermal conductivity and viscosity of liquid by dispersing ultra-fine particles. Dispersion of Al2O3, SiO2 and TiO2 ultra-fine particles. *Netsu Bussei(Japan)*, *7*(4), 227-223.

[46] Abu-Nada, E., & Oztop, H. F. (2009). Effects of inclination angle on natural convection in enclosures filled with Cu–water nanofluid. *International Journal of Heat and Fluid Flow*, *30*(4), 669-678.

[47] Khan, W. A., & Pop, I. (2010). Boundary-layer flow of a nanofluid past a stretching sheet. *International Journal of Heat and Mass Transfer*, *53*(11), 2477-2483.

[48] Ismoen, M., Kandasamy, R., & Abdul Kahar, R. (2011). Scaling group transformation for boundary-layer flow of a nanofluid past a porous vertical stretching surface in the presence of chemical reaction with heat radiation. *Computers and Fluids*, *52*(1), 15-21.

[49] Hady, F. M., Ibrahim, F. S., Abdel-Gaied, S. M., & Eid, M. R. (2012). Radiation effect on viscous flow of a nanofluid and heat transfer over a nonlinearly stretching sheet. *Nanoscale Research Letters*, *7*(1), 229.

[50] Nadeem, S., & Haq, R. U. (2014). Effect of thermal radiation for megnetohydrodynamic boundary layer flow of a nanofluid past a stretching sheet with convective boundary conditions. *Journal of Computational and Theoretical Nanoscience*, *11*(1), 32-40.

[51] Das, S. K., Putra, N., Thiesen, P., & Roetzel, W. (2003) Temperature dependence of thermal conductivity enhancement for nanofluids. *Journal of Heat Transfer, 125*(4), 567-574.

[52] Vajravelu, K., Prasad, K. V., Lee, J., Lee, C., Pop, I., & Van Gorder, R. A. (2011). Convective heat transfer in the flow of viscous Ag-water and Cu-water nanofluids over a stretching surface. *International Journal of Thermal Sciences*, *50*(5), 843-851.

[53] Turkyilmazoglu, M., & Pop, I. (2013). Heat and mass transfer of unsteady natural convection flow of some nanofluids past a vertical infinite flat plate with radiation effect. *International Journal of Heat and Mass Transfer*, *59*, 167-171.

[54] Vieru, D., Fetecau, C., & Sohail, A. (2011). Flow due to a plate that applies an accelerated shear to a second grade fluid between two parallel walls perpendicular to the plate. *Zeitschrift für angewandte Mathematik und Physik*, *62*(1), 161-172.

[55] Fetecau, C., Vieru, D., & Fetecau, C. (2011). Effect of side walls on the motion of a viscous fluid induced by an infinite plate that applies an oscillating shear stress to the fluid. *Central European Journal of Physics*, *9*(3), 816-824.

[56] Bég, O. A., Rashidi, M. M., Akbari, M., & Hosseini, A. (2014). Comparative numerical study of single-phase and two-phase models for bio-nanofluid transport phenomena. *Journal of Mechanics in Medicine and Biology*, *14*(01), 1450011.

[57] Unal, G. (2003). Symmetries of Itô and Stratonovich dynamical systems and their conserved quantities. *Nonlinear Dynamics*, *32*(4), 417-426.

[58] Unal, G., & Sun, J. Q. (2004). Symmetries and conserved quantities of stochastic dynamical control systems. *Nonlinear Dynamics*, *36*(1), 107-122.

[59] Unal, G. (2001). Approximate first integrals of weakly nonlinear, damped-driven oscillators with one degree of freedom. *Nonlinear Dynamics*, *26*(4), 309-329.

[60] Unal, G., & Sun, J. Q. (2008). New exact solutions to the Fokker–Planck–Kolmogorov equation. *Communications in Nonlinear Science and Numerical Simulation*, *13*(10), 2051-2059.

[61] Unal, G., Iyigünler, I., & Khalique, C. M. (2007). Linearization of one-dimensional nonautonomous jump-diffusion stochastic differential equations. *Journal of Nonlinear Mathematical Physics*, *14*(3), 430-442.

[62] Asghar, S., Jalil, M., Hussan, M., & Turkyilmazoglu, M. (2014). Lie group analysis of flow and heat transfer over a stretching rotating disk. *International Journal of Heat and Mass Transfer*, *69*, 140-146.

[63] Pop, I., & Soundalgekar, V. M. (1974). Effects of Hall current on hydromagnetic flow near a porous plate. *Acta Mechanica*, *20*(3), 315-318.

[64] Pop, I., Seddighi, S., Bachok, N., & Ismail, F. (2014). Boundary layer flow beneath a uniform free stream permeable continuous moving surface in a nanofluid. *Journal of Heat and Mass Transfer Research (JHMTR)*, *1*(1), 55-65.

[65] Pop, I., Naganthran, K., & Nazar, R. (2016). Numerical solutions of non-alignment stagnation-point flow and heat transfer over a stretching/shrinking surface in a nanofluid. *International Journal of Numerical Methods for Heat & Fluid Flow*, *26*(6), 1747-1767.

[66] Pop, I., & Na, T. Y. (1996). Unsteady flow past a stretching sheet. *Mechanics Research Communications*, *23*(4), 413-422.

[67] Pop, I., & Na, T. Y. (1998). A note on MHD flow over a stretching permeable surface. *Mechanics Research Communications*, *25*(3), 263-269.

[68] Fetecau, C., & Fetecau, C. (2005). Starting solutions for some unsteady unidirectional flows of a second grade fluid. *International Journal of Engineering Science*, *43*(10), 781-789.

[69] Fetecau, C., Fetecau, C., Kamran, M., & Vieru, D. (2009). Exact solutions for the flow of a generalized Oldroyd-B fluid induced by a constantly accelerating plate between

two side walls perpendicular to the plate. *Journal of Non-Newtonian Fluid Mechanics, 156*(3), 189-201.

[70] Fetecau, C., Nigar, N., Vieru, D., & Fetecau, C. (2015). First general solution for unidirectional motions of rate type fluids over an infinite plate. *Communications in Numerical Analysis, 2*, 125-138.

[71] Fetecau, C., Vieru, D., Fetecau, C., & Pop, I. (2015). Slip effects on the unsteady radiative MHD free convection flow over a moving plate with mass diffusion and heat source. *The European Physical Journal Plus, 130*(1), 6.

[72] Fetecau, C., Vieru, D., & Azhar, W. A. (2017). Natural convection flow of fractional nanofluids over an isothermal vertical plate with thermal radiation. *Applied Sciences, 7*(3), 247.

[73] Fetecau, C., Nigar, N., Vieru, D., & Fetecau, C. (2015). First general solution for unidirectional motions of rate type fluids over an infinite plate. *Communications in Numerical Analysis, 2*, 125-138.

[74] Fetecau, C., Vieru, D., & Fetecau, C. (2008). A note on the second problem of Stokes for Newtonian fluids. *International Journal of Non-Linear Mechanics, 43*(5), 451-457.

[75] Fetecau, C., Hayat, T., & Fetecau, C. (2006). Steady-state solutions for some simple flows of generalized Burgers fluids. *International Journal of Non-Linear Mechanics, 41*(8), 880-887.

[76] Turkyilmazoglu, M. (2014). Nanofluid flow and heat transfer due to a rotating disk. *Computers & Fluids, 94*, 139-146.

[77] Turkyilmazoglu, M. (2014). Unsteady convection flow of some nanofluids past a moving vertical flat plate with heat transfer. *Journal of Heat Transfer, 136*(3), 031704.

[78] Turkyilmazoglu, M., & Pop, I. (2013). Heat and mass transfer of unsteady natural convection flow of some nanofluids past a vertical infinite flat plate with radiation effect. *International Journal of Heat and Mass Transfer, 59*, 167-171.

[79] Turkyilmazoglu, M., & Pop, I. (2013). Exact analytical solutions for the flow and heat transfer near the stagnation point on a stretching/shrinking sheet in a Jeffrey fluid. *International Journal of Heat and Mass Transfer, 57*(1), 82-88.

[80] Turkyilmazoglu, M. (2013). The analytical solution of mixed convection heat transfer and fluid flow of a MHD viscoelastic fluid over a permeable stretching surface. *International Journal of Mechanical Sciences, 77*, 263-268.

[81] Asghar, S., Mohyuddin, M. R., & Hayat, T. (2005). Effects of Hall current and heat transfer on flow due to a pull of eccentric rotating disks. *International Journal of Heat and Mass Transfer, 48*(3), 599-607.

[82] Asghar, S., Mushtaq, M., & Hayat, T. (2010). Flow in a slowly deforming channel with weak permeability: an analytical approach. *Nonlinear Analysis: Real World Applications, 11*(1), 555-561.

[83] Asghar, S., Hanif, K., Hayat, T., & Khalique, C. M. (2007). MHD non-Newtonian flow due to non-coaxial rotations of an accelerated disk and a fluid at infinity. *Communications in Nonlinear Science and Numerical Simulation, 12*(4), 465-485.

[84] Asghar, S., Hayat, T., & Siddiqui, A. M. (2002). Moving boundary in a non-Newtonian fluid. *International Journal of Non-linear Mechanics, 37*(1), 75-80.

[85] Bég, O. A., Prasad, V. R., Vasu, B., Reddy, N. B., Li, Q., & Bhargava, R. (2011). Free convection heat and mass transfer from an isothermal sphere to a micropolar regime with Soret/Dufour effects. *International Journal of Heat and Mass Transfer*, *54*(1), 9-18.

[86] Bég, O. A., & Makinde, O. D. (2011). Viscoelastic flow and species transfer in a Darcian high-permeability channel. *Journal of Petroleum Science and Engineering*, *76*(3), 93-99.

[87] Bég, O. A., Takhar, H. S., Bhargava, R., Rawat, S., & Prasad, V. R. (2008). Numerical study of heat transfer of a third grade viscoelastic fluid in non-Darcy porous media with thermophysical effects. *Physica Scripta*, *77*(6), 065402.

[88] Bég, O. A., Zueco, J., & Takhar, H. S. (2009). Unsteady magnetohydrodynamic Hartmann–Couette flow and heat transfer in a Darcian channel with Hall current, ionslip, viscous and Joule heating effects: Network numerical solutions. *Communications in nonlinear science and numerical simulation*, *14*(4), 1082-1097.

[89] Bég, O. A., Bakier, A. Y., & Prasad, V. R. (2009). Numerical study of free convection magnetohydrodynamic heat and mass transfer from a stretching surface to a saturated porous medium with Soret and Dufour effects. *Computational Materials Science*, *46*(1), 57-65.

[90] 90 Anderson Jr, J. D. (2010). Fundamentals of aerodynamics. *Tata McGraw-Hill Education.*

[91] Andersson, H. I., & Valnes, O. A. (1998). Flow of a heated ferrofluid over a stretching sheet in the presence of a magnetic dipole. *Acta Mechanica, 128*(1), 39-47.

[92] Neuringer, J. L. (1966). Some viscous flows of a saturated ferro-fluid under the combined influence of thermal and magnetic field gradients. *International Journal of Non-Linear Mechanics, 1*(2), 123-137.

[93] Nadeem, S., & Akbar, N. S. (2009). Peristaltic flow of a Jeffrey fluid with variable viscosity in an asymmetric channel. *Zeitschrift für Naturforschung A, 64*(11), 713-722.

[94] Ali, N., Hayat, T., & Asghar, S. (2009). Peristaltic flow of a Maxwell fluid in a channel with compliant walls. *Chaos, Solitons & Fractals, 39*(1), 407-416.

[95] Rajagopal, K. R., Na, T. Y., & Gupta, A. S. (1984). Flow of a viscoelastic fluid over a stretching sheet. *Rheologica Acta, 23*(2), 213-215.

[96] Muhammad, A. (2012). Fluctuating hydromagnetic flow of viscous incompressible fluid past a magnetized heated surface (Doctoral dissertation), *Comsats Institute of Information Technology, Islamabad.*

[97] Sparrow, M. E. & Cess, D. R. (1970). Radiation Heat Transfer, Brooks/ Cole, Belmont, *Calif, USA*.

[98] Özisik, M. N. (1973). Radiative Transfer and Interactions with Conduction and Convection, John Wiley and Sons. *Inc., New York*.

[99] Siegel, R. H. J. R., & Howell, J. R. (1992). Thermal Radiation Heat Transfer, Hemisphere Pub. *Corp Wash DC*.

[100] Howell, J. R. (2000). Radiative transfer in porous media. In *Handbook of Porous Media*, 663-698. CRC Press.

[101] Bear, J. (1972). Dynamics of Fluids in Porous Media. *Dover New York Google Scholar*.

[102] Nield, D. A., & Bejan, A. (2006). Convection in porous media. *Springer Science & Business Media*.

[103] Darcy, H. (1856). Les fontaines publiques de la ville de Dijon: Exposition et Application. *Victor Dalmont*.

[104] Nakayama, A. (1995). PC-aided Numerical Heat Transfer and Convective Flow. *CRC press*.

[105] Hong, J. T., Yamada, Y., & Tien, C. L. (1987). Effect of non-Darcian and non-uniform porosity on vertical plate natural convection in porous medium. *Internal Journal of Heat and Mass Transfer, 109*, 356–362.

[106] Forchheimer, P. (1901). Wasserbewegung durch Boden. *Zeitschrift des Vereines Deutscher Ingenieure, 45*(1736-1741), 1781-1788.

[107] Chen, C. H., & Horng, J. H. (1999). Natural convection from a vertical cylinder in a thermally stratified porous medium. *Heat and Mass Transfer, 34*(5), 423-428.

[108] Poulikakos, D., & Bejan, A. (1985). The departure from Darcy flow in natural convection in a vertical porous layer. *The Physics of Fluids, 28*(12), 3477-3484.

[109] Prasad, V., & Tuntomo, A. (1987). Inertia effects on natural convection in a vertical porous cavity. *Numerical Heat Transfer, Part A Applications, 11*(3), 295-320.

[110] Brinkman, H. C. (1949). A calculation of the viscous force exerted by a flowing fluid on a dense swarm of particles. *Flow, Turbulence and Combustion, 1*(1), 27.

[111] Brinkman, H. C. (1949). On the permeability of media consisting of closely packed porous particles. *Flow, Turbulence and Combustion, 1*(1), 81.

[112] Al-Sanea, S. A. (2004). Mixed convection heat transfer along a continuously moving heated vertical plate with suction or injection. *International Journal of Heat and Mass Transfer, 47*(6), 1445-1465.

[113] Bhattacharyya, K. (2011). Effects of radiation and heat source/sink on unsteady MHD boundary layer flow and heat transfer over a shrinking sheet with suction/injection. *Frontiers of Chemical Science and Engineering, 5*(3), 376-384.

[114] Mukhopadhyay, S. (2013). Slip effects on MHD boundary layer flow over an exponentially stretching sheet with suction/blowing and thermal radiation. *Ain Shams Engineering Journal, 4*(3), 485-491.

[115] Erickson, L. E., Fan, L. T., & Fox, V. G. (1966). Heat and mass transfer on moving continuous flat plate with suction or injection. *Industrial & Engineering Chemistry Fundamentals, 5*(1), 19-25.

[116] Fox, V. G., Erickson, L. E., & Fan, L. T. (1968). Methods for solving the boundary layer equations for moving continuous flat surfaces with suction and injection. *AIChE Journal, 14*(5), 726-736.

[117] Char, M. I. (1988). Heat transfer of a continuous, stretching surface with suction or blowing. *Journal of Mathematical Analysis and Applications, 135*(2), 568-580..

[118] Abo-Eldahab, E. M., & El Aziz, M. A. (2004). Blowing/suction effect on hydromagnetic heat transfer by mixed convection from an inclined continuously stretching surface with internal heat generation/absorption. *International Journal of Thermal Sciences, 43*(7), 709-719.

[119] Kafoussias, N. G., & Williams, E. W. (1995). Thermal-diffusion and diffusion-thermo effects on mixed free-forced convective and mass transfer boundary layer flow with temperature dependent viscosity. *International Journal of Engineering Science, 33*(9), 1369-1384.

[120] Eckert, E. R. G., & Drake Jr, R. M. (1987). Analysis of heat and mass transfer.

[121] Hiemenz, K. (1911). Die Grenzschicht an einem inden gleichförmigen Flüssigkeitsstrom eingetauchten geraden Kreiszylinder, *Dingler's Polytechanic. Journal, 326*, 321-324.

[122] Sharma, K. (2012). Problems on ferrofluid flow due to rotating disk (Doctoral thesis). National Institute of Technology, Kurukshetra, India.

[123] Ram, P., Kumar, V., & Sharma, S. (2014). Magneto-viscous effects on unsteady nano-ferrofluid flow influenced by low oscillating magnetic field in the presence of rotating disk, *Recent Advances in Fluid Mechanics and Thermal Engineering*, 89-97.

[124] Ram, P., & Bhandari, A. (2013). Effect of phase difference between highly oscillating magnetic field and magnetization on the unsteady ferrofluid flow due to a rotating disk. *Results in Physics, 3*, 55-60.

[125] Boutros, Y. Z., Abd-el-Malek, M. B., Badran, N. A., & Hassan, H. S. (2007). Lie-group method solution for two-dimensional viscous flow between slowly expanding or contracting walls with weak permeability. *Applied Mathematical Modelling, 31*(6), 1092-1108.

[126] Chen, C. H. (1998). Laminar mixed convection adjacent to vertical, continuously stretching sheets. *Heat and Mass Transfer, 33*(5), 471-476.

[127] Ishak, A., Nazar, R., & Pop, I. (2008). Hydromagnetic flow and heat transfer adjacent to a stretching vertical sheet. *Heat and Mass Transfer, 44*(8), 921.

[128] Abel, M. S., Sanjayanand, E., & Nandeppanavar, M. M. (2008). Viscoelastic MHD flow and heat transfer over a stretching sheet with viscous and ohmic dissipations. *Communications in Nonlinear Science and Numerical Simulation, 13*(9), 1808-1821.

[129] Ali, M. E. (1994). Heat transfer characteristics of a continuous stretching surface. *Heat and Mass Transfer, 29*(4), 227-234.

[130] Wang, C. Y. (1989). Free convection on a vertical stretching surface. *ZAMM-Journal of Applied Mathematics and Mechanics/Zeitschrift für Angewandte Mathematik und Mechanik, 69*(11), 418-420.

[131] Hamad, M. A. A., & Ferdows, M. (2012). Similarity solution of boundary layer stagnation-point flow towards a heated porous stretching sheet saturated with a nanofluid with heat absorption/generation and suction/blowing: a Lie group analysis. *Communications in Nonlinear Science and Numerical Simulation, 17*(1), 132-140.

[132] Pal, D., Mandal, G., & Vajravelu, K. (2014). Flow and heat transfer of nanofluids at a stagnation point flow over a stretching/shrinking surface in a porous medium with thermal radiation. *Applied Mathematics and Computation, 238*, 208-224.

[133] Hamad, M. A., & Pop, I. (2011). Scaling transformations for boundary layer flow near the stagnation-point on a heated permeable stretching surface in a porous medium saturated with a nanofluid and heat generation/absorption effects. *Transport in Porous Media, 87*(1), 25-39.

[134] Grubka, L. J., & Bobba, K. M. (1985). Heat transfer characteristics of a continuous, stretching surface with variable temperature. *Journal of Heat Transfer, 107*(1), 248-250.

[135] Bachok, N., Ishak, A., & Nazar, R. (2011). Flow and heat transfer over an unsteady stretching sheet in a micropolar fluid. *Meccanica, 46*(5), 935-942.

[136] Crane, L. J. (1970). Flow past a stretching plate. *Zeitschrift für angewandte Mathematik und Physik ZAMP, 21*(4), 645-647.

[137] Christov, C. I. (2009). On frame indifferent formulation of the Maxwell-Cattaneo model of finite-speed heat conduction. *Mechanics Research Communications, 36*(4), 481-486.

[138] Tiwari, R. K., & Das, M. K. (2007). Heat transfer augmentation in a two-sided lid-driven differentially heated square cavity utilizing nanofluids. *International Journal of Heat and Mass Transfer, 50*(9), 2002-2018.

[139] Domkundwar, A. V., Domdundwar, V. M. (2004). Heat and Mass transfer data book, *Dhanparai and co (p) Ltd, Educational and Technical Publishers, Delhi*.

[140] Shliomis, M. I., & Morozov, K. I. (1994). Negative viscosity of ferrofluid under alternating magnetic field. *Physics of Fluids, 6*(8), 2855-2861.

[141] Ram, P., & Bhandari, A. (2013). Negative viscosity effects on ferrofluid flow due to a rotating disk. *International Journal of Applied Electromagnetics and Mechanics, 41*(4), 467-478.

[142] Shliomis, M. I. (2001). Ferrohydrodynamics: Testing a third magnetization equation. *Physical Review E, 64*(6), 060501.

[143] Brinkman, H. C. (1952). The viscosity of concentrated suspensions and solutions. *The Journal of Chemical Physics, 20*(4), 571-571.

[144] Hamilton, R. L., & Crosser, O. K. (1962). Thermal conductivity of heterogeneous two-component systems. *Industrial and Engineering Chemistry Fundamentals, 1*(3), 187-191

[145] Timofeeva, E. V., Routbort, J. L., & Singh, D. (2009). Particle shape effects on thermophysical properties of alumina nanofluids. *Journal of Applied Physics, 106*(1), 014304.

[146] Kelson, N., & Desseaux, A. (2000). Note on porous rotating disk flow. *Australian and New Zealand Industrial and Applied Mathematics Journal, 42*, 837-855.

[147] Rashidi, M. M., Abelman, S., & Mehr, N. F. (2013). Entropy generation in steady MHD flow due to a rotating porous disk in a nanofluid. *International Journal of Heat and Mass Transfer, 62*, 515-525.